Ice, Cloud, and Land Elevation Satellite 2 (ICESat-2) Project

Algorithm Theoretical Basis Document for Precision Pointing Determination

Prepared By:
Noah Smith, Sungkoo Bae, Bob Schutz
University of Texas Center for Space Research

Goddard Space Flight Center
Greenbelt, Maryland

National Aeronautics and Space Administration

Abstract

Pointing knowledge consists of time series of laser pointing unit vectors and their uncertainties expressed in the celestial reference frame. During processing the laser pointing vectors are expressed in the Laser Reference Sensor coordinate frame and then in the celestial frame using the estimated Laser Reference Sensor attitude. The Laser Reference Sensor is a custom instrument designed specifically for laser pointing determination and plays the central role for pointing knowledge. It simultaneously observes the altimetry lasers, stars, and reference signals, all in its own instrument coordinate frame. The star observations along with observations from the spacecraft star trackers and gyro unit are used to estimate the rotation between the Laser Reference Sensor coordinate frame and the celestial frame. Processing is similar to the previous ice altimetry mission, which also centered on a custom Laser Reference Sensor tying laser pointing to the celestial frame. The methods are mature and their complexities are understood.

CM Foreword

This document is an Ice, Cloud, and Land Elevation (ICESat-2) Project Science Office controlled document. Changes to this document require prior approval of the Science Development Team ATBD Lead or designee. Proposed changes shall be submitted in the ICESat-II Management Information System (MIS) via a Signature Controlled Request (SCoRe), along with supportive material justifying the proposed change.

In this document, a requirement is identified by "shall," a good practice by "should," permission by "may" or "can," expectation by "will," and descriptive material by "is."

Questions or comments concerning this document should be addressed to:

ICESat-2 Project Science Office
Mail Stop 615
Goddard Space Flight Center
Greenbelt, Maryland 20771

Preface

The ICESat-2 Science Development Team, in support of the ICESat-2 Project Science Office (PSO), assumes responsibility for this document and updates it, as required, to meet the needs of the ICESat-2 SIPS. Reviews of this document are performed when appropriate and as needed updates to this document are made. Changes to this document will be made by complete revision.

Changes to this document require prior approval of the Change Authority listed on the signature page. Proposed changes shall be submitted to the ICESat-2 PSO, along with supportive material justifying the proposed change.

Questions or comments concerning this document should be addressed to:

Thorsten Markus, ICESat-2 Project Scientist
Mail Stop 615
Goddard Space Flight Center
Greenbelt, Maryland 20771

Review/Approval Page

Prepared by:

Noah Smith
Postdoctoral Fellow
Center for Space Research

Reviewed by:

Approved by:

***** Signatures are available on-line at:** https:// /icesatiimis.gsfc.nasa.gov ***

Change History Log

Level	DESCRIPTION OF CHANGE	SCoRe No.	Date Approved
1.0	Initial Release		

List of TBDs/TBRs

Item No.	Location	Summary	Ind./Org.	Due Date

Table of Contents

List of Figures

List of Tables

1.0 Introduction

ICESat-2 uses a lidar system to make precision range measurements between the ICESat-2 observatory and the Earth. Pointing determination provides arcsecond-level knowledge of the laser pointing direction for each laser pulse, while orbit determination provides cm-level knowledge of the observatory position in space. The pointing and orbit products are combined with the range measurements to yield the positions of the laser spots on the surface of the Earth to a horizontal accuracy of 6.5 meters.

The intended pointing knowledge users are the Planetary Geodynamics Laboratory and the Science Investigator-Led Processing System at NASA's Goddard Space Flight Center for incorporation into the Level-2A data products. The pointing product consists of six 50 Hz time series of laser pointing unit vectors and their uncertainties, expressed in the celestial reference frame.

During pointing processing, the laser pointing vectors are expressed in the Laser Reference Sensor (LRS) coordinate frame, and then in the celestial reference frame using the estimated LRS attitude. The LRS simultaneously observes the lasers, stars, and alignment reference signals in the LRS coordinate frame. An LRS measurement model interprets these observations as three-dimensional unit vectors in the LRS coordinate frame and filters them along with data from the two spacecraft star trackers (SSTs) and gyro unit (SIRU) to estimate the LRS attitude.

The estimated uncertainties of the laser pointing vectors are important for downstream processing, particularly calculation of geolocation uncertainties. The primary sources of measurement uncertainty are the LRS and the SIRU. Much of the empirical information about pointing uncertainties due to high frequency motion will necessarily come from the SIRU output, which is recorded at 50 Hz and provides more bandwidth than the 10 Hz LRS star observations and 10 Hz SST attitude observations. The SIRU is also used to propagate the pointing vector estimates to the 50 Hz rate required in the pointing product.

The pointing algorithms are similar to the ICESat GLAS algorithms, which also centered on an LRS to tie laser pointing to the celestial reference frame. The GLAS heritage means that many pointing methods are mature and that their complexities are understood. The algorithms for LRS attitude estimation carry over directly from the GLAS LRS. Many of the specific questions for ATLAS pointing are related to the unique characteristics of the sensors.

Verification and quality measures for the pointing product and are based on LRS star residuals and ocean scan altimetry range residuals. LRS attitude estimates are equivalent to predictions of

the LRS star observations, and the observed minus predicted residuals reflect the attitude estimate accuracy. Ocean scan residuals reflect the accuracy of the estimated laser pointing vectors. Given accurate LRS attitude estimates, biases in the ocean scan residuals reflect biases in the measurement model used to express laser observations in the LRS coordinate frame. Pointing quality is also assessed using cross-over analysis.

2.0 Overview

The pointing algorithm uses the LRS observations with support from the SSTs and SIRU to determine the pointing of the altimetry laser. The LRS is a custom instrument designed specifically for laser pointing determination and plays the central role in pointing knowledge. It simultaneously observes the altimetry lasers, stars, and reference signals, all in the LRS coordinate frame. The star observations, along with the SST attitude observations, are used to estimate the rotation between the LRS coordinate frame and the celestial reference frame.

The processor is a filter moving sequentially forward in time through the input observations. A cycle consisting of a propagation and an update is performed for each incoming observation and the sensors can be roughly divided into two groups corresponding to cycle phase and measurement type. The LRS and SSTs make vector observations and are used for measurement updates, which generally tend to decrease pointing uncertainty. The SIRU makes angle and inferred-rate observations and is used for propagation, which tends to increase pointing uncertainty.

One question concerns the LRS measurement model for interpreting the observations of the lasers and reference signal spots as three-dimensional unit vectors in the LRS coordinate frame. This geometric transformation from two-dimensional image measurements to three-dimensional unit vectors requires calibration, preferably repeatedly throughout the mission. The LRS coordinate frame is defined by the LRS star tracker. Alignment variations between the star tracker and laser tracker are difficult to observe directly, but the effects are corrected with information from ocean scan calibrations.

The star observations themselves are a significant question. The catalog of predicted star observations for the LRS indicates that there are regions of the sky where LRS stars will be sparse. ICESat-1 LRS star observations were inherently sparse and heritage algorithms for incorporating observations from other star trackers based on their time-varying relative alignments carry over here.

Fully utilizing the SIRU is another question. The 50 Hz telemetry from the SIRU and the LRS laser tracker are monitored in both the time and frequency domains for evidence of high frequency pointing variations. Correlations with entering and exiting eclipse, solar panel motion, maneuvers, and other changes of state are of particular interest.

2.1 Telemetry

Telemetry is received as HDF5 data files containing 10 Hz star telemetry from the LRS star tracker and SSTs, 50 Hz laser measurements from the LRS laser tracker, and 50 Hz sense-axes angular increment measurements from the SIRU. Supporting inputs from telemetry concern the spacecraft state including position and velocity, onboard attitude estimates, temperatures, solar array motion, and the state of individual components such as the laser system and beam steering mechanism.

The LRS consists of two trackers joined back-to-back for two fields of view: one tracking stars near the zenith, and one tracking laser and reference spots near the nadir. Ideally the LRS has a single coordinate frame and two fields of view, one for stars, and one for the altimetry lasers and reference signals.

Because the LRS star tracker directly observes stars and the celestial reference frame it is used to define the LRS coordinate frame. The physical joint between the star and laser trackers is designed to be stable and the two tracker coordinate frames are ideally equivalent to a single LRS frame, but pointing determination accounts for the possibility of relative motion.

The term star telemetry is used here for all telemetry entering the processor as measurement updates and determining the propagation time intervals and filter cycle boundaries. It is a generic term for 10 Hz star measurements from the LRS and 10 Hz attitude estimates from the SSTs (which are based on SST star measurements).

The processor can be viewed as treating the SSTs as support components for the LRS star tracker. Each SST is a black box that outputs an attitude estimate. The processor filter states represent the time-varying alignment rotations between the SSTs and the LRS star tracker, in effect joining the SSTs with the LRS by tracking the alignment rotations and replacing physical joints with a software model of the physical geometry. This parallels the way two trackers are physically joined in the LRS to form a single LRS frame.

Laser telemetry is received from the LRS laser tracker, which measures laser and reference spot centroids at 50 Hz. The laser spots represent the directions of the lasers in the laser tracker coordinate frame. The directions in the LRS frame are then known, assuming that the alignment between the LRS star and laser trackers is known.

Gyro telemetry is received from the SIRU and used for propagation between measurement updates. The SIRU is a gyro unit and measures angular increments about its four sense axes. It provides greater angular resolution over short time scales and more information bandwidth than

the 10 Hz star telemetry. It consists of four hemispherical resonator gyros arranged with their axes forming an octahedral tetrad pyramid shape. The gyros are of the rate integrating type, outputting an angle expressed as an integer count which wraps as the output register overflows or underflows. One count is equal to 0.05 arcseconds. The overall unit is effectively a black box with four output registers that are updated at 100 Hz, one for each sense axis. The spacecraft records the values in the output registers asynchronously at 50 Hz.

2.2 Measurement and Error Models

Measurement and error models are the equations and parameters necessary for using the LRS, SST, and SIRU telemetry within the processor. Generally, measurement models are deterministic terms for transforming and interpreting the sensor measurements and error models are stochastic terms involving random processes and uncertainties.

Initial parameter estimates for the models come from ground testing. The overall pointing knowledge process emphasizes updating both the models and parameter estimates during the mission based on flight data. These updates are shared and documented where possible. There is experience from ICESat-1 with problems that can arise when the links between telemetry and measurement models become ambiguous or confused.

The key LRS measurements are two-dimensional positions expressed in pixels. The measurement model converts these pixel coordinates to three-dimensional unit vectors in the LRS coordinate frame. For the star tracker, another measurement model converts brightness counts to instrument magnitudes. The laser tracker models have to include the laser to star tracker alignment in order to produce unit vectors expressed in the LRS coordinate frame. This alignment is difficult to estimate from flight telemetry and the initial estimates from ground testing will play an important role throughout the mission.

Because the SSTs are effectively black boxes, their measurement models reduce to alignment rotations that relate the telemetered attitude estimates to the LRS frame. The processor tracks these alignment rotations and SST error modeling involves parameter estimation for the alignment process noise in addition to the uncertainties in the telemetered attitude estimates.

The SIRU measurement model combines angular increments from four sense axes and transforms them into a three-dimensional angular rate vector for the SIRU frame. Angular rate is simply calculated as angular increment per unit of time. The SIRU measurement model includes calibration parameters for each sense axis: geometric misalignment from the ideal octahedral tetrad, bias, and scale factors of various types.

SIRU error modeling represents the growth of attitude uncertainty during the propagation phase of the filter cycle. Gyro modeling can be complex but reduces here to three stochastic processes generically referred to as angular random walk (ARW), rate random walk (RRW), and angle white noise. ARW is linked to uncertainties over short time scales and can be referred to as noise. RRW is linked to uncertainties over long time scales and can be referred to as bias instability and associated with gyro drift.

2.3 Mission Star Catalog

The mission star catalog provides the reference parameters to predict and interpret the LRS star telemetry. Errors in the catalog can directly cause errors in the pointing products in certain circumstances, particularly when only one star is being tracked. The catalog is used to identify LRS stars and to provide their reference unit vectors in the celestial frame for comparison with the LRS measurements.

Stars with measurements that are biased relative to the catalog reference parameters are referred to here as bad stars. The biases can be in position and/or brightness but clearly position is primary concern. Adaptive checks within the filter are used to detect and reject bad stars by comparing the filter predictions and observations before they are used to perform a measurement update, but cases where the measurement bias is near the noise level require large samples to detect and characterize.

The mission catalog is intended to correct for measurement biases wherever possible by providing what are referred to as blended or center of light reference parameters. The catalog positions and instrument magnitudes are predictions of what the LRS actually observes on the sky. For a bad star with a small LRS position measurement bias, the mission catalog record should be corrected as soon as practical to either negate the bias or to flag the star for automatic rejection.

Mission catalog position and magnitude parameters are initially based on analysis of the astronomical star catalogs and ground testing of the LRS. During the mission the observed minus predicted filter residuals are stored and analyzed in order to improve the catalog records over time. Catalog information comes primarily from the LRS Team Catalog (LRSTC), NASA SKY2000 Version 5 star tracker catalog [1-5], and LRS telemetry.

Ancillary inputs from sources outside the mission are ephemerides for the sun, moon, Earth inertial velocity, and fundamental star catalogs (SKY2000, Hipparcos). Ephemerides with daily

values for 2016.01.01 to 2016.01.01 have been generated using the JPL HORIZONS system and accompany this document.

2.4 Processor and Products

The main path through the processor consists of a Kalman filter cycling sequentially forward in time through the telemetry. Star telemetry determines the cycle boundaries. When a new LRS star measurement or SST attitude estimate is received a measurement update is performed to incorporate the new information into the filter state. Between updates the SIRU is used to propagate the filter state forward in time. The conceptual discussion here focuses on the LRS and filter updates.

The combined filter states represent attitude estimates for the LRS and SSTs, along with a correction to the angular rate. The filter also maintains a representation of the uncertainties in the states. The attitude estimates are equivalent to predictions of the star telemetry. The observed minus predicted residuals are used to update the states and uncertainties.

The states represent three attitude estimates but only one is explicit. The other two combine the explicit attitude estimate with alignment estimates. The explicit attitude estimate is often identified with a generic coordinate frame referred to as the body frame. In practice the body frame can be associated with the LRS frame, an SST, the SIRU, or a combination of several sensor coordinate frames.

There are advantages to associating the body frame with a sensor providing frequent and uninterrupted observations, particularly star or attitude observations that provide direct information from the celestial coordinate frame. One possibility is to use a combination of the SSTs since they acquire and track a large number of stars and are aligned in such a way that they will not both be blinded simultaneously. On the other hand, the attitude of the LRS coordinate frame, identified with the LRS star tracker, is of central importance for the overall pointing product.

For the discussion here, the body frame is identified with the LRS coordinate frame unless stated otherwise. The attitude estimates for the SSTs are a combination of the body frame attitude estimate and SST alignment estimates. Other modes of defining and arranging the filter state are possible but are classed as contingencies here.

The pointing products are 50 Hz time series of laser unit vectors and their uncertainties expressed in the celestial frame. The vectors have two degrees of freedom because of the unit constraint and can be represented by two coordinates. The LRS frame orientation relative to the

celestial frame is given by its estimated attitude. A three-dimensional laser unit vector is specified by two coordinates in the LRS frame and then expressed by extension in the celestial frame.

The 50 Hz pointing product time tags correspond to the LRS laser telemetry time tags. In other words the laser telemetry time tags are the set of times at which the processor needs to estimate the laser unit vectors and uncertainties.

Unique higher frequency information concerning laser pointing is available in the gyro telemetry and an objective of the processor is to take advantage of this information where practical. The 50 Hz gyro telemetry is asynchronous with the 50 Hz laser telemetry and careful propagation and interpolation of the results is required.

The six pointing vectors are the means or first moments of six laser pointing probability distributions which represent the overall pointing knowledge. The Kalman filter which makes up the main path of the processor models the pointing probability distributions using first and second moments alone. An important question is whether the filter error covariance matrix adequately describes the pointing probability distributions and true laser pointing uncertainties. The pointing vector estimates may be relatively straightforward compared to their uncertainties.

Concepts and definitions for describing pointing uncertainty are adopted here from a sequence of papers on the topic [6-8]. Pointing uncertainty is defined for a specified length of time, generally the time needed for a sensor to make its observation. For an imager the length of time is the exposure or integration time.

For laser pointing knowledge the most significant time scales are a more complex question. The 20 millisecond time scale of the 50 Hz pointing product is adopted here by convention. This is a relatively small time scale and tends to make the question of jitter more significant for pointing uncertainty.

The term jitter has a very specific meaning, “motion occurring during an image exposure of specified duration” [7] or “line-of-sight motion within a time interval” [8]. It is rigorously defined as jitter variance, one of two components in the overall variance, along with the variance of the mean.

For the pointing product the estimated pointing vectors are the mean. At longer time scales the variance of the mean becomes smaller and the jitter variance becomes larger which agrees with intuition: the more time and observations available, the more certain the mean value becomes.

This is related to the concept of variance of the sample mean, where the variance for a sample size of n decreases by $1/n$.

3.0 Theory

Theory for the processor concerns estimation of attitude, instrument alignments, laser pointing, and related signal processing. This section begins with a general overview of processor parameters. It then discusses analytic theory underlying the processor. Dynamics and dynamical modeling do not play a major role and, in particular, no attempt is made to model the torques and structural dynamics that cause laser pointing variations.

3.1 Parameter Overview

Many of the model parameters correspond to three classes of telemetry and the two phases of the processor filter cycle: 10 Hz star telemetry (LRS star tracker, SSTs) is associated with filter measurement updates, 50 Hz gyro telemetry and 50 Hz laser telemetry is associated with filter propagation.

The sources of uncertainty that are explicitly modeled are gyro AWN, ARW, and RRW, LRS measurement uncertainty, SST attitude uncertainty, and LRS to SST alignment uncertainty. Gyro and alignment uncertainties enter the filter as process noise during propagation. LRS and SST uncertainties enter the filter as measurement noise during measurement updates. These sources, particularly gyro ARW and LRS measurement uncertainty, determine the filter model for pointing knowledge uncertainties.

The key parameters are summarized below in Table 1, along with the telemetry from each sensor.

Table 1 Overview of telemetry and model parameters

	10 Hz Star		50 Hz Gyro	50 Hz Laser
	LRS Star Tracker	SSTs		
Telemetry	x, y star centroid detector coordinates, pixels or mm b star brightness, counts	$\mathbf{A}_i^{SST1}, \mathbf{A}_i^{SST2}$ attitude estimates	$\boldsymbol{\theta}_s(t_k)$ sense axes angle increment counts, 0.05 arcseconds/count	x, y (x6), laser spot centroid detector coordinates, pixels or mm
Deterministic measurement model parameters	$\mathbf{A}_b^{LRS}$ alignment rotation from body frame $\mathbf{p}_1$ parameters to convert centroids to unit vectors $\mathbf{u}_1 = \mathbf{f}_1(x, y, \mathbf{p}_1)$ $\mathbf{p}_2$ parameters to correct unit vectors $\mathbf{u}_2 = \mathbf{f}_2(\mathbf{u}_1, \mathbf{p}_2)$ $\mathbf{p}_{ref}$ mission star catalog reference parameters for stars	$\mathbf{A}_b^{SST1}, \mathbf{A}_b^{SST2}$ alignment rotations from body frame	$\mathbf{A}_b^{SIRU}$ gyro unit alignment rotation from body frame $\boldsymbol{\omega}_s(t_k) = \mathbf{f}(\Delta\boldsymbol{\theta}_s(t_k))$ sense axes angular rates, radians/second $\mathbf{b}(t)$ gyro rate bias expressed in body frame, radians/second $\boldsymbol{\Lambda}$ sense axes scale factors $\mathbf{W}$ sense axes ideal geometry $\mathbf{U}, \mathbf{V}, \boldsymbol{\Delta}_\mathbf{u}, \boldsymbol{\Delta}_\mathbf{v}$ sense axes misalignments	$\mathbf{A}_{LT}^{LRS}$ alignment rotation from LRS laser tracker frame to LRS star tracker frame $\mathbf{p}_{LT}$ parameters to convert centroids to unit vectors $\mathbf{u}_{LT} = \mathbf{f}_{LT}(x, y, \mathbf{p}_{LT})$
Stochastic error model parameters	$\sigma_u^2(b)$ measurement noise variance as a function of star brightness σ_{LRS}^2 alignment rotation process noise, radians^2/second	$\mathbf{R}_{SST1}, \mathbf{R}_{SST2}$ uncertainty or effective noise in the attitude estimates $\sigma_{SST1}^2, \sigma_{SST2}^2$ alignment rotation process noise, radians^2/second	σ_{awn}^2 angular white noise variance, radians^2 σ_{arw}^2 angular random walk variance, radians^2/second σ_{rrw}^2 rate random walk variance, (radians/second)^2/second	$\mathbf{R}_{LT}$ uncertainty of the alignment rotation from LRS star tracker frame to LRS laser side frame, radians^2 σ_{LT}^2 measurement noise variance, radians^2

3.1.1 Star Model Parameters

These parameters characterized the coordinate frames and telemetry of the three star trackers. A fourth abstract body frame is included in the description. Ideally it is identified with a stable reference structure such as the IMSC. In practice one of the tracker frames usually plays the role of the body frame, but it is useful to keep the description general.

The three tracker coordinate frames are represented as reference alignment rotations from the body frame $\mathbf{A}_b^{LRS}$, $\mathbf{A}_b^{SST1}$, and $\mathbf{A}_b^{SST2}$. Alignment variations are characterized by the alignment process noises σ_{LRS}^2, σ_{SST1}^2, and σ_{SST2}^2 (radians^2/second) describing the growth of alignment uncertainty over time. If an alignment has a significant orbital variation its process noise reflects its magnitude. A tracker frame is effectively defined as the body frame by assuming that its alignment is constant and that its alignment uncertainty and process noise are zero.

Alignment rotations and process noises are effectively the measurement and error models for the SSTs. They are the parameters needed by the processor in order to utilize the SST telemetry.

The LRS star tracker model is more complex. The simplest possible model converts two-dimensional focal plane positions x, y to three-dimensional unit vectors $\mathbf{u}_1 = \mathbf{f}_1(x, y, \mathbf{p}_1)$ in the LRS coordinate frame based on a first-order geometric model (pinhole camera model). The model parameter vector $\mathbf{p}_1$ would have only one component (the effective focal length) for a true pinhole camera model. LRS ground calibration provides a quadratic model with three components in $\mathbf{p}_1$.

Deterministic corrections (for distortion, centroiding errors, aberration, etc) are included via a second model $\mathbf{u}_2 = \mathbf{f}_2(\mathbf{u}_1, \mathbf{p}_2)$ with parameter vector $\mathbf{p}_2$. The error model is summarized by $\mathbf{u} = \mathbf{h} + \boldsymbol{\eta}$ where $\mathbf{u}$ is the observed unit vector, $\mathbf{h}$ is the true unit vector, and $\boldsymbol{\eta}$ is zero-mean Gaussian white noise $E\{\boldsymbol{\eta}^T\boldsymbol{\eta}\} = \sigma_u^2\mathbf{I}$.

Three-dimensional unit vectors $\mathbf{u} = [u_1 \quad u_2 \quad u_3]^T$ are usually represented using $\mathbf{u}_{obs} = [u_{obs,1} \quad u_{obs,2} \quad u_{obs,3}]^T = [h_{obs} \quad v_{obs}]^T$ coordinates in an $\mathbf{ijk}$ tracker frame, where the tracker LOS is the $\mathbf{k}$ axis. Angles θ_h and θ_v are defined from the $\mathbf{k}$ axis towards the i and $\mathbf{j}$ axes. An intermediate vector $\mathbf{u}' = [h \quad v \quad 1]^T$ is defined using h, v coordinates

$$h \equiv \tan\theta_h = u_1/u_3 \tag{1}$$

$$v \equiv \tan\theta_v = u_2/u_3 \tag{2}$$

and $\mathbf{u}$ is the normalized version of $\mathbf{u}'$

$$\mathbf{u} = \begin{bmatrix} h & v & 1 \end{bmatrix}^T \Big/ \left(h^2 + v^2 + 1\right)^{1/2} \tag{3}$$

Near the $\mathbf{k}$ axis $h \equiv \tan\theta_h \cong \theta_h$ and $v \equiv \tan\theta_v \cong \theta_v$.

3.1.2 Laser Model Parameters

The LRS laser tracker observes six laser centroids at 50 Hz. The measurement model converts the centroids x_1, x_2 to unit vectors $\mathbf{u}_{LT}$ in the laser tracker coordinate frame. LRS ground calibration provides a quadratic model $\mathbf{u}_{LT} = \mathbf{f}_{LT}(x_1, x_2, \mathbf{p}_{LT})$ with parameters $\mathbf{p}_{LT}$. The alignment rotation $\mathbf{A}_{LT}^{LRS}$ from the LRS frame (LRS star tracker frame) to the laser tracker frame is used to express the laser unit vectors $\mathbf{u}_{LT}$ in the star tracker frame (and by extension in the ICRF).

The error model represents the uncertainty of the laser directions in the LRS frame. The main contributors are uncertainty in the unit vectors $\mathbf{u}_{LT}$ and in the alignment $\mathbf{A}_{LT}^{LRS}$. The uncertainties in the $\mathbf{u}_{LT}$ are characterized by the measurement noise variance σ_{LT}^2, radians^2. The alignment uncertainty is the covariance matrix $\mathbf{R}_{LT}$, radians^2.

3.1.3 Gyro Model Parameters

The four gyro unit sense axes are rate-integrating gyros outputting angular counts $\boldsymbol{\theta}_s(t_k)$, with units of 0.05 arcseconds per count. Angular rates about each sense axis $\boldsymbol{\omega}_s(t_k) = \mathbf{f}(\boldsymbol{\theta}_s(t_k))$ are calculated as observed angular change per unit time.

The measurement model parameters describe deterministic effects that are specific to each sense axis. With four sense axes there are four instances of each type of parameter collected into a parameter vector.

The gyro rate bias vector $\mathbf{b}$ represents the observed rate when the true rate is zero. This is a highly variable parameter. It is always estimated as a time-varying quantity if possible and is therefore always a member of the filter state. It absorbs the effects of multiple sources of error, most notably the alignment between the gyro unit frame and body frame. In effect the filter estimate of $\mathbf{b}(t)$ includes the effects of alignment variations for the gyro unit as a whole. Note that the components of $\mathbf{b}(t)$ are therefore in practice not strictly mapped one-for-one to the four sense axes.

Variations of $\mathbf{b}(t)$ are referred to as bias instability. Bias instability and gyro drift are closely associated concepts. In general they are a concern at longer time scales, whereas the concern over shorter time scales gyro noise. While star telemetry is coming in from at least one of the three star trackers, the effects of bias instability and gyro drift are kept small by measurement update corrections to the attitude estimate and $\mathbf{b}(t)$. OSC has stated that the SSTs will not be simultaneously blinded during normal or near-normal operations.

The rate scale factor vector $\boldsymbol{\lambda}$ represents the scaling between the observed and true rate. A linear scaling factor is often used but more sophisticated models (e.g. asymmetric scaling) are possible. Geometric misalignment vectors $\mathbf{u}, \mathbf{v}$ are used to correct for rate errors introduced by the fact that the sense axes do not form a perfect octahedral tetrad pyramid shape. The measurement model combines the four observed sense axes rates using a linear geometric transformation. The misalignments $\mathbf{u}, \mathbf{v}$ describe the deviations of the sense axes away from their ideal directions as two-component rotation vectors, expressed in the plane orthogonal to the ideal direction. Methods have been established for defining the necessary sense axis coordinate frames [9-12].

The basic measurement model for the estimated angular rate $\hat{\boldsymbol{\omega}}(t)$ expressed in the body frame is given by

$$\hat{\boldsymbol{\omega}}(t) = (\mathbf{A}_b^{SIRU})^T \boldsymbol{\omega}_{SIRU}(t) + \hat{\mathbf{b}}(t) \tag{4}$$

where the estimate $\hat{\mathbf{b}}(t)$ comes from the filter state and $\mathbf{A}_b^{SIRU}$ is a constant reference alignment rotation from the gyro unit frame to the body frame. Effects from variations in this alignment rotation are absorbed in $\hat{\mathbf{b}}(t)$. The observed gyro unit rate $\boldsymbol{\omega}_{SIRU}(t)$ expressed in the gyro unit frame is given by

$$\mathbf{G}_{4\times 3}\boldsymbol{\omega}_{SIRU}(t) = \boldsymbol{\omega}_s(t) \tag{5}$$

where $\mathbf{G}$ is a 4×3 matrix relating the four sense axes rates $\boldsymbol{\omega}_s(t)$ to $\boldsymbol{\omega}_{SIRU}(t)$. In practice $\boldsymbol{\omega}_{SIRU}(t)$ is calculated using the pseudo-inverse of $\mathbf{G}$

$$\boldsymbol{\omega}_{SIRU}(t) = (\mathbf{G}^T\mathbf{G})^{-1}\mathbf{G}^T\boldsymbol{\omega}_s(t) \tag{6}$$

$$\mathbf{G} = (\mathbf{I} - \boldsymbol{\Lambda})(\mathbf{W} - \mathbf{U}\boldsymbol{\Delta}_{\mathbf{v}} - \mathbf{V}\boldsymbol{\Delta}_{\mathbf{u}})^T \tag{7}$$

where $\boldsymbol{\Lambda} \equiv diag(\boldsymbol{\lambda})$, $\boldsymbol{\Delta}_{\mathbf{u}} \equiv diag(\mathbf{u})$, and $\boldsymbol{\Delta}_{\mathbf{v}} \equiv diag(\mathbf{v})$. The ideal sense axes directions expressed in the gyro unit frame are the columns of $\mathbf{W}_{3\times 4}$.

The error model characterizes uncertainties expressed in the gyro unit frame. It represents the growth of attitude uncertainty during the propagation phase of the filter cycle. The error model parameters are associated with three stochastic processes. Angular white noise variance σ_{awn}^2 is simple noise and has units of radians^2. Angular random walk variance σ_{arw}^2 is linked to uncertainties over short time scales. It describes the process noise for the angular output of the gyro unit (or ideally a sense axis) and has units of radians^2/second. Rate random walk (RRW) variance σ_{rrw}^2 describes the process noise for the angular rate observed by the gyro unit (or sense axis). It has units of (radians/second)^2/second.

The error model parameters appear in the filter as process noise. As discussed in following sections, the discrete time process noise matrix block associated with the attitude and gyro rate bias estimates is give by

$$\mathbf{Q}_k(t) = \begin{bmatrix} (\sigma_{awn}^2 + t\sigma_{arw}^2 + (t^3/3)\sigma_{rrw}^2)\mathbf{I} & (t^2/2)\sigma_{rrw}^2\mathbf{I} \\ (t^2/2)\sigma_{rrw}^2\mathbf{I} & t\sigma_{rrw}^2\mathbf{I} \end{bmatrix} \tag{8}$$

It is useful to note that RRW is associated with uncertainties over longer time scales. In fact the filter uses σ_{rrw}^2 to model bias instability and the variations of $\mathbf{b}(t)$. The link between σ_{rrw}^2 and $\mathbf{b}(t)$ is apparent from their units.

3.2 Attitude Filter

The filter is based on a standard attitude filter, referred to by reference [13] as the Multiplicative Extended Kalman Filter (MEKF). The description given here follows references [13] and [14].

Two central MEKF components are the reference attitude quaternion $q_{ref}(t)$, $|q_{ref}(t)| = 1$, and the attitude error quaternion $q(\mathbf{a}(t))$, where $\mathbf{a}(t)$ is a rotation vector and $q(\mathbf{a}(t))$ is a unit-norm quaternion function of the rotation vector. We also define $a \equiv |\mathbf{a}|$. The MEKF performs unconstrained estimation of the rotation vector $\hat{\mathbf{a}}(t)$ during each measurement update phase while maintaining the overall attitude estimate in the constrained (unit-norm) nonsingular reference attitude quaternion $q_{ref}(t)$. The true attitude $q(t)$ is represented as the product

$$q(t) = q(\mathbf{a}(t)) \otimes q_{ref}(t) \tag{9}$$

The covariance of $\mathbf{a}(t)$ is the covariance of the attitude error in the body frame. The multiplication in Eq. (9) is the reason for the term Multiplicative EKF. In the standard EKF, the true state $\mathbf{X}$ is represented as the sum of a reference state $\mathbf{X}_{ref}$ and a small error $\mathbf{x}$

$$\mathbf{X} = \mathbf{x} + \mathbf{X}_{ref} \tag{10}$$

Equation (9) for the MEKF corresponds directly to Eq. (10) for the EKF when $q(\mathbf{a}) \cong [\mathbf{a}^T/2 \quad 1]^T$.

The MEKF cycle has three phases: propagation, measurement update, and reset. Reference [13] discusses the relationship between Eq. (9) and the MEKF reset phase. An analogous EKF reset phase associated with Eq. (10) is normally absorbed and implicit within the EKF measurement update phase. Before reset $q_{ref}(t)$ is the prior (predicted) estimate $q_{ref}(-)$ of the attitude. After reset $q_{ref}(t)$ is the posterior (updated) estimate. The propagation phase inherently maintains $\hat{\mathbf{a}}(t) = \mathbf{0}$. The measurement update phase assigns a finite value $\hat{\mathbf{a}}(+)$ at $\hat{\mathbf{a}}(t)$ while the reference

quaternion retains its pre-update value $q_{ref}(-)$. The update information is moved from $\hat{\mathbf{a}}(+)$ to a post-update reference $q_{ref}(+)$ and $\hat{\mathbf{a}}(t)$ is reset to zero

$$q(\hat{\mathbf{a}}(+)) \otimes q_{ref}(-) = q(\mathbf{0}) \otimes q_{ref}(+) = q_{ref}(+) \tag{11}$$

The attitude error quaternion $q(\mathbf{a}(t))$ is calculated from the attitude error rotation vector $\mathbf{a}$ as

$$q(\mathbf{a}) = \begin{bmatrix} (\mathbf{a}/a)\sin(a/2) \\ \cos(a/2) \end{bmatrix} \tag{12}$$

or the second-order approximation

$$q(\mathbf{a}) \approx \begin{bmatrix} \mathbf{a}/2 \\ 1 - a^2/8 \end{bmatrix} \tag{13}$$

The equivalent attitude error rotation matrix is

$$\mathbf{A}(\mathbf{a}) \approx \mathbf{I}_{3\times 3} - [\mathbf{a}\times] - (a^2\mathbf{I}_{3\times 3} - \mathbf{a}\mathbf{a}^{\mathbf{T}})/2 \tag{14}$$

where $[\mathbf{a}\times]\mathbf{b} \equiv \mathbf{a}\times\mathbf{b}$. In practice $q(\mathbf{a})$ is normalized to ensure it is a unit quaternion, and the attitude error rotation matrix $\mathbf{A}$ can be computed from $q(\mathbf{a})$ to ensure it is orthonormal.

3.2.1 Summary

This section is a brief summary of the MEKF and is followed by detailed discussion in the following sections. The gyro unit outputs time-tagged angular increments which are used to compute the rate vector $\boldsymbol{\omega}_g(t)$. The true rate $\boldsymbol{\omega}(t)$ is modeled by $\boldsymbol{\omega}(t) = \boldsymbol{\omega}_g(t) + \mathbf{b}(t) + \boldsymbol{\eta}_a(t)$ where $d\mathbf{b}(t)/dt = \boldsymbol{\eta}_r(t)$. The angular rate estimate is $\hat{\boldsymbol{\omega}}(t_k) = \boldsymbol{\omega}_g(t_k) + \hat{\mathbf{b}}(t_k)$ and the propagation rotation vector is given by $\mathbf{a}_p = \Delta t\hat{\boldsymbol{\omega}}(t_k)$ where the time interval $\Delta t \equiv t_{k+1} - t_k$ is short enough that $\hat{\boldsymbol{\omega}}$ is approximately constant. Attitude propagation when the assumption of approximately constant $\hat{\boldsymbol{\omega}}$ is not valid is discussed in references [15]. Attitude and state propagations are given by $q_{ref}(t_{k+1}) = q(\mathbf{a}_p) \otimes q_{ref}(t_k)$ and $\hat{\mathbf{x}}(t_{k+1}) = \hat{\mathbf{x}}(t_k)$. Covariance propagation is given by $\mathbf{P}_{k+1} = \boldsymbol{\Phi}_k \mathbf{P}_k \boldsymbol{\Phi}_k^T + \mathbf{Q}_k$.

The measurement model is

$$\mathbf{y} \equiv \mathbf{h}(\mathbf{u}) + \boldsymbol{\varepsilon} = \begin{bmatrix} u_1/u_3 \\ u_2/u_3 \end{bmatrix} + \boldsymbol{\varepsilon} \tag{14}$$

where $\boldsymbol{\varepsilon}$ is zero-mean white noise and the measurement covariance is $\mathbf{R} = \sigma_y^2\mathbf{I}$. For an observed unit vector $\mathbf{u}$ with a corresponding reference unit vector $\mathbf{u}'$ in the inertial frame, the observation residual is $\Delta\mathbf{y} \equiv \mathbf{y} - \mathbf{h}(\mathbf{A}(q_{ref})\mathbf{u}')$ and with $[\mathbf{a}\times]\mathbf{b} \equiv \mathbf{a}\times\mathbf{b}$ the sensitivity matrix is given by

$$\mathbf{H} = \begin{bmatrix} 1/u_3 & 0 & -u_1/u_3^2 \\ 0 & 1/u_3 & -u_2/u_3^2 \end{bmatrix} [\mathbf{A}(q_{ref})\mathbf{u}'\times] \tag{15}$$

After propagation of the state and covariance from t_k to t_{k+1}, the measurement update at t_{k+1} is performed using the Kalman gain $\mathbf{K} = \mathbf{P}\mathbf{H}^T(\mathbf{H}\mathbf{P}\mathbf{H}^T + \mathbf{R})^{-1}$, state correction $[\Delta\hat{\mathbf{a}}^T(t) \quad \Delta\hat{\mathbf{b}}^T(t)]^T = \mathbf{K}\Delta\mathbf{y}$, and covariance update $\mathbf{P}_+ = (\mathbf{I} - \mathbf{K}\mathbf{H})\mathbf{P}_-$. The rate bias estimate is updated by $\hat{\mathbf{b}}_+ = \hat{\mathbf{b}}_- + \Delta\hat{\mathbf{b}}$ and the attitude error estimate is moved into the reference attitude $q_{ref+} = q(\Delta\hat{\mathbf{a}}) \otimes q_{ref-}$. The IST attitude time series $\hat{\mathbf{A}}_{IST}(t_k)$ is expressed as quaternions $q_{ref}(t_k)$ or as equivalent rotation matrices as convenient. MEKF filtering of 10 Hz IST star observations with 10 Hz gyro angular rates results in arcsecond level accuracies [16].

3.2.2 Attitude and State Propagation

The angular rate and kinematics of the reference attitude q_{ref} are represented by $\boldsymbol{\omega}_{ref}$ and

$$\frac{d}{dt} q_{ref} = \frac{1}{2} \begin{bmatrix} \boldsymbol{\omega}_{ref} \\ 0 \end{bmatrix} \otimes q_{ref} \tag{16}$$

$\boldsymbol{\omega}_{ref}$ is determined by the requirements that $\hat{\mathbf{a}} = \mathbf{0}$, so that q_{ref} is the optimal attitude estimate. Taking the time derivative of Eq. (9) and using Eq. (16)

$$\frac{1}{2} \begin{bmatrix} \boldsymbol{\omega} \\ 0 \end{bmatrix} \otimes q = \frac{d}{dt} q(\mathbf{a}) \otimes q_{ref} + q(\mathbf{a}) \otimes \frac{1}{2} \begin{bmatrix} \boldsymbol{\omega}_{ref} \\ 0 \end{bmatrix} \otimes q_{ref} \tag{17}$$

$$\left(\frac{1}{2} \begin{bmatrix} \boldsymbol{\omega} \\ 0 \end{bmatrix} \otimes q(\mathbf{a}) \otimes q_{ref} \right) \otimes q_{ref}^{-1} = \left(\frac{d}{dt} q(\mathbf{a}) \otimes q_{ref} + q(\mathbf{a}) \otimes \frac{1}{2} \begin{bmatrix} \boldsymbol{\omega}_{ref} \\ 0 \end{bmatrix} \otimes q_{ref} \right) \otimes q_{ref}^{-1} \tag{18}$$

$$2\frac{d}{dt} q(\mathbf{a}) = \begin{bmatrix} \boldsymbol{\omega} \\ 0 \end{bmatrix} \otimes q(\mathbf{a}) - q(\mathbf{a}) \otimes \begin{bmatrix} \boldsymbol{\omega}_{ref} \\ 0 \end{bmatrix} \tag{19}$$

The expectation of this nonlinear function of $\mathbf{a}$ and $\boldsymbol{\omega}$ is approximated by the same nonlinear function of the expectations $\hat{\mathbf{a}}$ and $\hat{\boldsymbol{\omega}}$, as normal in extended Kalman filtering

$$2\frac{d}{dt} q(\hat{\mathbf{a}}) = \begin{bmatrix} \hat{\boldsymbol{\omega}} \\ 0 \end{bmatrix} \otimes q(\hat{\mathbf{a}}) - q(\hat{\mathbf{a}}) \otimes \begin{bmatrix} \boldsymbol{\omega}_{ref} \\ 0 \end{bmatrix} \tag{20}$$

The requirement that $\hat{\mathbf{a}} = \mathbf{0}$ means that $q(\hat{\mathbf{a}})$ is the identity quaternion $q(\hat{\mathbf{a}}) = [0 \quad 0 \quad 0 \quad 1]^T$. Substituting this into Eq. (20) gives

$$\hat{\boldsymbol{\omega}}(t) = \boldsymbol{\omega}_{ref}(t) \tag{21}$$

This demonstrates that, because the reference attitude is the attitude estimate, the reference attitude rate is the rate estimate.

The gyro unit outputs time-tagged angular increments which are used to compute the rate vector $\boldsymbol{\omega}_g(t)$. The true rate $\boldsymbol{\omega}(t)$ is modeled using $\boldsymbol{\omega}_g(t)$, a rate bias $\mathbf{b}(t)$, and zero-mean white noise processes $\boldsymbol{\eta}_a(t)$ and $\boldsymbol{\eta}_r(t)$

$$\boldsymbol{\omega}(t) = \boldsymbol{\omega}_g(t) + \mathbf{b}(t) + \boldsymbol{\eta}_a(t) \tag{22}$$

$$d\mathbf{b}(t)/dt = \boldsymbol{\eta}_r(t) \tag{23}$$

For the noise processes, $E(\boldsymbol{\eta}_a \boldsymbol{\eta}_a^{\mathrm{T}}) = \sigma_a^2 \mathbf{I}\delta(t-\tau)$ where σ_a^2 is the angular random walk variance, and $E(\boldsymbol{\eta}_r \boldsymbol{\eta}_r^{\mathrm{T}}) = \sigma_r^2 \mathbf{I}\delta(t-\tau)$ where σ_r^2 is the rate random walk variance. The sign convention in Eq. (22) follows reference [14] rather than reference [13]. The rate estimate is defined as

$$\hat{\boldsymbol{\omega}}(t) = \boldsymbol{\omega}_g(t) + \hat{\mathbf{b}}(t) = \boldsymbol{\omega}_{ref}(t) \tag{24}$$

The MEKF state vector is

$$\mathbf{x}(t) = \begin{bmatrix} \mathbf{a}(t) \\ \mathbf{b}(t) \end{bmatrix} \tag{25}$$

The expectation $\hat{\mathbf{x}}$ of the state vector is constant during the propagation phase because $\hat{\mathbf{a}} = \mathbf{0}$ and Eq. (23) implies $d\hat{\mathbf{b}}/dt = \mathbf{0}$.

The angular rate estimate is $\hat{\boldsymbol{\omega}}(t_k) = \boldsymbol{\omega}_g(t_k) + \hat{\mathbf{b}}(t_k)$ and the rotation vector is given by $\mathbf{a} = (t_{k+1} - t_k)\hat{\boldsymbol{\omega}}(t_k)$, where the time interval $t_{k+1} - t_k$ is short enough that $\hat{\boldsymbol{\omega}}$ is approximately constant. To propagate the attitude and state estimates from t_k to t_{k+1}

$$q_{ref}(t_{k+1}) = q(\mathbf{a}) \otimes q_{ref}(t_k) \tag{26}$$

$$\hat{\mathbf{x}}(t_{k+1}) = \hat{\mathbf{x}}(t_k) \tag{27}$$

Attitude propagation when the assumption of approximately constant $\hat{\boldsymbol{\omega}}$ is not valid is discussed in references [15].

3.2.3 Covariance Propagation

The MEKF covariance matrix $\mathbf{P}$ is defined by

$$\mathbf{P} \equiv E((\mathbf{x} - \hat{\mathbf{x}})(\mathbf{x} - \hat{\mathbf{x}})^{\mathrm{T}} \mid \mathbf{y}) \equiv \begin{bmatrix} \mathbf{P_a} & \mathbf{P_c} \\ \mathbf{P_c} & \mathbf{P_b} \end{bmatrix} \tag{28}$$

where the vector $\mathbf{y}$ represents star observations and $\mathbf{P}$ is partitioned into 3×3 attitude, bias, and correlation sub-matrices. The objective here is a discrete-time state transition matrix $\mathbf{\Phi}_k(\tau)$ and process noise covariance $\mathbf{Q}_k(\tau)$ to propagate $\mathbf{P}$ over the time interval $\tau = t_{k+1} - t_k$ using

$$\mathbf{P}_{k+1|k} = \mathbf{\Phi}_k \mathbf{P}_k \mathbf{\Phi}_k^T + \mathbf{Q}_k \tag{29}$$

The following derivation of the linearized state equation follows reference [14]. The time derivative of the attitude error rotation vector $d\mathbf{a}/dt$ is given by the Bortz equation

$$\frac{d\mathbf{a}}{dt} = \boldsymbol{\omega} + \frac{1}{2}\mathbf{a}\times\boldsymbol{\omega} + \frac{1}{a^2}\left(1 - \frac{a\sin a}{2(1-\cos a)}\right)\mathbf{a}\times(\mathbf{a}\times\boldsymbol{\omega}) \tag{30}$$

which for small $\mathbf{a}$ is approximated by the Bortz equation for small rotations

$$d\mathbf{a}/dt = \boldsymbol{\omega} + (\mathbf{a}\times\boldsymbol{\omega})/2 + (\mathbf{a}\times(\mathbf{a}\times\boldsymbol{\omega}))/12 \tag{31}$$

Setting aside the bias equation $d\mathbf{b}(t)/dt = \boldsymbol{\eta}_r(t)$, the state equation $\dot{\mathbf{x}} = \mathbf{f}(\mathbf{x},t)$ is

$$\begin{bmatrix}\dot{\mathbf{a}}\\ \dot{\mathbf{b}}\end{bmatrix} = \begin{bmatrix}\boldsymbol{\omega} + (\mathbf{a}\times\boldsymbol{\omega})/2 + (\mathbf{a}\times(\mathbf{a}\times\boldsymbol{\omega}))/12\\ \mathbf{0}\end{bmatrix} \tag{32}$$

The objective is to linearize the state equation about a reference trajectory $\mathbf{x}_{ref}(t)$ and form a linearized state equation $\delta\dot{\mathbf{x}} = \mathbf{F}(\mathbf{x}_{ref})\delta\mathbf{x}$ for $\delta\mathbf{x}(t) = \mathbf{x}(t) - \mathbf{x}_{ref}(t)$. Let the reference trajectory $\mathbf{x}_{ref}(t)$ be defined by the solution $\mathbf{a}_{ref}(t)$ from the Bortz equation for small rotations

$$d\mathbf{a}_{ref}/dt = \boldsymbol{\omega}_{ref} + (\mathbf{a}_{ref}\times\boldsymbol{\omega}_{ref})/2 + (\mathbf{a}_{ref}\times(\mathbf{a}_{ref}\times\boldsymbol{\omega}_{ref}))/12 \tag{33}$$

for the time interval t_k to t_{k+1}, where the reference bias is $\mathbf{b}_{ref} = \hat{\mathbf{b}}$, the reference rate is $\boldsymbol{\omega}_{ref} = \boldsymbol{\omega}_g + \mathbf{b}_{ref}$, and the initial condition is $\mathbf{a}_{ref}(t_k) = \mathbf{0}$. The second order term $\mathbf{a}_{ref}\times(\mathbf{a}_{ref}\times\boldsymbol{\omega}_{ref})$ is negligible and the reference trajectory is approximately the solution to the coning equation

$$d\mathbf{a}_{ref}/dt = \boldsymbol{\omega}_{ref} + (\mathbf{a}_{ref}\times\boldsymbol{\omega}_{ref})/2 \tag{34}$$

From the composition rule for small rotations, the rotation error $\delta\mathbf{a}(t)$ between the true $\mathbf{a}(t)$ from Eq. (31) and the reference $\mathbf{a}_{ref}(t)$ is

$$\delta\mathbf{a} = \mathbf{a}\circ(-\mathbf{a}_{ref}) \approx \mathbf{a} - \mathbf{a}_{ref} + (\mathbf{a}\times\mathbf{a}_{ref})/2 \tag{35}$$

where $\delta\mathbf{a}(t_k) = \mathbf{0}$. Differentiating this and discarding higher order terms

$$d(\delta\mathbf{a})/dt = -\boldsymbol{\omega}_{ref}\times\delta\mathbf{a} + \delta\mathbf{b} + \boldsymbol{\eta}_a \tag{36}$$

where $\delta\mathbf{b} = \mathbf{b} - \mathbf{b}_{ref}$.

Including the bias equation $d\mathbf{b}(t)/dt = \boldsymbol{\eta}_r(t)$, the linearized state equation $\delta\dot{\mathbf{x}} = \mathbf{F}\delta\mathbf{x} + \mathbf{G}\boldsymbol{\eta}$ is

$$\begin{bmatrix} \delta\dot{\mathbf{a}} \\ \delta\dot{\mathbf{b}} \end{bmatrix} = \begin{bmatrix} -[\boldsymbol{\omega}_{ref}\times] & \mathbf{I}_{3\times3} \\ \mathbf{0}_{3\times3} & \mathbf{0}_{3\times3} \end{bmatrix} \begin{bmatrix} \delta\mathbf{a} \\ \delta\mathbf{b} \end{bmatrix} + \mathbf{I}_{6\times6} \begin{bmatrix} \boldsymbol{\eta}_a \\ \boldsymbol{\eta}_r \end{bmatrix} \tag{37}$$

The discrete-time solution is

$$\delta\mathbf{x}_{k+1} = \boldsymbol{\Phi}_k \delta\mathbf{x}_k + \boldsymbol{\Gamma}_k \mathbf{w}_k \tag{38}$$

where the state transition matrix for $\tau = t_{k+1} - t_k$ is

$$\boldsymbol{\Phi}_k(\tau) = \exp(\tau \mathbf{F}(\mathbf{x}_k)) = \begin{bmatrix} \mathbf{R}(\mathbf{a}_k(\tau)) & \mathbf{S}(\mathbf{a}_k(\tau)) \\ 0 & \mathbf{I} \end{bmatrix} \tag{39}$$

and where the rotation vector $\mathbf{a}_k(\tau)$ is the solution $\mathbf{a}_{ref}(t_k + \tau)$ to Eq. (34) with initial condition $\mathbf{a}_{ref}(t_k) = \mathbf{0}$. For $\mathbf{a} = \mathbf{a}_k(\tau)$, the matrices $\mathbf{R}$ and $\mathbf{S}$ are

$$\mathbf{R}(\mathbf{a}) = (\cos a)\mathbf{I} - \left(\frac{\sin a}{a}\right)[\mathbf{a}\times] + \left(\frac{1-\cos a}{a^2}\right)\mathbf{a}\mathbf{a}^{\mathrm{T}} \tag{40}$$

$$\mathbf{S}(\mathbf{a}) = \tau\left[\left(\frac{\sin a}{a}\right)\mathbf{I} - \left(\frac{1-\cos a}{a^2}\right)[\mathbf{a}\times] + \left(\frac{a-\sin a}{a^3}\right)\mathbf{a}\mathbf{a}^{\mathrm{T}}\right] \tag{41}$$

The continuous-time process noise covariance $\mathbf{Q}(t)$ is defined by

$$\mathbf{Q}(t) = E(\boldsymbol{\eta}(t)\boldsymbol{\eta}^{\mathrm{T}}(t'))\delta(t-t') = \begin{bmatrix} \sigma_a^2\mathbf{I}_{3\times3} & \mathbf{0}_{3\times3} \\ \mathbf{0}_{3\times3} & \sigma_r^2\mathbf{I}_{3\times3} \end{bmatrix} \tag{42}$$

and the discrete-time process noise covariance $\mathbf{Q}_k(\tau)$ for $E(\boldsymbol{\eta}_k\boldsymbol{\eta}_k^T) = \mathbf{I}$ is

$$\mathbf{Q}_k(\tau) = \boldsymbol{\Gamma}_k\boldsymbol{\Gamma}_k^T = \begin{bmatrix} (\sigma_w^2 + \tau\sigma_a^2 + (\tau^3/3)\sigma_r^2)\mathbf{I} & (\tau^2/2)\sigma_r^2\mathbf{I} \\ (\tau^2/2)\sigma_r^2\mathbf{I} & \tau\sigma_r^2\mathbf{I} \end{bmatrix} \tag{43}$$

where σ_w^2 is the gyro angle white noise variance.

3.2.4 Update

For filter measurement updates, an observation $\mathbf{y}$ is defined by the measurement model $\mathbf{h}(\mathbf{u})$

$$\mathbf{y} = \mathbf{h}(\mathbf{u}) + \boldsymbol{\varepsilon} = \begin{bmatrix} h \\ v \end{bmatrix} + \boldsymbol{\varepsilon} = \begin{bmatrix} u_1/u_3 \\ u_2/u_3 \end{bmatrix} + \boldsymbol{\varepsilon} \tag{43}$$

where $\boldsymbol{\varepsilon}$ is zero-mean white noise. The measurement noise covariance matrix $\mathbf{R}$ is

$$\mathbf{R} = \begin{bmatrix} \sigma_h^2 & 0 \\ 0 & \sigma_v^2 \end{bmatrix} \tag{43}$$

where σ_h^2 and σ_v^2 are the horizontal and vertical coordinate variances.

The objective here is the measurement sensitivity matrix $\mathbf{H} = \partial\mathbf{y}/\partial\mathbf{x}$ representing the relationship of the observations to the filter states. The observations are not sensitive to the gyro rate bias, $\partial\mathbf{h}(\mathbf{u})/\partial\mathbf{b} = \mathbf{0}$. They are, however, sensitive to a change of body frame attitude represented by the rotation vector $\mathbf{a}$

$$\mathbf{H} = \begin{bmatrix} \dfrac{\partial\mathbf{h}(\mathbf{u})}{\partial\mathbf{a}} & \dfrac{\partial\mathbf{h}(\mathbf{u})}{\partial\mathbf{b}} \end{bmatrix} = \begin{bmatrix} \dfrac{\partial\mathbf{h}}{\partial\mathbf{u}}\dfrac{\partial\mathbf{u}}{\partial\mathbf{a}} & \mathbf{0} \end{bmatrix} = \frac{\partial\mathbf{h}}{\partial\mathbf{u}}\begin{bmatrix} \dfrac{\partial\mathbf{u}}{\partial\mathbf{a}} & \mathbf{0} \end{bmatrix} \tag{43}$$

where, from Eq. (43),

$$\frac{\partial\mathbf{h}}{\partial\mathbf{u}} = \begin{bmatrix} 1/u_3 & 0 & -u_1/u_3^2 \\ 0 & 1/u_3 & -u_2/u_3^2 \end{bmatrix} \tag{43}$$

To derive $\partial\mathbf{u}/\partial\mathbf{a}$, the rotation from the inertial frame to the body frame can be represented by a rotation vector $\mathbf{a}_i^b$ and equivalent rotation matrix $\mathbf{A}(\mathbf{a}_i^b)$. With the alignment rotation from the body frame to the sensor coordinate frame represented by a rotation matrix $\mathbf{R}_b^s$, the observed unit vector in the sensor coordinate frame $\mathbf{u}$ is related to the same unit vector in the inertial frame $\mathbf{u}'$ by

$$\mathbf{u} = \mathbf{R}_b^s\mathbf{A}(\mathbf{a}_i^b)\mathbf{u}' \tag{44}$$

For a reference attitude $\mathbf{A}(\mathbf{a}_i^r)$ arbitrarily close to the body attitude $\mathbf{A}(\mathbf{a}_i^b)$

$$\mathbf{A}(\mathbf{a}_i^b) = \mathbf{A}(\mathbf{a})\mathbf{A}(\mathbf{a}_i^r) = (\mathbf{I} - [\mathbf{a}\times])\mathbf{A}(\mathbf{a}_i^r) \tag{45}$$

where $\mathbf{a}$ is a small rotation vector and the first-order approximation is $\mathbf{A}(\mathbf{a}) \approx (\mathbf{I} - [\mathbf{a}\times])$. Substituting into Eq. (45)

$$\mathbf{u} = \mathbf{R}_b^s(\mathbf{I} - [\mathbf{a}\times])\mathbf{A}(\mathbf{a}_i^r)\mathbf{u}' \tag{46}$$

$$\mathbf{u} = \mathbf{R}_b^s\mathbf{A}(\mathbf{a}_i^r)\mathbf{u}' - \mathbf{R}_b^s[\mathbf{a}\times]\mathbf{A}(\mathbf{a}_i^r)\mathbf{u}' \tag{47}$$

$$\mathbf{u} = \mathbf{R}_b^s\mathbf{A}(\mathbf{a}_i^r)\mathbf{u}' + \mathbf{R}_b^s[\mathbf{A}(\mathbf{a}_i^r)\mathbf{u}'\times]\mathbf{a} \tag{48}$$

Taking the partial with respect to $\mathbf{a}$ and noting that $\mathbf{a}_i^r \to \mathbf{a}_i^b$ as $\mathbf{a} \to \mathbf{0}$

$$\left.\frac{\partial\mathbf{u}}{\partial\mathbf{a}}\right|_{\mathbf{a}=\mathbf{0}} = \mathbf{R}_b^s[\mathbf{A}(\mathbf{a}_i^b)\mathbf{u}'\times] \tag{49}$$

and substituting

$$\mathbf{H} = \begin{bmatrix} 1/u_3 & 0 & -u_1/u_3^2 \\ 0 & 1/u_3 & -u_2/u_3^2 \end{bmatrix} \mathbf{R}_b^s [\mathbf{A}(\mathbf{a}_i^b)\mathbf{u}'\times] \tag{50}$$

After propagation of the state and covariance from t_k to t_{k+1}, the measurement update at t_{k+1} is performed using the Kalman filter equations

$$\mathbf{K}_{k+1} = \mathbf{P}_{k+1|k}\mathbf{H}_{k+1}^{\mathrm{T}}(\mathbf{H}_{k+1}\mathbf{P}_{k+1|k}\mathbf{H}_{k+1}^{\mathrm{T}} + \mathbf{R}_{k+1})^{-1} \tag{51}$$

$$\begin{bmatrix} \Delta\hat{\mathbf{a}}_{k+1} \\ \Delta\hat{\mathbf{b}}_{k+1} \end{bmatrix} = \mathbf{K}_{k+1}(\mathbf{y} - \mathbf{h}(\mathbf{R}_b^s\mathbf{A}(\mathbf{a}_i^b)\mathbf{u}')) \tag{52}$$

$$\mathbf{P}_{k+1|k+1} = (\mathbf{I} - \mathbf{K}_{k+1}\mathbf{H}_{k+1})\mathbf{P}_{k+1|k} \tag{53}$$

The estimated bias error is added to the bias estimate

$$\hat{\mathbf{b}}_{k+1} = \Delta\hat{\mathbf{b}}_{k+1} + \hat{\mathbf{b}}_k \tag{54}$$

and as described above the reset phase moves the estimated attitude error information into the attitude estimate $\hat{q}(t) = q_{ref}(t)$ by multiplication

$$\hat{q}_{k+1} = q(\Delta\hat{\mathbf{a}}_{k+1}) \otimes \hat{q}_k \tag{55}$$

3.3 Alignment Filter

An alignment filter is used to simultaneously predict the measurements from all three star trackers. The measurement residuals are used to update the filter states, which represent the body frame attitude and time-varying corrections to reference alignments. The combined states represent the attitudes of all three trackers. Alignment filtering has been discussed in the literature (references [17-22]), particularly since 2000 by Pittelkau (references [23-27]).

3.3.1 Attitude, State, and Covariance

Time-varying rotation vectors $\mathbf{a}_{TRK}(t)$ representing small alignment corrections are included in the attitude models for the three trackers

$$\mathbf{A}_i^{LRS}(t) = \mathbf{A}(\mathbf{a}_{LRS}(t))\mathbf{A}_b^{LRS}\mathbf{A}_i^b(t) \tag{56}$$

$$\mathbf{A}_i^{SST1}(t) = \mathbf{A}(\mathbf{a}_{SST1}(t))\mathbf{A}_b^{SST1}\mathbf{A}_i^b(t) \tag{57}$$

$$\mathbf{A}_i^{SST2}(t) = \mathbf{A}(\mathbf{a}_{SST2}(t))\mathbf{A}_b^{SST2}\mathbf{A}_i^b(t) \tag{58}$$

where $\mathbf{A}(\mathbf{a}_{TRK}(t))$ is a rotation matrix equivalent to a rotation vector $\mathbf{a}_{TRK}(t)$, and $\mathbf{A}_b^{TRK}$ is a reference alignment.

Normally the LRS frame is identified with the body frame by holding $\mathbf{a}_{LRS}(t) \cong \mathbf{0}$. This is easily accomplished by setting the uncertainty and process noise associated with $\mathbf{a}_{LRS}(t)$ to be very small. The results is $\mathbf{A}_i^{LRS}(t) \cong \mathbf{A}_b^{LRS}\mathbf{A}_i^b(t)$. $\mathbf{a}_{LRS}(t)$ is included in the filter state here because in some circumstances it may be useful to identify one of the SSTs with the body frame instead of the LRS, by holding $\mathbf{a}_{SST1}(t) \cong \mathbf{0}$ or $\mathbf{a}_{SST2}(t) \cong \mathbf{0}$.

The state vector is

$$\mathbf{x}(t) = [\mathbf{a}(t)^T \quad \mathbf{b}(t)^T \quad \mathbf{a}_{LRS}(t)^T \quad \mathbf{a}_{SST1}(t)^T \quad \mathbf{a}_{SST2}(t)^T]^T \tag{59}$$

where $\mathbf{a}(t)$ is the attitude error rotation vector and $\mathbf{b}(t)$ is the gyro rate bias. These states are estimated sequentially using an alignment filter based on the standard attitude filter, referred to by reference [13] as the Multiplicative Extended Kalman Filter (MEKF). The description here follows references [13, 14, 24, 25].

The filter performs unconstrained estimation of $\mathbf{a}(t)$ during each measurement update phase while maintaining the overall body frame attitude estimate in the unit-norm reference attitude quaternion $q_{ref}(t)$ and $\hat{\mathbf{A}}_i^b(t) = \mathbf{A}(q_{ref}(t))$. The true attitude $q(t)$ is modeled as $q(t) = q(\mathbf{a}(t)) \otimes q_{ref}(t)$ where $q(\mathbf{a}(t))$ is a unit-norm quaternion function of the rotation vector. The measurement update phase assigns a finite value $\hat{\mathbf{a}}(+)$ to $\hat{\mathbf{a}}(t)$ while the reference quaternion retains its pre-update value $q_{ref}(-)$. The update information is moved from $\hat{\mathbf{a}}(+)$ to a post-update reference $q_{ref}(+)$ and $\hat{\mathbf{a}}(t)$ is reset to zero so that $q(\hat{\mathbf{a}}(+)) \otimes q_{ref}(-) = q(\mathbf{0}) \otimes q_{ref}(+)$.

The covariance matrix $\mathbf{P}$ is given by

$$\mathbf{P}_{15\times15} \equiv E\{(\mathbf{x}-\hat{\mathbf{x}})(\mathbf{x}-\hat{\mathbf{x}})^{\mathbf{T}}\} = \begin{bmatrix} \mathbf{P_a} & \mathbf{P_{ab}} & & & \\ \mathbf{P_{ab}} & \mathbf{P_b} & & & \\ & & \mathbf{P}_{LRS} & & \\ & & & \mathbf{P}_{SST1} & \\ & & & & \mathbf{P}_{SST2} \end{bmatrix} \tag{60}$$

where $\mathbf{P}$ is partitioned into 3×3 attitude error $\mathbf{P_a}$, gyro rate bias $\mathbf{P_b}$, correlation $\mathbf{P_{ab}}$, and alignment $\mathbf{P}_{TRK}$ sub-matrices. In the continuous-time linearized state equation given by

$$\begin{bmatrix} \dot{\boldsymbol{\delta a}} \\ \dot{\boldsymbol{\delta b}} \\ \dot{\boldsymbol{\delta a}}_{LRS} \\ \dot{\boldsymbol{\delta a}}_{SST1} \\ \dot{\boldsymbol{\delta a}}_{SST2} \end{bmatrix} = \begin{bmatrix} -[\boldsymbol{\omega}_{ref}\times] & \mathbf{I}_{3\times3} & & & & \\ \mathbf{0}_{3\times3} & \mathbf{0}_{3\times3} & & & & \\ & & \mathbf{0}_{3\times3} & & & \\ & & & \mathbf{0}_{3\times3} & & \\ & & & & \mathbf{0}_{3\times3} & \\ & & & & & \mathbf{0}_{3\times3} \end{bmatrix} \begin{bmatrix} \boldsymbol{\delta a} \\ \boldsymbol{\delta b} \\ \boldsymbol{\delta a}_{LRS} \\ \boldsymbol{\delta a}_{SST1} \\ \boldsymbol{\delta a}_{SST2} \end{bmatrix} + \mathbf{I}_{15\times15} \begin{bmatrix} \boldsymbol{\eta}_{ARW} \\ \boldsymbol{\eta}_{RRW} \\ \boldsymbol{\eta}_{LRS} \\ \boldsymbol{\eta}_{SST1} \\ \boldsymbol{\eta}_{SST2} \end{bmatrix} \tag{61}$$

the gyro rate bias $\boldsymbol{\delta b}$ and alignments $\boldsymbol{\delta a}_{LRS}$, $\boldsymbol{\delta a}_{IST}$, $\boldsymbol{\delta a}_{BST2}$ are driven by process noise alone, with $E\{\boldsymbol{\eta}_{ARW}\boldsymbol{\eta}_{ARW}^T\} = \sigma_{ARW}^2\mathbf{I}$, $E\{\boldsymbol{\eta}_{RRW}\boldsymbol{\eta}_{RRW}^T\} = \sigma_{RRW}^2\mathbf{I}$, $E\{\boldsymbol{\eta}_{LRS}\boldsymbol{\eta}_{LRS}^T\} = \sigma_{LRS}^2\mathbf{I}$, $E\{\boldsymbol{\eta}_{SST1}\boldsymbol{\eta}_{SST1}^T\} = \sigma_{SST1}^2\mathbf{I}$, $E\{\boldsymbol{\eta}_{SST2}\boldsymbol{\eta}_{SST2}^T\} = \sigma_{SST2}^2\mathbf{I}$. The discrete-time process noise matrix for a propagation interval $t \equiv t_{k+1} - t_k$ is given by

$$\mathbf{Q}_k(t) = \begin{bmatrix} (\sigma_{AWN}^2 + t\sigma_{ARW}^2 + (t^3/3)\sigma_{RRW}^2)\mathbf{I} & (t^2/2)\sigma_{RRW}^2\mathbf{I} & & & & \\ (t^2/2)\sigma_{RRW}^2\mathbf{I} & t\sigma_{RRW}^2\mathbf{I} & & & & \\ & & t\sigma_{LRS}^2\mathbf{I} & & & \\ & & & t\sigma_{SST1}^2\mathbf{I} & & \\ & & & & t\sigma_{SST2}^2\mathbf{I} & \end{bmatrix} \tag{62}$$

Parameter estimates for the alignment process noises $\sigma_{LRS}, \sigma_{SST1}, \sigma_{SST2}$ are discussed in a following section.

3.3.2 Propagation

The gyro unit outputs time-tagged angular increments which are used to compute the rate vector $\boldsymbol{\omega}_g(t)$. The true rate $\boldsymbol{\omega}(t)$ is modeled by $\boldsymbol{\omega}(t) = \boldsymbol{\omega}_g(t) + \mathbf{b}(t) + \boldsymbol{\eta}_{ARW}(t)$ where $d\mathbf{b}(t)/dt = \boldsymbol{\eta}_{RRW}(t)$. The angular rate estimate is $\hat{\boldsymbol{\omega}}(t_k) = \boldsymbol{\omega}_g(t_k) + \hat{\mathbf{b}}(t_k)$ and the propagation rotation vector is $\mathbf{a}_p = t\hat{\boldsymbol{\omega}}(t_k)$ where the time interval $t \equiv t_{k+1} - t_k$ is short enough that $\hat{\boldsymbol{\omega}}$ is approximately constant. Attitude propagation when the assumption of approximately constant $\hat{\boldsymbol{\omega}}$ is not valid is discussed in reference [15]. The propagated attitude estimate and state are $q_{ref}(t_{k+1}) = q(\mathbf{a}_p) \otimes q_{ref}(t_k)$ and $\hat{\mathbf{x}}_{k+1} = \hat{\mathbf{x}}_k$.

The discrete-time state transition matrix is given by

$$\boldsymbol{\Phi}_k(t) = \begin{bmatrix} \mathbf{R}(\mathbf{a}_p) & \mathbf{S}(\mathbf{a}_p) & & & & \\ \mathbf{0}_{3\times3} & \mathbf{I}_{3\times3} & & & & \\ & & \mathbf{I}_{3\times3} & & & \\ & & & \mathbf{I}_{3\times3} & & \\ & & & & \mathbf{I}_{3\times3} & \end{bmatrix} \tag{63}$$

$$\mathbf{R}(\mathbf{a}) = (\cos a)\mathbf{I} - \left(\frac{\sin a}{a}\right)[\mathbf{a}\times] + \left(\frac{1-\cos a}{a^2}\right)\mathbf{a}\mathbf{a}^{\mathbf{T}} \tag{64}$$

$$\mathbf{S}(\mathbf{a}) = t\left[\left(\frac{\sin a}{a}\right)\mathbf{I} - \left(\frac{1-\cos a}{a^2}\right)[\mathbf{a}\times] + \left(\frac{a-\sin a}{a^3}\right)\mathbf{a}\mathbf{a}^{\mathbf{T}}\right] \tag{65}$$

and the propagated covariance is $\mathbf{P}_{k+1} = \mathbf{\Phi}_k \mathbf{P}_k \mathbf{\Phi}_k^T + \mathbf{Q}_k$.

3.3.3 Update

The input to a measurement update phase consists of one or more observed star unit vectors $\mathbf{u}$ in an $\mathbf{i,j,k}$ sensor coordinate frame with the $\mathbf{k}$ axis along the LOS and the $\mathbf{i,j}$ axes in the focal plane. The star unit vectors are expressed in h, v coordinates using Eqs. (1) and (2). The measurement model $\mathbf{h}(\mathbf{u})$ is given by

$$\mathbf{y} = \mathbf{h}(\mathbf{u}) + \mathbf{\eta}_y = \begin{bmatrix} h \\ v \end{bmatrix} + \mathbf{\eta}_y = \begin{bmatrix} u_1/u_3 \\ u_2/u_3 \end{bmatrix} + \mathbf{\eta}_y \tag{66}$$

where the measurement covariance $\mathbf{R} = E\{\mathbf{\eta}_y \mathbf{\eta}_y^T\} = \sigma_y^2 \mathbf{I}$. The jth sensor attitude is $\mathbf{A}_i^j(t) = \mathbf{A}(\mathbf{a}_j(t))\mathbf{A}_b^j \mathbf{A}_i^b(t)$ and the measurement residuals are $\Delta\mathbf{y} \equiv \mathbf{y} - \mathbf{h}(\mathbf{A}(\mathbf{a}_j(t))\mathbf{A}_b^j \mathbf{A}_i^b(t)\mathbf{u}')$ where $\mathbf{u}'$ is a reference unit vector in the inertial frame.

The measurement sensitivity matrix representing the relationship of the observations to the filter states is

$$\mathbf{H} = \frac{\partial \mathbf{y}}{\partial \mathbf{x}} = \frac{\partial \mathbf{h}}{\partial \mathbf{u}}\frac{\partial \mathbf{u}}{\partial \mathbf{x}} = \frac{\partial \mathbf{h}}{\partial \mathbf{u}}\left[\frac{\partial \mathbf{u}}{\partial \mathbf{a}} \quad \mathbf{0} \quad \frac{\partial \mathbf{u}}{\partial \mathbf{a}_{LRS}} \quad \frac{\partial \mathbf{u}}{\partial \mathbf{a}_{SST1}} \quad \frac{\partial \mathbf{u}}{\partial \mathbf{a}_{SST2}}\right] \tag{67}$$

where from Eq. (43)

$$\frac{\partial \mathbf{h}}{\partial \mathbf{u}} = \begin{bmatrix} 1/u_3 & 0 & -u_1/u_3^2 \\ 0 & 1/u_3 & -u_2/u_3^2 \end{bmatrix} \tag{68}$$

The factors $\partial\mathbf{u}/\partial\mathbf{a}$ and $\partial\mathbf{u}/\partial\mathbf{a}_j$ represent the sensitivity of star unit vectors to body frame attitude and jth sensor alignment variations. Their derivation here follows references [24, 25].

For $\partial\mathbf{u}/\partial\mathbf{a}$ the jth alignment is held constant and absorbed in $\mathbf{A}_b^j$. For a reference attitude $\mathbf{A}_i^r(t)$ arbitrarily close to $\mathbf{A}_i^b(t)$ and a small attitude error rotation vector $\mathbf{a}$ with the first-order approximation $\mathbf{A}(\mathbf{a}) \approx (\mathbf{I} - [\mathbf{a}\times])$, the attitude is modeled as $\mathbf{A}_i^b(t) = (\mathbf{I} - [\mathbf{a}\times])\mathbf{A}_i^r(t)$. Observed and reference unit vectors are related by $\mathbf{u} = \mathbf{A}_b^j \mathbf{A}_i^b(t)\mathbf{u}'$ and substitution gives

$$\mathbf{u} = \mathbf{A}_b^j \mathbf{A}_i^r(t)\mathbf{u}' - \mathbf{A}_b^j[\mathbf{a}\times]\mathbf{A}_i^r(t)\mathbf{u}' \tag{69}$$

$$\mathbf{u} = \mathbf{A}_b^j \mathbf{A}_i^r(t)\mathbf{u}' + \mathbf{A}_b^j[\mathbf{A}_i^r(t)\mathbf{u}'\times]\mathbf{a} \tag{70}$$

$$\partial\mathbf{u}/\partial\mathbf{a} = \mathbf{A}_b^j[\mathbf{A}_i^b(t)\mathbf{u}'\times] \tag{71}$$

for $\mathbf{a}_i^r \to \mathbf{a}_i^b$ as $\mathbf{a} \to \mathbf{0}$.

For $\partial\mathbf{u}/\partial\mathbf{a}_j$ with a reference alignment $\mathbf{A}_b^r$ arbitrarily close to $\mathbf{A}_b^j$ and the approximation $\mathbf{A}(\mathbf{a}_j) \approx (\mathbf{I} - [\mathbf{a}_j\times])$, the *j*th sensor alignment is modeled as $\mathbf{A}(\mathbf{a}_j)\mathbf{A}_b^r = (\mathbf{I} - [\mathbf{a}_j\times])\mathbf{A}_b^r$. Observed and reference unit vectors are related by $\mathbf{u} = \mathbf{A}(\mathbf{a}_j)\mathbf{A}_b^r\mathbf{A}_i^b(t)\mathbf{u}'$ and substitution gives

$$\mathbf{u} = \mathbf{A}_b^r\mathbf{A}_i^b(t)\mathbf{u}' - [\mathbf{a}_j\times]\mathbf{A}_b^r\mathbf{A}_i^b(t)\mathbf{u}' \tag{72}$$

$$\mathbf{u} = \mathbf{A}_b^r\mathbf{A}_i^b(t)\mathbf{u}' + [\mathbf{A}_b^r\mathbf{A}_i^b(t)\mathbf{u}'\times]\mathbf{a}_j \tag{73}$$

$$\partial\mathbf{u}/\partial\mathbf{a}_j = [\mathbf{A}_b^j\mathbf{A}_i^b(t)\mathbf{u}'\times] \tag{74}$$

for $\mathbf{a}_b^r \to \mathbf{a}_b^j$ as $\mathbf{a}_j \to \mathbf{0}$.

After propagation of the state and covariance from t_k to t_{k+1} the measurement update at t_{k+1} is performed using the Kalman gain $\mathbf{K} = \mathbf{P}\mathbf{H}^T(\mathbf{H}\mathbf{P}\mathbf{H}^T + \mathbf{R})^{-1}$, estimated state correction

$$\Delta\hat{\mathbf{x}} = [\Delta\hat{\mathbf{a}}^T \quad \Delta\hat{\mathbf{b}}^T \quad \Delta\hat{\mathbf{a}}_{LRS}^T \quad \Delta\hat{\mathbf{a}}_{SST1}^T \quad \Delta\hat{\mathbf{a}}_{SST2}^T]^T = \mathbf{K}\Delta\mathbf{y} \tag{75}$$

and covariance update $\mathbf{P}_+ = (\mathbf{I} - \mathbf{K}\mathbf{H})\mathbf{P}_-$. The rate bias estimate is updated by $\hat{\mathbf{b}}_+ = \hat{\mathbf{b}}_- + \Delta\hat{\mathbf{b}}$ and the attitude error estimate is moved into the reference attitude $q_{ref+} = q(\Delta\hat{\mathbf{a}}) \otimes q_{ref-}$. The sensor alignments are updated by $\hat{\mathbf{a}}_{LRS+} = \hat{\mathbf{a}}_{LRS-} + \Delta\hat{\mathbf{a}}_{LRS}$, $\hat{\mathbf{a}}_{SST1+} = \hat{\mathbf{a}}_{SST1-} + \Delta\hat{\mathbf{a}}_{SST1}$, and $\hat{\mathbf{a}}_{SST2+} = \hat{\mathbf{a}}_{SST2-} + \Delta\hat{\mathbf{a}}_{SST2}$.

3.3.4 Alignment Process Noise

Multiple-Model Adaptive Estimation (MMAE) is used to estimate alignment process noise values $\sigma_{LRS}, \sigma_{SST1}, \sigma_{SST2}$ by testing a set of candidates. Each candidate is implemented in its own filter H_i and the set of candidates form a filter bank $H_i; i = 1,...,n$. Simulated measurements are input to the filter bank and the results are compared with simulation truth to select the best candidate. The description here follows reference [28].

The simulation represents a sensor frame as a rotation $\mathbf{A}_i^{TRK}(t) = \mathbf{A}(\mathbf{a}_{TRK}(t))\mathbf{A}_i^r(t)$ where $\mathbf{A}_i^r(t)$ is a reference attitude and $\mathbf{A}(\mathbf{a}_{TRK}(t))$ is a rotation matrix equivalent to a small alignment rotation vector $\mathbf{a}_{TRK}(t)$. $\mathbf{A}_i^r(t)$ includes the orbital rate of 223 arcseconds per second for motion of the stars through the sensor field of view. The simulation state $\mathbf{x}(t)$ is the sensor alignment $\mathbf{a}_{TRK}(t)$ and includes a sinusoidal orbital variation

$$\mathbf{x}(t) \equiv \mathbf{a}_{TRK}(t) = [a\sin(2\pi t / t_p + \theta_0) \quad 0 \quad 0]^T \tag{76}$$

with amplitude a, a period t_p equal to the orbital period ($t_p = 5790$ seconds), and a random initial phase θ_0. The sensor alignment is driven by zero-mean Gaussian noise $E\{\boldsymbol{\eta}_{TRK}\boldsymbol{\eta}_{TRK}^T\} = \sigma_{TRK}^2\mathbf{I}$ and the continuous-time state equation is $\boldsymbol{\delta}\dot{\mathbf{x}} = \boldsymbol{\eta}_{TRK}$. Filter propagation over an interval $t \equiv t_{k+1} - t_k$ is given by $\hat{\mathbf{x}}_{k+1} = \hat{\mathbf{x}}_k$, $\mathbf{Q}_k = t\sigma_{TRK}^2\mathbf{I}$, and $\mathbf{P}_{k+1} = \mathbf{P}_k + \mathbf{Q}_k$. Measurement updates are performed as in Section IIIC except for the sensitivity matrix which reduces to

$$\mathbf{H} = \frac{\partial \mathbf{y}}{\partial \mathbf{x}} = \frac{\partial \mathbf{h}}{\partial \mathbf{u}}\frac{\partial \mathbf{u}}{\partial \mathbf{x}} = \frac{\partial \mathbf{h}}{\partial \mathbf{u}}\frac{\partial \mathbf{u}}{\partial \mathbf{a}_{TRK}} \tag{77}$$

After propagation of the state and covariance from t_k to t_{k+1} the measurement update at t_{k+1} is performed using the Kalman gain $\mathbf{K} = \mathbf{P}\mathbf{H}^T(\mathbf{H}\mathbf{P}\mathbf{H}^T + \mathbf{R})^{-1}$, estimated state correction $\Delta\hat{\mathbf{x}} = \Delta\hat{\mathbf{a}}_{TRK} = \mathbf{K}\Delta\mathbf{y}$, and covariance update $\mathbf{P}_+ = (\mathbf{I} - \mathbf{K}\mathbf{H})\mathbf{P}_-$.

The measurement probability for a candidate and filter bank member H_i is given by

$$P(\mathbf{y}_k \mid H_i) = (2\pi)^{-m/2} \mid \mathbf{S}_k \mid^{-1/2} \exp(-\Delta\mathbf{y}_k^T\mathbf{S}_k^{-1}\Delta\mathbf{y}_k / 2) \tag{78}$$

where $\mathbf{S}_k = \mathbf{H}_k\mathbf{P}_k\mathbf{H}_k^T + \mathbf{R}_k$ and m is the number of filter states. At the beginning of a simulation each of the H_i are assigned the same probability $P_0(H_i) = n^{-1}$ of being the best. The probabilities are updated at each filter measurement update by

$$P_k(H_i) = \frac{P(\mathbf{y}_k \mid H_i)P_{k-1}(H_i)}{\sum_{j=1}^{n} P(\mathbf{y}_k \mid H_j)P_{k-1}(H_j)} \tag{79}$$

If a $P_k(H_i)$ approaches 1 as t_k increases, it is evidence that the associated filter H_i and candidate are the most correct.

Two cases are considered here with simulated alignment variation amplitudes $a_1 = 2$ and $a_2 = 10$ arcseconds. In both cases seven candidates and filter bank members $H_i; i = 1,...,7$ are tested. The candidate values associated with the H_i are shown in the columns 2 and 4 of Table 2.

Table 2 MMAE results for alignment process noise σ_{TRK}

	a_1 = 2, arcsec		a_2 = 10, arcsec	
	σ_{TRK}, arcsec/sec$^{1/2}$	$P(H_i)$	σ_{TRK}, arcsec/sec$^{1/2}$	$P(H_i)$
H_1	.002	0	.015	0

H_2	.005	0	.02	0
H_3	.007	0	.025	0.001
H_4	.01	1	.03	0.985
H_5	.015	0	.035	0.014
H_6	.02	0	.04	0
H_7	.025	0	.045	0

The final hypothesis probabilities $P(H_i)$ are used to select the best candidates: $\sigma_{TRK} = 0.01$ arcsec/sec$^{1/2}$ and $\sigma_{TRK} = 0.03$ arcsec/sec$^{1/2}$.

3.4 Batch Least Squares Differential Correction

Estimation of the gyro rate bias is an essential step in using the SIRU output. A batch least squares method provides an alternative to sequential filtering. This description of batch least squares differential correction follows reference [29].

A time series of attitude estimates $\hat{\mathbf{A}}(t_i)$ is computed by propagating an initial attitude $\hat{\mathbf{A}}(t_0)$ forward in time using $\boldsymbol{\omega}_g(t)$ and $\hat{\mathbf{b}}(t_0)$. The angular rate is $\hat{\boldsymbol{\omega}}(t_i) = \mathbf{A}_g^b \boldsymbol{\omega}_g(t_i) + \hat{\mathbf{b}}(t_0)$ and the rotation vector is given by $\mathbf{a} = (t_{i+1} - t_i)\hat{\boldsymbol{\omega}}(t_i)$, where the time interval is short enough that $\hat{\boldsymbol{\omega}}$ is approximately constant. Propagation is performed using

$$\hat{\mathbf{A}}(t_{i+1}) = \mathbf{R}(t_{i+1}, t_0)\hat{\mathbf{A}}(t_0) \tag{80}$$

where the state transition sub-matrix $\mathbf{R}(t_{i+1}, t_0)$ is computed recursively beginning with $\mathbf{R}(t_0, t_0) = \mathbf{I}_{3\times 3}$

$$\mathbf{R}(t_{i+1}, t_0) = \mathbf{R}(t_{i+1}, t_i)\mathbf{R}(t_i, t_0) = \mathbf{R}(\mathbf{a})\mathbf{R}(t_i, t_0) \tag{81}$$

and $\mathbf{R}(\mathbf{a})$ is defined in Eq. (40). The $\mathbf{R}$ matrices must be orthonormal rotation matrices. This can be ensured by converting to a quaternion, normalizing, and converting back to a rotation matrix. The state transition sub-matrix $\mathbf{S}(t_{i+1}, t_0)$ is also computed recursively beginning with $\mathbf{S}(t_0, t_0) = \mathbf{0}_{3\times 3}$

$$\mathbf{S}(t_{i+1}, t_0) = \mathbf{S}(t_{i+1}, t_i) + \mathbf{R}(t_{i+1}, t_i)\mathbf{S}(t_i, t_0) = \mathbf{S}(\mathbf{a}) + \mathbf{R}(\mathbf{a})\mathbf{S}(t_i, t_0) \tag{82}$$

where $\mathbf{S}(\mathbf{a})$ is defined in Eq. (41) for $\tau = t_{i+1} - t_i$.

The gyro propagated attitudes $\hat{\mathbf{A}}(t_i)$ are used to compute predictions of the star observations. For a star observation $\mathbf{y}_i$ with an observed vector $\mathbf{u}$ in the tracker coordinate frame and a catalog vector $\mathbf{u}'$ in the celestial coordinate frame, the predicted vector in the tracker coordinate frame is $\mathbf{u}'' = \hat{\mathbf{A}}(t_i)\mathbf{u}'$. The measurement noise variance for $\mathbf{y}_i$ is σ_i^2 and the effective observation is the residual $\Delta\mathbf{y}_i = \mathbf{y}_i - \mathbf{h}(\mathbf{u}_i'')$.

The correction vector is $\Delta\hat{\mathbf{x}} \equiv [\Delta\hat{\mathbf{a}}^{\mathbf{T}} \quad \Delta\hat{\mathbf{b}}^{\mathbf{T}}]^{\mathbf{T}}$ and the observation residual is $\Delta\mathbf{y}_i \equiv \mathbf{H}_i\Delta\hat{\mathbf{x}} + \boldsymbol{\varepsilon}_i$ where the measurement sensitivity is

$$\mathbf{H}_i = \begin{bmatrix} 1/u_3 & 0 & -u_1/u_3^2 \\ 0 & 1/u_3 & -u_2/u_3^2 \end{bmatrix} [\mathbf{u}_i \times] [\mathbf{R}(t_i, t_0) \quad \mathbf{S}(t_i, t_0)] \tag{83}$$

The least squares solution minimizing the sum of the squares of $\boldsymbol{\varepsilon}_i$ is

$$\Delta\hat{\mathbf{x}} = \left(\sum_{i=1}^{n} \sigma_i^{-2} \mathbf{H}_i^T \mathbf{H}_i \right)^{-1} \sum_{i=1}^{n} \sigma_i^{-2} \mathbf{H}_i^T \Delta\mathbf{y}_i \tag{84}$$

To end each iteration the corrections are applied using $\hat{\mathbf{b}}(t_0)_+ = \hat{\mathbf{b}}(t_0)_- + \Delta\hat{\mathbf{b}}$ and $\hat{\mathbf{A}}(t_0)_+ = \mathbf{R}(\Delta\hat{\mathbf{a}})\hat{\mathbf{A}}(t_0)_-$.

Since all of the observations in batch differential correction are transitioned backwards in time to t_0, time as a variable and information about variations with respect to time are deemphasized. The useful result here is a single point $\hat{\mathbf{b}}(t_0)$ representing a cluster of observations at t_0 and it is natural to interpret this point as a type of expected or mean value given the observations.

3.5 Attitude Filter Uncertainty Estimates

The following discussion of attitude filter uncertainties follows reference [16]. The term attitude observer is used interchangeably with the term attitude filter. Here the filter is assumed to be made up of three decoupled single-axis observers and the discussion focuses on one axis.

Single-axis star tracker measurements y are modeled in continuous time as

$$y = \theta + v \tag{85}$$

where θ is a small angle in the instrument coordinate frame and v is zero-mean white Gaussian noise $E\{v(t)v(t+\tau)\} = r\delta(\tau)$. The units of r are $rad^2 / Hz = rad^2 s$. In discrete time with star tracker measurement updates every Δ seconds

$$r = \Delta\sigma_{nea}^2 / N \tag{86}$$

where σ_{nea} is the 1σ noise equivalent angle in radians per star measured, and N is the number of stars per update.

Single-axis gyro measurements ω_g are modeled as

$$\omega = \omega_g + b + n_1 \tag{87}$$

$$\dot{b} = n_2 \tag{88}$$

where ω is the true rate and b is the gyro bias. The two zero-mean white Gaussian noise terms n_1 and n_2 represent angular random walk and rate random walk, with $E\{n_1(t)n_1(t+\tau)\} = q_1\delta(\tau)$ and $E\{n_2(t)n_2(t+\tau)\} = q_2\delta(\tau)$. The units of n_1 and n_2 are $rad/s^{1/2}$ and $rad/s^{3/2}$, and the units of q_1 and q_2 are rad^2/s and rad^2/s^3.

For the single-axis observer, the state $\mathbf{x}$ is the angle θ and gyro bias b, $\mathbf{x} = [\theta \quad b]^T$. The state error $\boldsymbol{\varepsilon}$ is the difference between the true and estimated states

$$\boldsymbol{\varepsilon} = \mathbf{x} - \hat{\mathbf{x}} \tag{89}$$

and the error covariance is

$$\mathbf{P} = E\{\mathbf{x}\mathbf{x}^{\mathbf{T}}\} = \begin{bmatrix} p_{11} & p_{12} \\ p_{12} & p_{22} \end{bmatrix} \tag{90}$$

The angle error covariance p_{11} represents the uncertainty in the attitude. Reference [16] demonstrates that if the observer uses the standard Kalman filter gain calculations and is in steady-state, so that $\dot{\mathbf{P}} = \mathbf{0}$, then

$$p_{11} = r^{1/2}(q_1 + 2\sqrt{q_2 r})^{1/2} \tag{91}$$

This variance describes the steady-state attitude error in terms of the star tracker and gyro unit characteristics alone. The current geolocation error budget (released July 31, 2012) allocates 2.9 microradians 1σ for attitude determination error in PPD. This can be interpreted as the highest allowable value for $\sqrt{p_{11}}$.

For the LRS, $\Delta = 0.1$ seconds and $\sigma_{nea} = 16.8$ microradians. The number of stars per measurement update N is variable and its probability distribution is not yet known. A mean value $N = 3.5$ is specified in the geolocation error budget. For the SIRU, based on documentation from OSC $n_1 = 4.3633E-8 \ rad/s^{1/2}$ and $n_2 = 2.4241E-11 \ rad/s^{3/2}$. Figure 1 shows $\sqrt{p_{11}}$ from Equation (91) for a range of N values on the horizontal axis. The plotted curves are for σ_{nea} values of 5, 10, 15, 20, and 25 microradians.

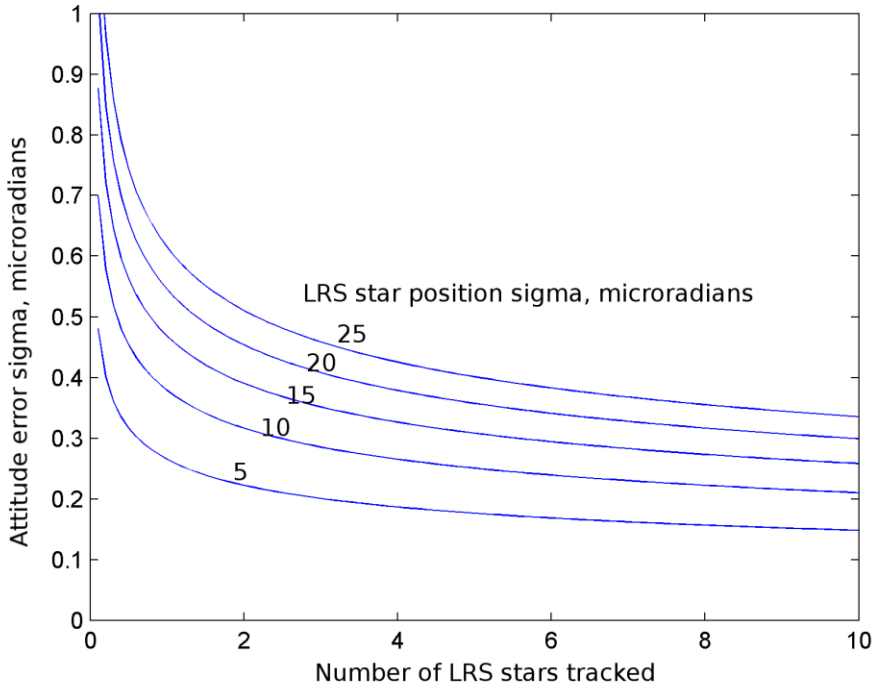

Figure 1. PPD filter attitude uncertainty as a function of the number of LRS stars tracked, and LRS star measurement errors.

Figure 1 demonstrates that when the LRS is tracking stars so that N is greater than zero, the filter attitude error is significantly less than 2.9 microradians.

4.0 Implementation

Processing is based on observing the laser pointing vectors in the LRS coordinate frame while estimating the LRS attitude relative to the celestial reference frame. The processor is closely related to the ICESat-1 processor, which also centered on an LRS to tie laser pointing to the celestial reference frame. This heritage means that many of the methods are mature and that their complexities are understood. The focus of this implementation section is on the unique characteristics of the sensors within the context of the processor.

4.1 Star Passes and the Mission Catalog

This section discusses the use of information from star observations at the level of individual unique stars (Sirius, Polaris, etc), their mission catalog records, and adaptive aspects of processing as a star passes through the LRS field of view. This is a higher-level perspective than the discussion of 10 Hz star tracker measurements from telemetry in the next section (Section 4.2) and is intended to provide a wider context for using stars in alignment and attitude filtering.

The mission catalog is tied to the LRS star tracker alone and can also be referred to as the LRS catalog. The spacecraft star trackers are completely independent from the mission catalog. They are effectively black boxes containing their own manufacturer defined catalogs which have no relation to the mission catalog.

The plural term mission catalogs could be used here since there are at least two significant catalogs: one onboard the spacecraft for real-time attitude control, and one for ground-based processing. There will also be multiple versions of both of these catalogs as revisions and improvements are made over the life of the mission. The most recent version of the mission catalog for ground processing is the topic here unless noted otherwise.

The mission catalog contains reference parameters (star positions and instrument magnitudes) compiled specifically for interpreting the LRS star tracker telemetry. Significant sources for this information are the LRS Team Catalog (LRSTC), the NASA SKY2000 star tracker catalog, and flight data from LRS telemetry.

The catalog reflects what the LRS actually sees on the sky based on prelaunch night-sky test results, analytic methods using astronomical data and flight data from other missions, and LRS flight data after launch. It describes the apparent sky for the LRS, not the true sky. Catalog records correspond to the observed objects that the LRS acquires and tracks, not individual true astronomical objects. For example a binary star system that is acquired and tracked as a single

object by the LRS has a single record with parameters describing the location and brightness of the measured object, not separate records for both true objects in the binary system. Such cases and their corresponding records in the catalog are also referred to as blended objects or blended stars [1-4, 30-32].

An important question is whether the catalog includes all of the observed objects that the LRS can acquire. If the catalog has one record for each observed object it is an adequate representation of the apparent sky seen by the LRS.

4.1.1 Terminology and Conventions

The term star is used here for an object observed crossing the field of view. The set of observations is termed a star pass or simply a pass. The situation is more complex in a small fraction of cases but this terminology is convenient because most of the tracked objects are in fact astronomical point sources. With these conventions a star can be a transient (dust particle, cosmic ray, satellite, etc) moving with a unique velocity across the field of view, or an object that is acquired, lost, and reacquired as it crosses the field of view. The object is still termed a star and the observations from multiple acquisitions make up a single pass.

The principal here is that the word star is simply a generic term for an object tracked by a star tracker or star sensor. The focus is on the information content. If a star is actually a dust particle the information content is low and it should be classed as a bad star and rejected. If the star is truly an astronomical point source but the sensor observations are biased by nearby astronomical sources then the information content is higher but still problematic and the bias should either be corrected (preferably via the mission catalog record for the star) or rejected. Only when the star is an astronomical point source with unbiased sensor observations is the information sufficient to perform a filter update.

The set of observations comprising a star pass is determined sequentially: if two sequential observations are nearby in space and time and have similar brightness values then they are the same star. Time gaps between observations can introduce complexity but the predictable ICESat motion and relatively high observation rate mean that linking star pass observations is not a practical problem.

4.1.2 Initial Checks

Several initial checks are performed to reject invalid stars. Every observation includes two binary flags set by the LRS: a trackstat bit, and a quality bit. A star pass is strictly defined to consist

only of observations with both binary flags set indicating valid tracking and full accuracy. In principal an otherwise good astronomical point source can be acquired and tracked by the LRS but be rejected because of insufficient observations with the quality bit set. This can happen in practice for a star that is only marginally bright enough for the LRS to track. The LRS acquires the star and makes observations with the trackstat bit set but the accuracy is low and the quality bit is not set.

An initial check is also made of star velocity across the field of view, calculated from two or more observations using two-dimensional x, y pixel coordinates or h, v coordinates (Section 4.2.1). The velocity should be consistent with other stars in the field of view (or recently in the field of view) and with the estimated angular rate. Stars with inconsistent velocities are rejected as transients.

4.1.3 Residuals

When a new star is observed at least two decisions have to be made: which mission catalog record is associated with the star, and should the pass observations be accepted for performing filter updates. These questions are answered as early in the pass as possible and ideally used for all of the following pass observations. In practice, additional decisions to accept individual observations are also made sequentially throughout the pass.

Identification and assessment are both based on residuals representing the differences between predicted and observed unit vectors. Residuals can be expressed in various forms, for example a scalar angular separation or a three-dimensional vector difference. Here they are defined to be the two-component vector difference $\Delta\mathbf{u}$ between predicted and observed unit vectors expressed in h, v coordinates (Section 4.2.1).

The predicted unit vector $\mathbf{u}_{pred}$ is based on the reference unit vector $\mathbf{u}_{ref}$ from the mission catalog, the estimated attitude $\mathbf{A}_i^b(t)$, and the estimated LRS alignment $\mathbf{A}_b^{LRS}(t)$. Normally the LRS frame (LRS star tracker frame) is identified with the body frame by holding $\mathbf{A}_b^{LRS}(t)$ approximately constant so that

$$\mathbf{u}_{pred} = \mathbf{A}_b^{LRS}\mathbf{A}_i^b(t)\mathbf{u}_{ref} \tag{92}$$

and $\mathbf{u}_{pred}$ depends on the mission catalog $\mathbf{u}_{ref}$ and attitude estimate $\mathbf{A}_i^b(t)$ alone. This demonstrates the central role of the mission catalog. To identify a star, the catalog is searched for nearby candidates using the method discussed in Section 4.1.8. Residuals are calculated for each candidate and the candidates are assessed using the adaptive criteria discussed in Section 4.1.5.

For the predicted unit vector

$$\mathbf{u}_{pred} = [u_{pred,1} \quad u_{pred,2} \quad u_{pred,3}]^T = [h_{pred} \quad v_{pred}]^T \tag{93}$$

and the observed unit vector

$$\mathbf{u}_{obs} = [u_{obs,1} \quad u_{obs,2} \quad u_{obs,3}]^T = [h_{obs} \quad v_{obs}]^T \tag{94}$$

the residual is given by

$$\Delta\mathbf{u}_{LRS} = [\Delta h \quad \Delta v]^T = [h_{obs} - h_{pred} \quad v_{obs} - v_{pred}]^T \tag{95}$$

This residual is expressed in the LRS frame and is also the information needed for estimating deterministic corrections to the LRS star tracker measurement model (Section 4.2.4).

A body frame residual $\Delta\mathbf{u}_{body}$ and celestial frame residual $\Delta\mathbf{u}_{ICRF}$ are computed along with $\Delta\mathbf{u}_{LRS}$. The $\Delta\mathbf{u}_{body}$ can be directly correlated with attitude and sensor alignment variations. The $\Delta\mathbf{u}_{ICRF}$ from multiple passes of a particular star can be combined for statistical analysis of bias and noise characteristics for improving the star's mission catalog record.

To compute $\Delta\mathbf{u}_{body}$ the predicted unit vector is

$$(\mathbf{u}_{pred})_{body} = \mathbf{A}_i^b(t)\mathbf{u}_{ref} \tag{96}$$

And the observed unit vector is

$$(\mathbf{u}_{obs})_{body} = (\mathbf{A}_b^{LRS})^T(\mathbf{u}_{obs})_{LRS} \tag{97}$$

These two unit vectors are expressed as h, v coordinates in a local tangent plane frame. The $\mathbf{i}, \mathbf{j}, \mathbf{k}$ axes of the local tangent plane frame are constructed based on the spacecraft frame $\mathbf{x}$ axes (the centerline from the spacecraft through the science instrument) and $(\mathbf{u}_{pred})_{body}$

$$\mathbf{i} = \mathbf{k} \times \mathbf{j} \tag{98}$$

$$\mathbf{j} = \mathbf{x} \times (\mathbf{u}_{pred})_{body} = [1 \quad 0 \quad 0]^T \times (\mathbf{u}_{pred})_{body} \tag{99}$$

$$\mathbf{k} = (\mathbf{u}_{pred})_{body} \tag{100}$$

The body frame residual is given by

$$\Delta\mathbf{u}_{body} = [\Delta h_{body} \quad \Delta v_{body}]^T = [(h_{obs} - h_{pred})_{body} \quad (v_{obs} - v_{pred})_{body}]^T \tag{101}$$

See Section 4.2.1 for more discussion of local tangent plane coordinates.

To compute $\Delta\mathbf{u}_{ICRF}$ the predicted unit vector is

$$(\mathbf{u}_{pred})_{ICRF} = \mathbf{u}_{ref} \tag{102}$$

And the observed unit vector is

$$(\mathbf{u}_{obs})_{ICRF} = (\mathbf{A}_b^{LRS}\mathbf{A}_i^b(t))^T(\mathbf{u}_{obs})_{LRS} \tag{103}$$

These two unit vectors are expressed as h, v coordinates in a local tangent plane frame on the celestial sphere that is aligned with astronomical right ascension and declination. The $\mathbf{i, j, k}$ axes of the frame are constructed based on the ICRF $\mathbf{z}$ axes (pointing to the celestial north pole) and $(\mathbf{u}_{pred})_{ICRF}$

$$\mathbf{i} = \mathbf{k} \times \mathbf{j} \tag{104}$$

$$\mathbf{j} = \mathbf{z} \times \mathbf{k} = [0 \quad 0 \quad 1]^T \times \mathbf{u}_{ref} \tag{105}$$

$$\mathbf{k} = (\mathbf{u}_{pred})_{ICRF} = \mathbf{u}_{ref} \tag{106}$$

The ICRF frame residual is given by

$$\Delta\mathbf{u}_{ICRF} = [\Delta h_{ICRF} \quad \Delta v_{ICRF}]^T = [(h_{obs} - h_{pred})_{ICRF} \quad (v_{obs} - v_{pred})_{ICRF}]^T \tag{107}$$

An array arrPassJ for pass j is generated sequentially as each observation is processed. Each row contains a time tag, $\Delta\mathbf{u}_{LRS}$, $\Delta\mathbf{u}_{body}$, $\Delta\mathbf{u}_{ICRF}$ and $\mathbf{u}_{obs} = [h_{obs} \quad v_{obs}]^T$. The $\mathbf{u}_{obs}$ vectors are included in the array for estimation of distortion corrections (LRS measurement model deterministic corrections). After processing n observations from pass j the dimensions of arrPassJ are $n \times 9$.

4.1.4 Pass Statistics

After a pass is complete its array is reduced to a relatively small set of statistics. The same reduction is performed at any time during the pass using the observations that have already been sequentially processed and stored in the array. The reduced pass statistics are used for identification and assessment and the question becomes what are effective and efficient statistics to include in the reduction.

The obvious candidates are the mean μ and square root of the variance σ, and the median $Q2$ and associated quartiles $Q1, Q3$. μ and σ are straightforward but assume the residuals have a Gaussian distribution. This assumption can be a problem when there are significant trends or outliers in the residuals. The first, second, and third quartiles ($Q1, Q2, Q3$) are termed robust statistics because they are less sensitive to the effects of outliers.

A practical difference is that μ, σ can be computed sequentially, whereas $Q1, Q2, Q3$ cannot. μ, σ can be computed from the sequentially accumulated parameters $n, \Sigma x, \Sigma x^2$. To compute $Q1, Q2, Q3$ a complete batch of residuals is required. For a star with thousands of passes and

millions of total observations, each pass should be reduced to $Q1, Q2, Q3$ values rather than storing every residual.

There are 5 statistics $\mu, \sigma, Q1, Q2, Q3$ characterizing each of the 6 h, v components in $\Delta\mathbf{u}_{LRS}$, $\Delta\mathbf{u}_{body}$, and $\Delta\mathbf{u}_{ICRF}$ for a total of 30 reduced statistics or parameters characterizing the pass. For pass j with n processed observations, the full $n \times 9$ pass array arrPassJ is reduced to a 31 component (including a timetag) vector vecRedPassJ. This discussion assumes that adequate $Q2_{LRS}$ estimates are available and focuses on processing a single pass, referred to as the current pass, based on the $Q1_{pass}, Q2_{pass}, Q3_{pass}$ values of its residuals. Because of their importance for characterizing the filter status, the 6 $Q1_{LRS}, Q2_{LRS}, Q3_{LRS}$ values are added to each vecRedPassJ record for a total of 37 components.

An additional parameter is the interquartile range $IQR = Q3 - Q1$. A standard robust definition of an outlier is given by

$$< Q1 - 1.5(IQR) \text{ or } > Q3 + 1.5(IQR) \tag{108}$$

Outlier residuals are excluded from calculations of $\mu, \sigma, Q1, Q2, Q3$ based on an initial calculation of $Q1, Q2, Q3$. Because the sensitivity of $Q1, Q2, Q3$ to outliers is relatively low, the initial and final $Q1, Q2, Q3$ values are usually the same.

Residuals are evaluated based on adaptive criteria that are sequentially adjusted for:

1. The current overall condition of the filter as determined empirically from the $Q1, Q2, Q3$ pass statistics for stars that were recently in the field of view. These overall values are maintained in $Q1_{LRS}, Q2_{LRS}, Q3_{LRS}$. The subscript LRS specifies that these values characterize the overall LRS attitude estimate, which is the key component of the filter state.
2. Whether a positive identification of the current pass (the pass being assessed) has been made. The binary identification value is represented by ID_{pass} here.
3. The $Q1, Q2, Q3$ statistics for the previous residuals of the current pass. These values are maintained in $Q1_{pass}, Q2_{pass}, Q3_{pass}$.

The data structures and parameters used in pass identification and assessment are summarized in Table 3.

A constantly recurring process is determination of the overall condition of the filter based on the $Q2_{LRS}$ values. Non-zero $Q2_{LRS}$ indicates a bias in the LRS attitude estimate

$$\mathbf{A}_i^{LRS} = \mathbf{A}(\mathbf{a}_{LRS})\mathbf{A}_b^{LRS}\mathbf{A}_i^b \tag{109}$$

Assuming that the LRS is identified with the body frame (because $\mathbf{A}(\mathbf{a}_{LRS})$ is held approximately constant at zero) this means a bias in the body frame attitude $\mathbf{A}_i^b$. For example if the $Q2_{LRS}$ value for the h residuals of recent passes is 10 arcseconds, then the $Q2_{pass}$ value for the h residuals of the current pass are expected to be near 10 arcseconds. $Q2_{LRS}$ is calculated from the current and previous star passes over a memory interval of length t_{memory}. The oldest pass residuals included have timetags $t_{timetag} > t_{current} - t_{memory}$.

Table 3 Data structures and parameters used in star pass identification and assessment.

Object	Description
arrPassJ	Array for pass j with rows comprised of a timetag, $\Delta\mathbf{u}_{LRS}$, $\Delta\mathbf{u}_{body}$, $\Delta\mathbf{u}_{ICRF}$ and $\mathbf{u}_{obs} = [h_{obs} \quad v_{obs}]^T$, generated sequentially as each observation is processed. With n processed observations the array is $n \times 9$.
vecRedPassJ	For pass j with n processed observations the $n \times 9$ arrPassJ is reduced to a 37 component (including a timetag and $Q1_{LRS}, Q2_{LRS}, Q3_{LRS}$ values) vector vecRedPassJ.
binIDPassJ, ID_{pass}	Binary value indicating whether a positive identification of pass J (including the current pass ID_{pass}) has been made.
t_{memory}	$Q2_{LRS}$ is calculated from passes with timetags $t_{timetag} > t_{current} - t_{memory}$.
$Q2_{LRS}$	Median values of multiple pass residuals from recent passes. A non-zero value indicates a bias in the LRS attitude estimate.
$Q1_{LRS}, Q3_{LRS}$	First and third quartile values of multiple pass residuals from recent passes. Used for outlier detection.
$Q2_{pass}$	Median value of residuals from the current pass. If $Q2_{LRS}$ is approximately zero and $Q2_{pass}$ is non-zero then the current pass contains biased measurements and is a bad star.
$Q1_{pass}, Q3_{pass}$	First and third quartile values of residuals from the current pass. Used to detect outliers within the current pass.
$L_{\Delta h}$, $L_{\Delta v}$, $L_{\Delta m}$	Adaptive limits for the criteria (identification and assessment criteria).

4.1.5 Positive Identification

If ID_{pass} is false then the pass needs to be positively identified. $\mathbf{A}_i^b$ is adequate for star identification because filter updates are coming from the spacecraft star trackers. The mission catalog is searched for stars near $(\mathbf{A}_b^{LRS}\mathbf{A}_i^b)^T\mathbf{u}_{obs}$ using the search method described in Section 4.1.8. The search result with the smallest $(\mathbf{A}_b^{LRS}\mathbf{A}_i^b)^T\mathbf{u}_{obs} - \mathbf{u}_{ref}$ residual is the identification candidate.

Positive identification means that the observations are indeed of the star described by the candidate mission catalog record. With positive identification, if the residuals for the current pass $Q2_{pass}$ include a bias while $Q2_{LRS}$ is near zero then the mission catalog record should be corrected and improved over time to better reflect the empirical LRS response to the real sky. In other words, positive identification is an important step in recognizing and characterizing bad stars.

Positive identification is based on the $Q2_{LRS}$ and $Q2_{pass}$ values for position residuals, and the predicted and observed magnitudes $m_{pred} = m_{ref}$ and m_{obs}. The magnitude residual is defined by

$$\Delta m = m_{obs} - m_{pred} \tag{110}$$

The prediction m_{pred} is taken directly from the reference value m_{ref} provided by the mission catalog record. In effect brightness is the critical confirmation that the mission catalog record is correct and adequate. Because the magnitude residuals Δm are not a function of the attitude estimate and filter state, there is less need for the type of statistical analysis and reduction represented by the median function $Q2()$. The available magnitude observations are simply compared with the prediction from the mission catalog.

It is useful however to monitor the magnitude residuals as a function of predicted (or reference magnitude). A function $\Delta\hat{\hat{m}}(m_{pred})$ is fit to a large batch of residuals and used as an estimate.

The three criteria for positive identification are

$$\left|Q2_{pass}(\Delta h) - Q2_{LRS}(\Delta h)\right| < L_{\Delta h} \tag{111}$$

$$\left|Q2_{pass}(\Delta v) - Q2_{LRS}(\Delta v)\right| < L_{\Delta v} \tag{112}$$

$$\left|\Delta m\right| < L_{\Delta m} \tag{113}$$

where the limits $L_{\Delta h}$, $L_{\Delta v}$, and $L_{\Delta m}$ effectively determine the strictness of the criteria. The same criteria are used in the next section for assessing individual observations with different values for

$L_{\Delta h}, L_{\Delta v}, L_{\Delta m}$. These three values are the focus of the identification and assessment process. Implementation reduces to a question of adaptively setting appropriate $L_{\Delta h}, L_{\Delta v}, L_{\Delta m}$ values.

4.1.6 Assessment for Use in Filter Updates

Assessment of the current pass and individual observations is based on the same criteria as positive identification, Eqs. (111) to (113). The difference is smaller values for $L_{\Delta h}, L_{\Delta v}, L_{\Delta m}$. The concept is that a star pass can be positively identified but then not used for filter updates because its residuals are abnormally high. In other words only normal passes with relatively small $L_{\Delta h}, L_{\Delta v}, L_{\Delta m}$ should be used for filter updates.

There are three cases to consider. In case A the filter is performing a cold start and has not yet converged. Residuals from the LRS and spacecraft star trackers may be high. In case B a period without LRS stars observations is ending. Residuals from the spacecraft star trackers are low, but the LRS residuals may be high. This can be classed as a type of filter warm start since there are estimated, non-default states and uncertainties, but they may be stale and have high uncertainties depending on the length of the blinding. In case C the filter is converged and functioning normally with recent updates from the LRS and spacecraft star trackers. Residuals from the LRS and the spacecraft star trackers are low.

Table 4 describes the three cases. Positive identification can be classed as a fourth case and is also included. The final column shows the adaptive values for the limits $L_{\Delta h}, L_{\Delta v}$. They are based on a scaling of the Interquartile Range (IQR) of the overall LRS residuals $Q3_{LRS} - Q1_{LRS}$. The IQR introduces the adaptive element into the criteria. The scaling factors k_A, k_B, k_C, k_{ID} determine the relative tightness of the criteria. The scaling factors are found empirically from simulation and flight data. It is natural that

$$k_{ID} > k_A > k_B > k_C \tag{114}$$

representing the principle that the criteria become tighter as knowledge increases and uncertainty decreases.

Table 4 Cases for assessing star passes and positive identification

Case	Description	$Q2_{LRS}$	SST residuals	$L_{\Delta h}, L_{\Delta v}$
-	Positive Identification	Can be high or low	-	$k_{ID} \times IQR$
A	Filter is performing a cold start and has not yet converged.	High	High	$k_A \times IQR$
B	A period without LRS stars observations is ending.	High	Low	$k_B \times IQR$
C	Filter is converged and functioning normally with recent updates from the LRS and spacecraft star trackers.	Low	Low	$k_C \times IQR$

4.1.7 Improving the Mission Catalog Using Archived Pass Statistics

As described above, there are 5 statistics $\mu, \sigma, Q1, Q2, Q3$ characterizing each of the 6 h, v components in $\Delta\mathbf{u}_{LRS}$, $\Delta\mathbf{u}_{body}$, and $\Delta\mathbf{u}_{ICRF}$ for a total of 30 reduced statistics or parameters characterizing a pass. For pass j with n processed observations, the full $n \times 9$ pass array arrPassJ is reduced to a 31 component (including a timetag) vector vecRedPassJ. Because of their importance for characterizing the filter status, the 6 $Q1_{LRS}, Q2_{LRS}, Q3_{LRS}$ values are added to each vecRedPassJ record for a total of 37 components. These vectors are computed and archived for millions of star passes, creating a significant database to mine for correlations and outliers.

The residuals expressed on the sky $\Delta\mathbf{u}_{ICRF}$ are of primary interest and significance. The objective is to improve the mission catalog by correcting the reference positions in the catalog so that the $\Delta\mathbf{u}_{ICRF}$ values

$$\Delta h_{ICRF} = (h_{obs} - h_{pred})_{ICRF} \tag{115}$$

$$\Delta v_{ICRF} = (v_{obs} - v_{pred})_{ICRF} \tag{116}$$

are normally approximately zero for all observed stars.

For pass i the residuals are represented by the median values $Q2(\Delta h_{ICRF})_i$ and $Q2(\Delta v_{ICRF})_i$. The interquartile ranges

$$IQR(\Delta h_{ICRF})_i = Q3(\Delta h_{ICRF})_i - Q1(\Delta h_{ICRF})_i \tag{117}$$

$$IQR(\Delta v_{ICRF})_i = Q3(\Delta v_{ICRF})_i - Q1(\Delta v_{ICRF})_i \tag{118}$$

are measures of uncertainty in the residuals. The scale of the median residuals relative to their uncertainties is a measure of the overall significance s_i

$$s(\Delta h_{ICRF})_i = \frac{Q2(\Delta h_{ICRF})_i}{IQR(\Delta h_{ICRF})_i} = \frac{Q2(\Delta h_{ICRF})_i}{Q3(\Delta h_{ICRF})_i - Q1(\Delta h_{ICRF})_i} \tag{119}$$

$$s(\Delta v_{ICRF})_i = \frac{Q2(\Delta v_{ICRF})_i}{IQR(\Delta v_{ICRF})_i} = \frac{Q2(\Delta v_{ICRF})_i}{Q3(\Delta v_{ICRF})_i - Q1(\Delta v_{ICRF})_i} \tag{120}$$

of the pass in terms of improving the mission catalog. If the significance ratio is low then the result from the pass should have relatively little effect on the catalog. If the significance is high the pass should be weighted up when correcting the catalog.

The measures of significance above only include uncertainty estimates for the residuals and by extension the observations. Uncertainties in the overall filter state should also be included. If the filter state uncertainties are high then large residuals can be expected and are not significant. The

six $Q1_{LRS}, Q2_{LRS}, Q3_{LRS}$ values are used to estimate the filter uncertainties, particularly $Q2_{LRS}$ alone. Augmented significance measures are given by

$$s(\Delta h_{ICRF})_i = \frac{Q2(\Delta h_{ICRF})_i}{Q2(\Delta h_{LRS})_i + IQR(\Delta h_{ICRF})_i} \tag{121}$$

$$s(\Delta v_{ICRF})_i = \frac{Q2(\Delta v_{ICRF})_i}{Q2(\Delta v_{LRS})_i + IQR(\Delta v_{ICRF})_i} \tag{122}$$

This is directly analogous to how the Kalman filter uncertainty $\mathbf{HPH^T + R}$ combines the uncertainty from the filter states $\mathbf{HPH^T}$ with the uncertainty from the measurements $\mathbf{R}$.

With the median residuals $Q2(\Delta h_{ICRF})_i, Q2(\Delta v_{ICRF})_i$ and significance parameters $s(\Delta h_{ICRF})_i, s(\Delta v_{ICRF})_i$ for $i = 1,...,n$ passes of a particular star, and the analogous values for hundreds of other stars, it is straightforward to detect cases with significant biases. Stars with relatively high $Q2$ and s values are flagged for assessment as possible bad stars. With flight experience, the detection thresholds are determined from the empirical probability distributions of the parameters. The biases represented by the high $Q2$ values can then be corrected in the mission catalog.

4.1.8 Search a Star Catalog for Stars Near a Point on the Sky

Given an arbitrary search point on the sky the objective is to find the records from a star catalog that are near the search point. Complexity is only introduced by efforts to optimize or reduce the computational cost of the search and these efforts are often not be necessary with modern ground-based computers. Brute force is not necessarily a problem for ground processing.

The key to this method is the coordinates used to represent the search point and the star catalog records. They are not represented using right ascension and declination. This would make the search much more difficult, particularly near the poles.

The coordinates are three-dimensional unit vectors in the celestial frame, and they are viewed simply as triplets of numbers between -1 and 1. The frame axes are: $\mathbf{z}$ axis pointing to the north celestial pole, $\mathbf{x}$ axis pointing to the vernal equinox, $\mathbf{y} = \mathbf{z} \times \mathbf{x}$. Star catalog records reduce to an integer record identifier and three coordinates x,y,z

Table 5 Example of a star catalog reduced to x,y,z coordinates

record	x	y	z	Note
1	1	0	0	Star at vernal equinox

2	0	0	1	Star at north celestial pole
3	-.53	-.21	.65	Some star
4	.86	-.54	.03	Some star

This allows the search to be decomposed into three simple independent sub-searches:

Sub-search 1. Find the set A of records with x values near the search point x value.

Sub-search 2. Find the set B of records with y values near the search point y value.

Sub-search 3. Find the set C of records with z values near the search point z value.

The intersection of sets A, B, and C are the catalog records near the search point. This completes the search. The only questions are related to how a sub-search is performed. The same sub-search method is used for each of the three sub-searches, with only the coordinate x,y,z changing. The remainder of this section discusses sub-search methods and optimizations. We note here that, for example, the Mortari K-vector search is one method for optimizing the sub-search method [33].

Within a sub-search, there is a list of $i = 1,...,n$ catalog coordinates $-1 \le c_i \le 1$ and a search point coordinate s. There is also an input parameter r specifying the radius in radians about the search point inside which catalogs records are accepted as nearby. The lower bound $cmin$ and upper bound $cmax$ for acceptable c_i values are given by:

If $s \ge \cos(r)$

$$\begin{aligned} cmin &= \cos(r)s - \sin(r)(1-s^2)^{1/2} \\ cmax &= 1 \end{aligned} \tag{123}$$

Elseif $s \le -\cos(r)$

$$\begin{aligned} cmin &= -1 \\ cmax &= \cos(r)s + \sin(r)(1-s^2)^{1/2} \end{aligned} \tag{124}$$

Else

$$\begin{aligned} cmin &= \cos(r)s - \sin(r)(1-s^2)^{1/2} \\ cmax &= \cos(r)s + \sin(r)(1-s^2)^{1/2} \end{aligned} \tag{125}$$

Matlab provides a function find( ) which can be used to find the c_i between the lower and upper bounds in a single line of code. Without a find( ) function, an obvious approach is to first sort the

list of c_i values and then step through to find the first $c_i \geq cmin$ and the last $c_i \leq cmax$. This type of sequential search in a sorted list is the basis of the Morari K-vector search. It takes advantage of the ordering in the sorted list to fit a low-order polynomial function. The positions of the first $c_i \geq cmin$ and the last $c_i \leq cmax$ can then be estimated by evaluating the polynomial rather than stepping sequentially through the list.

4.2 Star Telemetry and Model Parameters

LRS star tracker telemetry provides two-dimensional centroid positions in units of pixels. The field of view is $12^{\circ} \times 12^{\circ}$ and the detector is 1024×1024 with approximately $43.12 arcsec / pixel$ ($209 \mu rad / pixel$). Centroids are converted to unit vectors using the measurement models detailed in this section. The models include deterministic corrections to the measurements that can be thought of as higher-order terms augmenting a first-order geometric model. Some of the important corrections discussed here include integration time, distortion, centroiding error, and stellar aberration [34-36].

LRS telemetry also includes a brightness value for each star position measurement. The definition of the brightness value is not yet set, but may be an instrument magnitude calculated using the astronomical convention

$$m - m_{ref} = -2.5 log_{10}(b / b_{ref}) \tag{126}$$

where the m are instrument magnitudes, the b are brightness counts, and the subscript ref indicates a specified reference star.

The two spacecraft star trackers are functionally closely related to the LRS, and can be viewed as supporting components of the LRS star tracker. From this perspective, the SSTs provide attitude estimates that are useful for interpreting and using the LRS star telemetry. During periods when the LRS star tracker is blinded the SSTs naturally take on additional importance. Each SST is a black box that outputs an attitude estimate and uncertainty for its own coordinate frame. In practice the measurement model needed to interpret and SST attitude estimate is simply the estimated rotation $\mathbf{A}_b^{LRS}(\mathbf{A}_b^{SST})^T$ between the SST and LRS coordinate frames, and the error model represents the uncertainties $\mathbf{R}_{SST}$ and σ_{SST}^2 in $\mathbf{A}_i^{SST}$ and $\mathbf{A}_b^{SST}$.

4.2.1 Unit Vector Representations, Focal Plane and LTP Coordinates

Three-dimensional unit vectors $\mathbf{u}$ have only two degrees of freedom because of the unit constraint $\|\mathbf{u}\| = 1$. One way to take advantage of this is to express a given $\mathbf{u}$ using two coordinates with respect to a reference unit vector $\mathbf{u}_{ref}$. Typically $\mathbf{u}_{ref}$ is the $\mathbf{k}$ axis of an $\mathbf{i,j,k}$ frame and the question is how the $\mathbf{i,j,k}$ frame is defined. A common case is the $\mathbf{i,j,k}$ frame of a sensor, for example the LRS star tracker $\mathbf{i,j,k}$ frame. This case can be referred to as sensor frame coordinates or focal plane coordinates. Another common case is an $\mathbf{i,j,k}$ frame derived from the body frame and referred to as local tangent plane (LTP) coordinates. Unit vectors in a sensor frame, and their two-coordinate representations, are instrument independent. Conversion

from centroids to unit vectors is a conversion from instrument dependent to instrument independent coordinates.

In all cases, within a given $\mathbf{i, j, k}$ frame two coordinates are used to represent unit vectors relative to the $\mathbf{k}$ axis, usually either angles θ_h, θ_v or scaled tangent "horizontal and vertical" h, v coordinates. Scaled tangents are often preferable because they can reduce the number of trigonometric function evaluations. In this document the terms horizontal and vertical coordinates or h, v coordinates are a flag that the topic being discussed is three-dimensional unit vectors. Horizontal and vertical coordinates are simply a convenient two-dimensional way to work with three-dimensional unit vectors.

Focal plane coordinates are commonly used here to represent three-dimensional unit vectors in the LRS star tracker coordinate frame. They are typically expressed using two-dimensional h, v coordinates. The LRS coordinate frame is defined by orthogonal $\mathbf{i, j, k}$ axes with the $\mathbf{k}$ axis along the line-of-sight and the $\mathbf{i, j}$ axes in the image or focal plane. Star observations are represented by unit vectors $\mathbf{u} = [u_1 \quad u_2 \quad u_3]^T$ pointing from the origin and clustering within six degrees of the $\mathbf{k}$ axis due to the field of view limits. Each unit vector can be specified by an angle θ_h from the $\mathbf{k}$ axis towards the $\mathbf{i}$ axis, and an angle θ_v from the $\mathbf{k}$ axis towards the $\mathbf{j}$ axis. The angles θ_h and θ_v are given in the output of some commercial star trackers, for example the two ICESat-1 bus trackers output $a\theta_h$ and $a\theta_v$ where the scaling factor $a \equiv 180 \cdot 60 \cdot 60 / \pi$. To compute a unit vector $\mathbf{u}$, an intermediate vector $\mathbf{u}' = [h \quad v \quad 1]^T$ is defined using the h, v coordinates

$$h \equiv \tan\theta_h = u_1 / u_3 \tag{127}$$

$$v \equiv \tan\theta_v = u_2 / u_3 \tag{128}$$

and $\mathbf{u}$ is the normalized version of $\mathbf{u}'$

$$\mathbf{u} = \left[h \quad v \quad 1\right]^T \Big/ \left(h^2 + v^2 + 1\right)^{1/2} \tag{129}$$

The ICESat-1 LRS1 computed the ratios $h = x/f$ and $v = y/f$ internally and the ICESat-1 GLA04 flight data files gave the values ah and av.

Local tangent plane (LTP) coordinates are expressed relative to the body frame $\mathbf{x}$ axis and used to represent clusters of two or more similar unit vectors in the body frame. These clusters of unit vectors can be star observations, star predictions from the filter, sensor LOS vectors, etc. One of the unit vectors is defined as a reference $\mathbf{u}_{ref}$ around which an $\mathbf{i, j, k}$ LTP coordinate frame is formed by

$$\mathbf{i} \equiv \mathbf{j} \times \mathbf{k} \tag{130}$$

$$\mathbf{j} \equiv \mathbf{u}_{ref} \times \mathbf{x} \tag{131}$$

$$\mathbf{k} \equiv \mathbf{u}_{ref} \tag{132}$$

Unit vectors are expressed in an $\mathbf{i,j,k}$ LTP frame by $\mathbf{u} = [u_1 \quad u_2 \quad u_3]^T$ or angles θ_h and θ_v from the $\mathbf{k}$ axis towards the $\mathbf{i}$ and $\mathbf{j}$ axes. An intermediate vector $\mathbf{u}' = [h \quad v \quad 1]^T$ is defined where

$$h \equiv \tan\theta_h = u_1/u_3 \tag{133}$$

$$v \equiv \tan\theta_v = u_2/u_3 \tag{134}$$

and $\mathbf{u} = \mathbf{u}'/\|\mathbf{u}'\|$. The $\mathbf{i,j}$ plane is tangent to the unit sphere around the body frame origin at the point $\mathbf{k} \equiv \mathbf{u}_{ref}$ and the h, v coordinates are referred to as LTP coordinates. Near the $\mathbf{k}$ axis $h \cong \theta_h$ and $v \cong \theta_v$ and the LTP coordinates are approximately equivalent to angles. The $\mathbf{i}$ axis points as directly as possible (within the tangent plane) towards the body frame $\mathbf{x}$ axis and the h coordinate represents a rotation from $\mathbf{u}_{ref}$ towards or away from the body frame $\mathbf{x}$ axis (depending on its sign). Correlations of the LTP h, v coordinates for LOS variations and measurement residuals (star observations and star predictions) are significant when interpreting filter results.

4.2.2 Conversion of Centroids to Unit Vectors

Conversion from centroids to unit vectors is treated here as the first step in processing telemetry, partly because it converts from instrument dependent coordinates (centroid position) to instrument independent coordinates (focal plane h, v coordinates).

To agree with previous sections of this document, the notation here represents the conversion of two-dimensional centroids x, y to three-dimensional unit vectors $\mathbf{u}_1 = \mathbf{f}_1(x, y, \mathbf{p}_1)$ with model parameter vector $\mathbf{p}_1$. Deterministic corrections (for distortion, centroiding errors, aberration, etc) are then included via a second model $\mathbf{u}_2 = \mathbf{f}_2(\mathbf{u}_1, \mathbf{p}_2)$ with parameter vector $\mathbf{p}_2$.

The simplest measurement model is based on a pinhole camera and represents the optics as an infinitesimal hole allowing light rays from the stars to pass though with no change of direction [34, 37, 38]. The focal plane sits behind the pinhole and the minimum distance between the focal plane and pinhole is the focal length f. The point on the focal plane where the distance to the pinhole is a minimum is referred to as the principal point x_0, y_0, and is the origin of the two-dimensional focal plane coordinate frame and the three-dimensional instrument coordinate

frame. The direction of a light ray hitting the focal plane is specified to first-order by the focal plane coordinates and the focal length.

LRS star position telemetry consists of two-dimensional centroid positions x, y on the focal plane expressed in units of linear distance such as pixels or millimeters. Millimeters will be assumed here because they are also the natural units for f .

With parameter estimates for the three pinhole camera model parameters $\mathbf{p}_1 = [f, x_0, y_0]$, a centroid is converted to a unit vector $\mathbf{u}$ by

$$h = (x - x_0)/f \tag{135}$$

$$v = (y - y_0)/f \tag{136}$$

and $\mathbf{u}_1 = [h \quad v \quad 1]^T / (h^2 + v^2 + 1)^{1/2} = \mathbf{f}_1(x, y, \mathbf{p}_1)$, taking advantage of the similar triangles

$$h = \tan\theta_h = (x - x_0)/f = u_1/u_3 \tag{137}$$

$$v = \tan\theta_v = (y - y_0)/f = u_2/u_3 \tag{138}$$

Note that trigonometric functions are not involved and f, x_0, y_0 are the only instrument dependent parameters. Once h, v coordinates are computed, f, x_0, y_0 are no longer involved, leaving only the instrument independent unit vector $\mathbf{u} = [h \quad v \quad 1]^T / (h^2 + v^2 + 1)^{1/2}$.

The LRS ICD (ICESat-2-LRS-IFACE-1794) defines a more sophisticated measurement model including a quadratic term to represent radial deviation from a simple linear model. This will be referred to as the LRSICD model here[1].

The LRSICD model uses five parameters: $\mathbf{p}_1 = [p_{11}, p_{12}, p_{13}, x_0, y_0]$. The radial distance of a centroid from the principal point is $d = ((x - x_0)^2 + (y - y_0)^2)^{1/2}$. A scaling factor k is given by

$$k = p_{11}d^2 + p_{12}d + p_{13} \tag{139}$$

The h, v coordinates of the unit vector are

[1] There is a difference between the notations used in this document and the LRSICD. Here pixel value (or millimeter) positions on the detector (centroids, principal point locations, etc) have the notation x, y and the notation h, v is reserved for unit vector h, v coordinates. In the LRSICD the notation H, V is used for pixel value position on the detector and is equivalent to x, y here. The principal in this document is that horizontal and vertical coordinates are always associated with unit vectors, not detector centroids or positions.

$$h = \tan\theta_h = \tan(k(x - x_0)) \tag{140}$$

$$v = \tan\theta_v = \tan(k(y - y_0)) \tag{141}$$

and $\mathbf{u}_1 = [h \quad v \quad 1]^T / (h^2 + v^2 + 1)^{1/2} = \mathbf{f}_1(x, y, \mathbf{p}_1)$. The quadratic radial term $p_{11}d^2$ means that similar triangles can not be taken advantage of to bypass the tan( ) function evaluation during the conversion from instrument dependent coordinates to instrument independent unit vectors.

Near the center of the field of view $h \approx \theta_h$ and $v \approx \theta_v$, so h, v coordinates are approximately angular measures with units of radians. This approximation is commonly used across the field of view for noise estimation using the triangle method.

4.2.3 Integration Time Correction

After conversion to instrument independent three-dimensional unit vectors, an LRS 10 Hz star data packet consists of up to thirty star observations $\mathbf{u}_i(t - \Delta\tau_i); i = 1, ..., 30$, each with its own center of integration time offset $\Delta\tau_i$ from the packet time tag t (also referred to as the center of integration base time or simply base time).

The 10 Hz base time t is the sum of two time tag values provided in each packet: the packet header time $t_{\text{Packet Header}}$, and the center of integration base time offset $\Delta t_{\text{COI Base}}$

$$t \equiv t_{\text{Packet Header}} - \Delta t_{\text{COI Base}} \tag{142}$$

The $i = 1, ..., 30$ individual star observation time tags τ_i are

$$\tau_i = t - \Delta\tau_i \tag{143}$$

The objective here is to propagate each $\mathbf{u}_i(t - \Delta\tau_i)$ to $\mathbf{u}_i(t)$ so that all of the observations are simultaneous at t. In other words, a deterministic correction of each unit vector so that $\Delta\tau_i = 0$ and $\tau_i = t$ for every $i = 1, ..., 30$.

When all of the observations have $\Delta\tau_i = 0$ and $\tau_i = t$ they can be referred to as a *frame of observations* or *observation frame*. This is standard jargon from the literature, for example discussing *single-frame* attitude determinations methods (Triad, q-Method, Markley SVD, Quest, etc).

Integration time correction is a question of propagating each unit vector $\mathbf{u}_i(t - \Delta\tau_i)$ over a small time interval $\Delta\tau_i$. Given the observed SIRU coordinate frame angular rate $\boldsymbol{\omega}_{SIRU}(t)$, the angular rate of the LRS coordinate frame is $\mathbf{A}_b^{LRS}(\mathbf{A}_b^{SIRU})^T \hat{\boldsymbol{\omega}}_{SIRU}$. Over a time interval $\Delta\tau_i$ the LRS frame rotation expressed as a rotation vector $\mathbf{a}$ is given by

$$\mathbf{a}(\Delta\tau_i) = \mathbf{A}_b^{LRS}(\mathbf{A}_b^{SIRU})^T \boldsymbol{\omega}_{SIRU}\Delta\tau_i \tag{144}$$

where the time interval $\Delta\tau_i$ is short enough that $\boldsymbol{\omega}_{SIRU}(t)$ is approximately constant. The equivalent rotation matrix is $\mathbf{A}(\mathbf{a}(\Delta\tau_i))$. The transpose $\mathbf{A}^T(\mathbf{a}(\Delta\tau_i))$ rotates unit vectors rather than the frame and $\mathbf{u}_i(t)$ is given by

$$\mathbf{u}_i(t) = \mathbf{A}^T(\mathbf{a}(\Delta\tau_i))\mathbf{u}_i(t-\Delta\tau_i) \tag{145}$$

Equation (145) is an exact correction. In practice approximations can be adequate, for example correcting the h, v coordinates of the unit vectors using their local, observed rate of change $\Delta h/\Delta t$ and $\Delta v/\Delta t$.

4.2.4 Deterministic Corrections for Star Unit Vectors

This section discusses deterministic corrections to the star unit vectors $\mathbf{u}_1 = \mathbf{f}_1(x, y, \mathbf{p}_1)$ from the previous section, using a second model $\mathbf{u}_2 = \mathbf{f}_2(\mathbf{u}_1, \mathbf{p}_2)$ with parameter vector $\mathbf{p}_2$. The real optics and focal plane are not an ideal pinhole camera, and the deviations of the real measurements from the first-order transformation are described by higher-order terms. The effects of these higher-order geometric terms are referred to generically as distortion. The terms and their estimated parameter values comprise most of $\mathbf{p}_2$ and $\mathbf{u}_2 = \mathbf{f}_2(\mathbf{u}_1, \mathbf{p}_2)$. Some additional terms are included to correct for stellar aberration and any other deterministic corrections.

Distortion errors or low spatial frequency errors (LSFE) refers here to deviations away from the simple pinhole camera model that are a function of the overall position on the focal plane [35, 37, 39]. These deviations vary slowly over large spatial scales, corresponding to low spatial frequencies. In other words distortion corrections do not change significantly on the scale of individual pixels, but do change over tens or hundreds of pixels.

Distortion corrections are applied to the measured star unit vectors before use in the alignment filter. The ICESat-1 IST distortion correction map is shown in Figure 2 as an example. The largest corrections in the corners of the field of view are approximately 2.5 arcseconds.

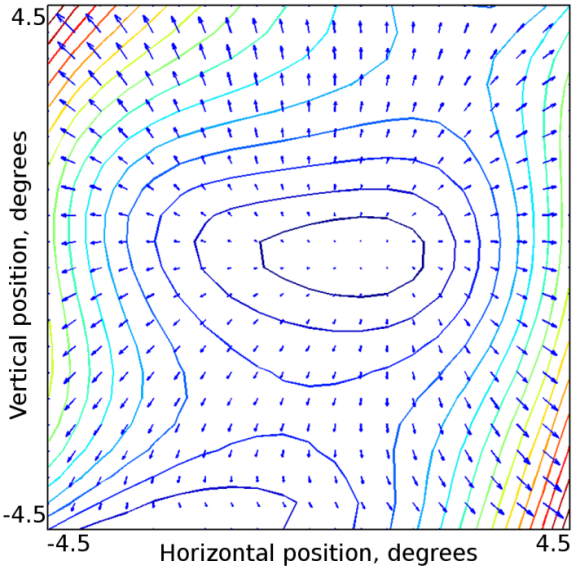

Figure 2 Distortion corrections of up to 2.5 arcseconds for the IST.

The PPD algorithm estimates the parameter values by comparing the observed and predicted focal plane h, v coordinates for large numbers of star observations, distributed as uniformly as possible across the focal plane. A three-dimensional surface is fit to the observed minus predicted residuals representing the h, v corrections to be applied to the observations.

Unit vectors are assumed here to be represented by h, v coordinates and all calculations are performed in the two-dimensional h, v plane. Near the center of the field of view $h \approx \theta_h$ and $v \approx \theta_v$, so h, v coordinates are approximately angular measures with units of radians. This approximation is used across the field of view for distortion estimation.

Distortion is estimated based on measurements $\mathbf{u}_1 = [h \quad v]^T$ and measurement residuals $\Delta\mathbf{u}_1 \equiv [\Delta h \quad \Delta v]^T$ calculated during filter measurement updates. A method for estimating the correction parameters $\mathbf{p}_2$ is summarized here, followed by a more detailed discussion of implementation.

As a summary, the measurement residuals are modeled by $\Delta h = \mathbf{h}_h \mathbf{p}_2 + \eta_h$ and $\Delta v = \mathbf{h}_v \mathbf{p}_2 + \eta_v$ where

$$\mathbf{h}_h = \begin{bmatrix} 1 & h & v & h^2 & hv & v^2 & h^3 & h^2 v & hv^2 & v^3 & \mathbf{0}_{1\times 10} \end{bmatrix} \tag{146}$$

$$\mathbf{h}_v = \begin{bmatrix} \mathbf{0}_{1\times 10} & 1 & h & v & h^2 & hv & v^2 & h^3 & h^2 v & hv^2 & v^3 \end{bmatrix} \tag{147}$$

and η_h, η_v are zero-mean Gaussian white noise. For a sample of measurements and residuals the observation vector $\mathbf{H}^T \Delta\mathbf{u}_1$ and information matrix $\mathbf{H}^T\mathbf{H}$ are accumulated by

$(\mathbf{H}^T\Delta\mathbf{u}_1)_i = (\mathbf{H}^T\Delta\mathbf{u}_1)_{i-1} + \mathbf{h}_h^T\Delta h + \mathbf{h}_v^T\Delta v$ and $(\mathbf{H}^T\mathbf{H})_i = (\mathbf{H}^T\mathbf{H})_{i-1} + \mathbf{h}_h^T\mathbf{h}_h + \mathbf{h}_v^T\mathbf{h}_v$ beginning with $(\mathbf{H}^T\Delta\mathbf{u}_1)_0 = \mathbf{0}_{20\times1}$ and $(\mathbf{H}^T\mathbf{H})_0 = \mathbf{0}_{20\times20}$. The least squares estimate of the distortion parameters $\mathbf{p}_2$ is given by $\hat{\mathbf{p}}_2 = \left(\mathbf{H}^\mathbf{T}\mathbf{H}\right)^{-1}\mathbf{H}^\mathbf{T}\Delta\mathbf{u}_1$.

In more detail, let $\mathbf{u}_{1j}$ be the *j*th observed unit vector and $\mathbf{u}'_{1j}$ be the *j*th predicted unit vector

$$\mathbf{u}_{1j} = [u_{11} \quad u_{12} \quad (u_{11}^2 + u_{12}^2)^{1/2}]^T \tag{148}$$

$$\mathbf{u}'_{1j} = [u'_{11} \quad u'_{12} \quad (u'^2_{11} + u'^2_{12})^{1/2}]^T \tag{149}$$

The effective observations $\mathbf{y} = \begin{bmatrix} y_h & y_v \end{bmatrix}^T$ are modeled by

$$y_h = u_{11} - u'_{11} = \mathbf{h}_h\mathbf{p}_2 + \eta_h \tag{150}$$

$$y_v = u_{12} - u'_{12} = \mathbf{h}_v\mathbf{p}_2 + \eta_v \tag{151}$$

where $\boldsymbol{\eta} = [\eta_h \quad \eta_v]^T$ is zero-mean Gaussion white noise $E\{\boldsymbol{\eta}^T\boldsymbol{\eta}\} = \sigma_y^2\mathbf{I}$. The information matrix $\mathbf{H}^T\mathbf{H}$ and observations vector $\mathbf{H}^T\mathbf{y}$ are accumulated from $(\mathbf{H}^T\mathbf{H})_0 = \mathbf{0}_{20\times20}$ and $(\mathbf{H}^T\mathbf{y})_0 = \mathbf{0}_{20\times1}$

$$(\mathbf{H}^T\mathbf{H})_j = (\mathbf{H}^T\mathbf{H})_{j-1} + \mathbf{h}_h^T\mathbf{h}_h + \mathbf{h}_v^T\mathbf{h}_v \tag{152}$$

$$(\mathbf{H}^T\mathbf{y})_j = (\mathbf{H}^T\mathbf{y})_{j-1} + \mathbf{h}_h^T y_h + \mathbf{h}_v^T y_v \tag{153}$$

and the parameter estimate is given by

$$\hat{\mathbf{p}}_2 = (\mathbf{H}^T\mathbf{H})^{-1}\mathbf{H}^T\mathbf{y} \tag{154}$$

This generalization allows for various models $\mathbf{h}_h$ and $\mathbf{h}_v$ to be used.

Centroiding errors or **high spatial frequency errors (HSFE)** refer here to deviations away from the pinhole camera model that are a function of small changes of position on the focal plane, on the scale of individual pixels [34, 36]. These deviations vary rapidly over small spatial scales, corresponding to high spatial frequencies, and are generally caused by the spatial quantization of the star images, in other words converting continuous light distributions into discrete pixel brightness values.

The optics are slightly defocused to spread a star image over multiple pixels, making it possible to estimate the centroid at sub-pixel levels, but there is always some centroiding error due to the discrete sampling of the image. This error is apparent as the star image moves across pixel boundaries. If the spacecraft is rotating with a constant rate, a star image moves across the focal plane at approximately a constant rate as well (there can be higher-order optical effects near the edges of the field of view). The rate of the measured centroid has a small periodic variation as

the image moves across pixel boundaries. Deterministic centroiding errors are expected to be at the sub-arcsecond level, per star. For n star observations the effects on attitude estimation decrease by $1/\sqrt{n}$.

Centroiding error has a significantly smaller effect than distortion and is typically treated as a small stochastic (noise) error that is averaged out by the processor filtering of large numbers of star observations. In effect it is included in the observation uncertainty $\mathbf{R}$ and is not explicitly treated as a deterministic error and corrected in $\mathbf{u}_2 = \mathbf{f}_2(\mathbf{u}_1, \mathbf{p}_2)$.

4.2.5 Stellar Aberration Correction

The telemetry value of the spacecraft velocity vector is used for stellar aberration correction. Supporting telemetry included in HDF5 data concern the spacecraft state including position and velocity, temperatures, solar array position, and the state of individual components such as the laser system and beam steering mechanism.

In stellar aberration, the observed direction $\mathbf{u}$ of a star is displaced from its true direction by an amount which depends on the transverse velocity of the observer. In practice this velocity is the sum of the Earth velocity and spacecraft velocity, both expressed in the ICRF. The displacement of the observed star direction can have a magnitude on the order of 20 arcseconds. The aberration correction can be applied either to the star predictions, or to the star observations [40].

Here all vectors including the observer velocity vector $\mathbf{v}$ are expressed in the observer's coordinate frame (observer frame). In practice this is a sensor frame, usually the LRS frame (LRS star tracker frame). Give the Earth velocity vector in the ICRF $\mathbf{v}_{EARTH,ICRF}$, the spacecraft velocity vector in the ICRF $\mathbf{v}_{SC,ICRF}$, and the LRS attitude $\mathbf{A}_i^{LRS}$

$$\mathbf{v} = \mathbf{A}_i^{LRS}(\mathbf{v}_{EARTH,ICRF} + \mathbf{v}_{SC,ICRF}) \tag{155}$$

For an observed star direction $\mathbf{u}$ in the LRS frame, the direction corrected for stellar aberration is

$$\mathbf{u}' = (\mathbf{u} - \mathbf{v}/c)/\left\|\mathbf{u} - \mathbf{v}/c\right\| \tag{156}$$

Aberration correction can be incorporated with the deterministic corrections $\mathbf{u}_2 = \mathbf{f}_2(\mathbf{u}_1, \mathbf{p}_2)$, but for simplicity and clarity the implementation is usually separate and easily distinguishable.

4.2.6 Noise Estimation Using the Triangle Method

In this section unit vectors are assumed to be represented by h, v coordinates and all calculations are performed in the two-dimensional h, v plane. Near the center of the field of view $h \approx \theta_h$ and $v \approx \theta_v$, so h, v coordinates are approximately angular measures with units of radians. This approximation is commonly used across the field of view for noise estimation using the triangle method.

The error model is $\mathbf{u} = \mathbf{h} + \boldsymbol{\eta}$ where $\mathbf{u}$ is the observed unit vector, $\mathbf{h}$ is the true unit vector, and $\boldsymbol{\eta}$ is zero-mean Gaussian white noise $E\{\boldsymbol{\eta}^T \boldsymbol{\eta}\} = \sigma_u^2 \mathbf{I}$. Measurement noise σ_u is estimated empirically for use in the measurement covariance $\mathbf{R} = E\{\boldsymbol{\eta}_u \boldsymbol{\eta}_u^T\} = \sigma_u^2 \mathbf{I}$. The estimate is based on variations of the angular separations between pairs of stars [41]. The variance of the separations between stars a and b is equal to the sum of their individual noise variances $\sigma_{ab}^2 = \sigma_a^2 + \sigma_b^2$, where σ_{ab}^2 is calculated directly from a set of simultaneous measurements of stars a and b. For a set of simultaneous measurements of three stars a, b and c the variances of the separations form 3 equations $\sigma_{ab}^2 = \sigma_a^2 + \sigma_b^2$, $\sigma_{ac}^2 = \sigma_a^2 + \sigma_c^2$, and $\sigma_{bc}^2 = \sigma_b^2 + \sigma_c^2$ with 3 unknowns σ_a^2, σ_b^2 and σ_c^2. When there are $n > 3$ measured stars over a given time period there is a variable number m of measured angular separations. If $m > n$ the resulting system of equations is solved using least squares methods. Estimated noise as a function of star brightness for ICESat-1 is shown in Figure 3.

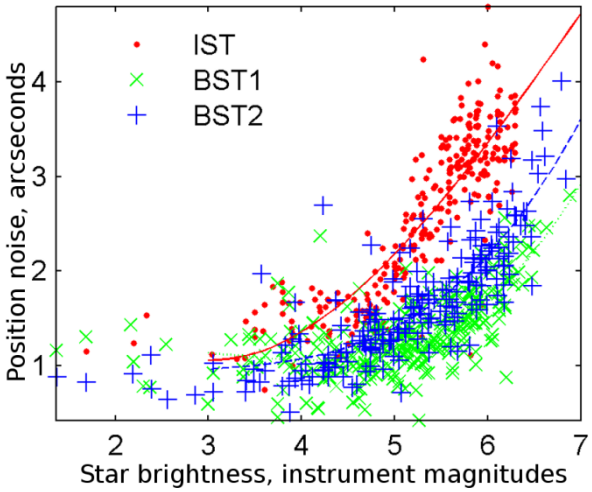

Figure 3 Measurement noise.

Note that the identities of the stars used for noise estimation do not appear in the estimation process. In other words noise estimation can be performed before and independently from star

identification. As far as noise estimation is concerned, there are simply some spots being tracked by the sensor. The only question is how much the angles between the spots vary over time.

The simplest implementation is clearly a batch estimation process in which a large batch of interstar variances σ_{xy}^2 are stored over time and then a single least squares estimate of the individual star positions variances $\sigma_a^2, \sigma_b^2, \sigma_c^2, \sigma_d^2, \ldots$ is calculated. Extension to a sequential algorithm and implementation is clearly both possible and practical but may not be worthwhile unless there is evidence that the noise depends on time as well as star brightness. If the noise is time varying a sequential method capable of tracking the variations may be worthwhile. Otherwise a lookup table of noise as a function of star brightness should be sufficient.

4.3 Laser Telemetry and Model Parameters

The LRS laser tracker observes for six laser unit vectors $\mathbf{u}_{LT} = \mathbf{f}_{LT}(x, y, \mathbf{p}_{LT})$ in the laser tracker frame at 50 Hz. The telemetry values are centroid positions x, y on the detector with units of pixels or equivalent millimeters[2]. The field of view is $1.3^{\circ} \times 1.3^{\circ}$ ($23.3 mrad \times 23.3 mrad$) and the detector is 1024×1024 with approximately $9.385 arcsec/pixel$ ($45.5 \mu rad/pixel$). The estimated alignment $\mathbf{A}_{LT}^{LRS}$ between the laser tracker frame and LRS frame (LRS star tracker frame) is used to transform the laser unit vectors into the LRS frame $\mathbf{u}_{LRS} = \mathbf{A}_{LT}^{LRS}\mathbf{u}_{LT}$.

The alignment $\mathbf{A}_{LT}^{LRS}$ can be classed as part of the laser tracker measurement model. In the ideal situation with a stable and well known $\mathbf{A}_{LT}^{LRS}$ the laser tracker effectively observes the laser vectors directly in the LRS frame $\mathbf{A}_{b}^{LRS}$ which is connected with the ICRF by $\mathbf{A}_{b}^{LRS}\mathbf{A}_{i}^{b}$. $\mathbf{A}_{LT}^{LRS}$ is determined in ground testing and the geolocation error budget allocates $5.0 \mu rad$ for its variability. Variations of $\mathbf{A}_{LT}^{LRS}$ may not be directly observable from flight data, but the effects should be significantly reduced by corrections to $\mathbf{A}_{LT}^{LRS}$ from ocean scan calibration.

4.3.1 6.25 Degree Yaw of the LRS

The body frame $\mathbf{A}_{i}^{b}$ is assumed here to be defined similarly to the OSC spacecraft frame:

1. X axis along the centerline of the spacecraft and positive out through the ATLAS instrument.
2. Y axis anti-parallel to the rotation axis of the solar array.
3. Z axis parallel to the ATLAS telescope line of sight.

The LRS as a whole is rotated by 6.25° about its optical axes relative to the body frame. The LRS laser tracker line of sight (nadir pointing) is parallel to the body frame Z axis. Its X and Y axes are yawed 6.25° from the body frame X and Y axes.

This yaw rotation is included in $\mathbf{A}_{b}^{LRS}$ and does not have any other direct effects on the processor. Normally the LRS frame is effectively defined as the body frame by holding $\mathbf{A}_{b}^{LRS}$

---

[2] There is a difference between the notations used in this document and the LRSICD. Here pixel value (or millimeter) positions on the detector (centroids, principal point locations, etc) have the notation x, y and the notation h, v is reserved for unit vector h, v coordinates. In the LRSICD the notation H, V is used for pixel value position on the detector and is equivalent to x, y here. The principal in this document is that horizontal and vertical coordinates are always associated with unit vectors, not detector centroids or positions.

approximately constant. The 6.25° LRS yaw is then effectively incorporated directly in the body frame attitude estimate $\mathbf{A}_i^b$. In this case one can say that the spacecraft is yawed 6.25° from the LRS and body frames, but the semantics have no practical significance.

The only question that matters is: does the processor adequately predict the LRS star observations and interpret the LRS laser observations. The answer depends entirely on the accuracy of $\mathbf{A}_i^{LRS} = \mathbf{A}_b^{LRS}\mathbf{A}_i^b$. The effects of the 6.25° yaw are absorbed in $\mathbf{A}_b^{LRS}\mathbf{A}_i^b$. A laser tracker unit vector $\mathbf{u}_{LT} = \mathbf{f}_{LT}(x_1, x_2, \mathbf{p}_{LT})$ in the laser tracker frame is transformed into the LRS the ICRF normally, $\mathbf{u}_{ICRF} = (\mathbf{A}_b^{LRS}\mathbf{A}_i^b)^T \mathbf{A}_{LT}^{LRS}\mathbf{u}_{LT}$.

4.3.2 LRS to ATLAS Frame Alignment Estimation

Motion of the laser tracker observations (centroids or unit vectors) can be caused by motion of the LRS as a whole relative to the ATLAS frame. This provides a possible method for detecting and characterizing LRS alignment variations even when there are no LRS star tracker observations (during LRS star tracker blinding). For example, if the laser tracker observations are clearly moving but the laser beams are fixed in the ATLAS frame (beam steering mechanism is constant), then what is actually moving is the LRS. This makes the LRS frame alignment $\mathbf{A}_b^{LRS}$ observable and provides a basis for parameter or state estimation of its time variations $\mathbf{A}_b^{LRS}(t)$.

4.3.3 Conversion of Centroids to Unit Vectors

As for the star tracker, a laser tracker measurement model $\mathbf{u}_{LT} = \mathbf{f}_{LT}(x, y, \mathbf{p}_{LT})$ including a quadratic radial term is provided by the LRS group. The model parameters are

$$\mathbf{p}_{LT} = [p_{LT1}, p_{LT2}, p_{LT3}, x_{LT0}, y_{LT0}] \tag{157}$$

The radial distance of a centroid from the laser tracker principal point is

$$d = ((x - x_{LT0})^2 + (y - y_{LT0})^2)^{1/2} \tag{158}$$

A scaling factor k is given by

$$k = p_{LT1}d^2 + p_{LT2}d + p_{LT3} \tag{159}$$

The h, v coordinates of the unit vector are

$$h = \tan\theta_h = \tan(k(x - x_{LT0})) \tag{160}$$

$$v = \tan\theta_v = \tan(k(y - y_{LT0})) \tag{161}$$

and $\mathbf{u}_{LT} = [h \quad v \quad 1]^T / (h^2 + v^2 + 1)^{1/2} = \mathbf{f}_{LT}(x, y, \mathbf{p}_{LT})$. Near the center of the field of view $h \approx \theta_h$ and $v \approx \theta_v$, so h, v coordinates are approximately angular measures with units of radians. This approximation is commonly used across the field of view for noise estimation using the triangle method.

There is a fundamental difference between the LRS laser tracker and star tracker with regard to on-orbit calibration. The star tracker observes nearly ideal external reference points - the stars. Star observations provide adequate information for calibration, with a nearly uniform distribution over the star tracker focal plane given a large enough sample. The information available for calibrating the laser tracker on-orbit is much more limited.

The available references for calibration of the laser tracker are the six laser spots and four reference signal TAMS spots. In other words, on-orbit calibration will necessarily depend on the geometry of the six laser spots and four reference signal spots.

The angles between the reference signal TAMS spots are approximately constant. The same should be true for the angles between the laser spots. Comparing the true angles with the observed angles is a potential source of calibration information for estimating laser tracker measurement model parameters.

The positions of the spots on the focal plane are normally approximately static, making the spatial distribution of calibration information across the focal plane sparse. It is possible in principal to scan the laser spots over the field of view using the beam steering mechanism to improve spatial coverage.

4.3.4 Noise Estimation Using the Triangle Method

In this section unit vectors are assumed to be represented by h, v coordinates and all calculations are performed in the two-dimensional h, v plane. Near the center of the field of view $h \approx \theta_h$ and $v \approx \theta_v$, so h, v coordinates are approximately angular measures with units of radians. This approximation is commonly used across the field of view for noise estimation using the triangle method.

The laser tracker error model for laser unit vector observations $\mathbf{u} = \mathbf{u}_{LT}$ is $\mathbf{u} = \mathbf{h} + \boldsymbol{\eta}$ where $\mathbf{u}$ is the observed unit vector, $\mathbf{h}$ is the true unit vector, and $\boldsymbol{\eta}$ is zero-mean Gaussian white noise $E\{\boldsymbol{\eta}^T \boldsymbol{\eta}\} = \sigma_u^2 \mathbf{I}$.

Measurement noise σ_u is estimated based on variations of the angular separations between pairs of laser vectors. The variance of the separations between vectors a and b is equal to the sum of their individual noise variances $\sigma_{ab}^2 = \sigma_a^2 + \sigma_b^2$, where σ_{ab}^2 is calculated directly from a set of

simultaneous measurements of vectors a and b. For a set of simultaneous measurements of three vectors a, b and c the variances of the separations form 3 equations $\sigma_{ab}^2 = \sigma_a^2 + \sigma_b^2$, $\sigma_{ac}^2 = \sigma_a^2 + \sigma_c^2$, and $\sigma_{bc}^2 = \sigma_b^2 + \sigma_c^2$ with 3 unknowns σ_a^2, σ_b^2 and σ_c^2. For the 6 laser vectors there are $6(6-1)/2 = 15$ angular separation variances σ_{xy}^2. The system of equations for the 6 unknown noise variances is over-determined and solved using least squares.

4.3.5 Alignment of Laser Tracker Frame and Ocean Scan Correction

The alignment $\mathbf{A}_{LT}^{LRS}$ between the laser tracker frame and LRS frame (star tracker frame) is a key factor in transforming laser tracker observations $\mathbf{u}_{LT} = \mathbf{f}_{LT}(x, y, \mathbf{p}_{LT})$ into laser vectors $\mathbf{u}_{ICRF}$ in the ICRF

$$\mathbf{u}_{ICRF} = (\mathbf{A}_b^{LRS}\mathbf{A}_i^b)^T \mathbf{A}_{LT}^{LRS}\mathbf{u}_{LT} \tag{162}$$

A reference alignment $\mathbf{B}$ is provided by ground testing and is a constant throughout the mission. A time-varying correction $\mathbf{C}(t)$ is included in the measurement model in order to incorporate flight data. By including $\mathbf{C}(t)$, the alignment becomes time dependent and given by

$$\mathbf{A}_{LT}^{LRS}(t) = \mathbf{C}(t)\mathbf{B} \tag{163}$$

so

$$\mathbf{u}_{ICRF} = [(\mathbf{A}_b^{LRS}\mathbf{A}_i^b(t))^T \mathbf{A}_{LT}^{LRS}(t)]\mathbf{u}_{LT} = [(\mathbf{A}_b^{LRS}\mathbf{A}_i^b(t))^T \mathbf{C}(t)\mathbf{B}]\mathbf{u}_{LT} \tag{164}$$

Parameter estimation for $\mathbf{C}(t)$ using flight data plays a major role in improving the overall laser tracker measurement model. In general $\mathbf{C}(t)$ reflects results from ocean scan calibration and is referred to as the ocean scan correction.

This discussion of ocean scan calibration is based on Ref. [42], where an expression similar to Eq. (164) is given (Ref. [42] Eq. (2) with minor notational changes) by

$$\mathbf{u}_{ICRF} = \mathbf{A}_{SBF}^{ICRF}(t)\mathbf{A}_{SBFC}^{SBF}(t)\mathbf{A}_{LT}^{SBFC}\mathbf{u}_{LT} \tag{165}$$

The objective of ocean scan calibration is estimation of the rotation $\mathbf{A}_{SBFC}^{SBF}$. Comparing Eqs. (165) to (164), $\mathbf{C}(t) = \mathbf{A}_{SBFC}^{SBF}(t)$ for $(\mathbf{A}_b^{LRS}\mathbf{A}_i^b(t))^T \equiv \mathbf{A}_{SBF}^{ICRF}(t)$ and $\mathbf{B} \equiv \mathbf{A}_{LT}^{SBFC}$. In other words, ocean scan calibration provides an estimate of the correction $\mathbf{C}(t)$.

4.3.6 Laser Pointing Product

The overall product is a set of 6 laser unit vectors in the ICRF $\mathbf{u}_{ICRF,i}(t_k)$ for $i = 1,...,6$ at each LRS laser tracker observation time tag t_k.

$$\mathbf{u}_{ICRF,i}(t_k) = [(\mathbf{A}_b^{LRS}\mathbf{A}_i^b(t_k))^T \mathbf{C}(t_k)\mathbf{B}]\mathbf{u}_{LT,i}(t_k) \quad (166)$$

The product $\mathbf{u}_{ICRF,i}(t_k)$ at t_k is fully specified by:

1. The 6 laser unit vectors $\mathbf{u}_{LT,i}(t_k)$ expressed in the laser tracker frame using h, v coordinates (or other convenient two-component representations).
2. The ocean scan correction $\mathbf{C}(t_k)$.
3. The attitude estimate $\mathbf{A}_i^b(t_k)$.

The significant question here is: what is the attitude estimate $\mathbf{A}_i^b(t_k)$ at the essentially arbitrary laser tracker output time tag t_k?

Table 7 and Table 8 on the next two pages demonstrate propagation of the attitude estimate to the arbitrary time tags of laser tracker observations and filter updates (star observations). The gyro observation time tags are included in the time series since the gyro observations provide the empirical basis for the propagation. The SIRU provides all of the available higher frequency pointing information and is necessarily the basis for propagation over short time scales.

The objective is to find the rotation vectors $\mathbf{a}_{k-1}^k$ from t_{k-1} to t_k representing the attitude change between successive pairs of time tags. All of the propagation information comes from the SIRU and is encoded into and transmitted by the rotation vectors.

Table 7 presents the overall structure of the propagation and the role of the rotation vectors but says nothing about where the rotation vectors come from (how they are estimated). That is the job of Table 8 which is entirely focused on estimating the rotation vectors. Explanatory discussion is included below each table.

4.4 Gyro Telemetry and Model Parameters

The SIRU is used to propagate the attitude estimate forward in time. In practice, propagation covers the time span between two measurement updates. SIRU output is recorded at 50 Hz, providing pointing information at higher frequencies than the 10 Hz star observations. With a precision on the order of tenths of an arcsecond, it also provides higher angular resolution.

Even with more bandwidth and precision, SIRU attitude propagation is associated with the growth of pointing uncertainty, while the LRS and SSTs are associated with reduced pointing uncertainties. Over shorter time scales the error characteristics of the SIRU dominate the uncertainties and drive their growth, appearing directly in the filter as process or state noise.

The time tags of the 50 Hz LRS laser observations determine the time tags of the 50 Hz PPD product. This means that the time tags of the LRS laser observations are effectively a set of target times at which the processor needs to estimate the six laser pointing vectors and uncertainties. The 50 Hz SIRU output is used to propagate and interpolate the pointing estimates to the target time tags.

The SIRU consists of four hemispherical resonator gyros arranged with their sense axes forming an octahedral tetrad pyramid shape. The gyros are of the rate integrating type, outputting an angle expressed as an integer count which wraps as the output register overflows or underflows. One count is equal to 0.05 arcseconds. The overall unit is effectively a black box with four output registers that are updated at 100 Hz, one for each sense axis. The spacecraft records the values in the output registers asynchronously at 50 Hz, along with a time tag.

The angular output is transformed into rates by calculating the angular change per unit time in a preprocessor. The same preprocessor edits out repeated records, outliers, and other problem data. One reason for converting from angles to rates is that the filter state represents attitude and rate but requires the rate to come from an external source. No attempt is made to model the rotational dynamics of the spacecraft and integrate the angular accelerations. Instead, rates are taken directly from the SIRU. This is referred to as model replacement.

In model replacement, the dynamical model found in many Kalman filters is replaced by empirical rate observations. The contribution to rate knowledge from the filter is the time-varying rate bias correction $\hat{\mathbf{b}}$ estimated during the measurement updates. Though no attempt is made to model and predict the rate in the filter, the information in the LRS star observations and SST attitude observations enable estimation of the rate correction $\hat{\mathbf{b}}$. This is particularly important because $\hat{\mathbf{b}}$ absorbs the effects of SIRU alignment variations. Variations of $\mathbf{A}_b^{SIRU}$ appear directly as variations in $\hat{\mathbf{b}}$.

SIRU output is used for several specific, discrete tasks within the implementation of the processor:

1. Propagating the body frame attitude estimate $\mathbf{A}_i^b$ forward in time from one star update to the next.
2. Calculating the state transition matrix $\mathbf{\Phi}$ for propagation of the state covariance $\mathbf{P}$ forward in time from one star update to the next.
3. Propagation of LRS star and laser observations over short time intervals (<<0.1 seconds). These are effectively small corrections to align time tags and closely related to simple interpolation.
4. Monitoring for higher-frequency pointing variations (jitter).

More indirectly, parameter estimates characterizing the SIRU also appear directly in the process noise matrix $\mathbf{Q}$ and determine the growth of body frame attitude uncertainty between star updates.

4.4.1 SIRU Geometry and Coordinate Frame Definitions

Several high-level SIRU characteristics can be inferred from OSC and NG documentation. Figure 4 illustrates the OSC spacecraft coordinate frame with +Z in the nadir direction, +Y opposite the solar array (orbit normal direction and pitch axis), and +X out of the page (velocity direction and roll axis). The first question is how does the SIRU frame (gyro unit coordinate frame) relate to the spacecraft frame?

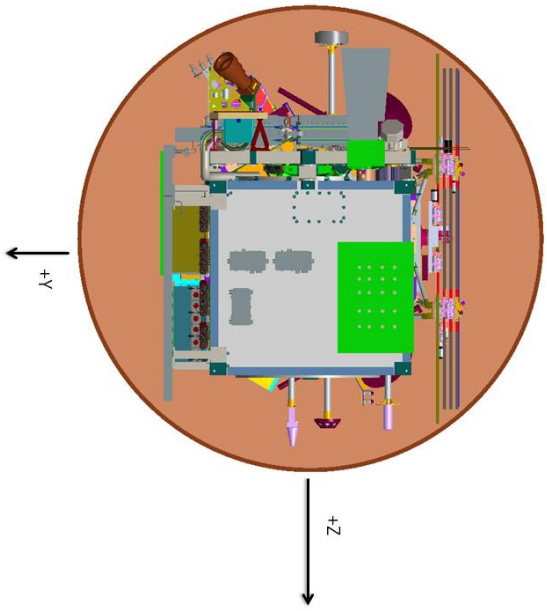

Figure 4 OSC spacecraft frame and SIRU (upper left).

Figure 5 is taken from OSC documentation of the IMSC and seems to show an early SST orientation that has since been changed. Comparing the three IMSC support feet or brackets to other figures indicates that the OSC spacecraft frame +Y direction is to the right. This orientation and the details of the SIRU agree with Figure 6 below.

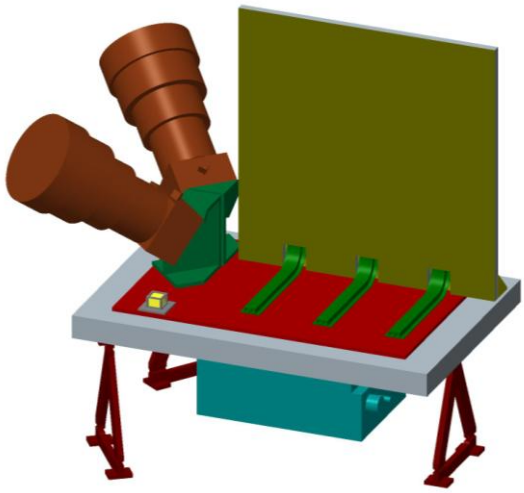

Figure 5 IMSC and SIRU. OSC spacecraft frame +Y is towards the right.

Figure 6 is taken from NG documentation and shows the SIRU coordinate frame definition. This definition seems to agree with the OSC spacecraft frame in the previous two figures. The

inference is that the SIRU frame and spacecraft frame are meant to be aligned and have similar axes and definitions. This is the working assumption here. If this assumption is incorrect, it is probably wrong by a simple 90° or 180° rotation about the +Z axis and does not have a qualitative effect on the discussion below.

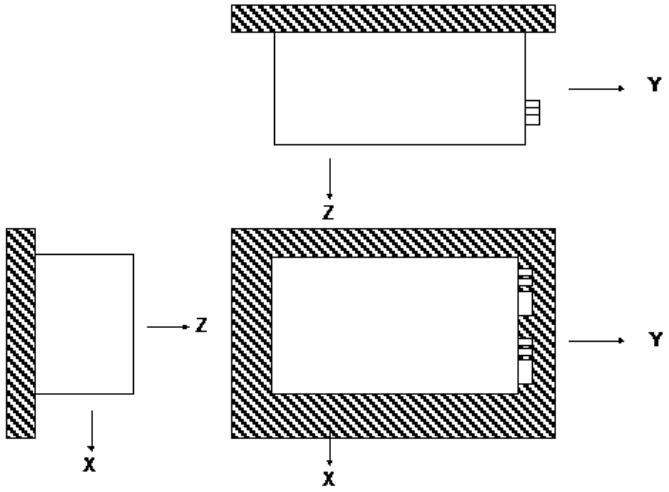

Figure 6 SIRU coordinate frame. This seems to match the OSC spacecraft frame.

Figure 7 is from NG documentation and shows the sense axes relative to the SIRU frame (and therefore the spacecraft frame as well). In summary, the four sense axes symmetrically divide the four spacecraft frame roll and pitch directions (+X, +Y, -X, –Y). Each sense axis is 54.736° from the roll and pitch axes (or their negatives). $\cos(54.736^\circ) = 0.5774$ so the sense axes measure 0.5774 of the rotation about their neighboring roll and pitch axes.

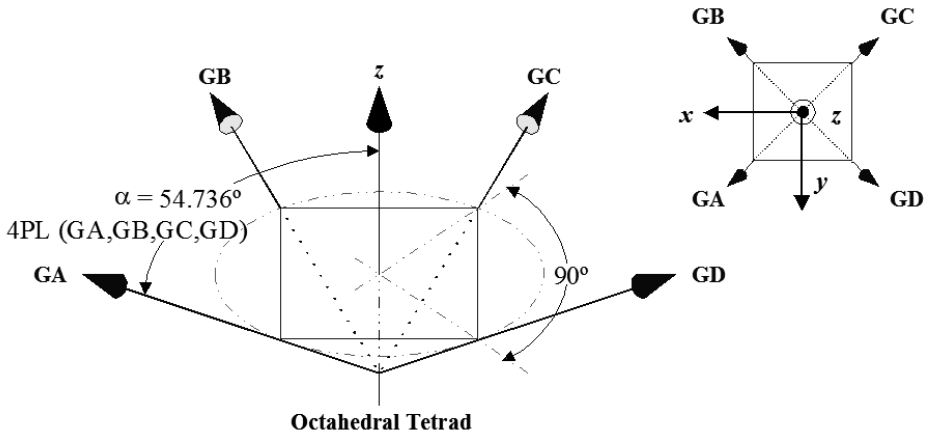

Figure 7 SIRU coordinate frame and sense axes

The observed SIRU frame rate $\boldsymbol{\omega}_{SIRU}(t)$ expressed in the SIRU frame is given by

$$\mathbf{G}_{4\times3}\boldsymbol{\omega}_{SIRU}(t) = \boldsymbol{\omega}_s(t) \tag{167}$$

where $\mathbf{G}$ is a 4×3 matrix relating the four sense axes rates $\boldsymbol{\omega}_s(t)$ to $\boldsymbol{\omega}_{SIRU}(t)$. For the simplest case $\mathbf{G} = \mathbf{W}^T$ where the ideal sense axes directions expressed in the gyro unit frame are the columns of $\mathbf{W}$ and $\boldsymbol{\omega}_{SIRU}(t)$ is given by

$$\mathbf{W}^T\boldsymbol{\omega}_{SIRU}(t) = \boldsymbol{\omega}_s(t) \tag{168}$$

$$\boldsymbol{\omega}_{SIRU}(t) = (\mathbf{W}\mathbf{W}^T)^{-1}\mathbf{W}\boldsymbol{\omega}_s(t) \tag{169}$$

The ideal sense axes directions expressed in the SIRU frame are the columns of $\mathbf{W}$ and NG documentation provides the following definition

$$\mathbf{W} = \frac{1}{\sqrt{3}}\begin{bmatrix} 1 & 1 & -1 & -1 \\ 1 & -1 & -1 & 1 \\ 1 & 1 & 1 & 1 \end{bmatrix} \tag{170}$$

The estimated body frame rate $\hat{\boldsymbol{\omega}}$ expressed in the body frame is given by $\hat{\boldsymbol{\omega}} = (\mathbf{A}_b^{SIRU})^T\boldsymbol{\omega}_{SIRU} + \hat{\mathbf{b}}$, and if the body frame definition is equivalent to the OSC spacecraft frame then $\mathbf{A}_b^{SIRU} = \mathbf{I}$ and $\hat{\boldsymbol{\omega}} = \boldsymbol{\omega}_{SIRU} + \hat{\mathbf{b}}$.

4.4.2 Sense Axes Angular Counts and Angular Rates

The four sense axes are rate-integrating gyros and the SIRU outputs a vector $\boldsymbol{\theta}_s(t_k)$ of four angular counts with units of 0.05 arcseconds per count. The counts range from 0 to 65,535 and wrap on underflow or overflow. When counts increase past 65,535 they wrap to 0, and when they decrease past 0 they wrap to 65,535. Some significant angular count quantities for nadir pointing are shown in Table 6.

Table 6 SIRU sense axis angular counts during nadir pointing

	50 Hz, 0.02 seconds	10 Hz, 0.1 seconds	1 Hz, 1 second
Pitch axis, arcsec	4.56 arcsec	22.8 arcsec	228 arcsec
Sense axis, arcsec	2.63 arcsec	13.16 arcsec	131.65 arcsec
Sense axis, counts	53 counts	263 counts	2632 counts

In general, the significant information in the SIRU output is the angular increment $\Delta\boldsymbol{\theta}_s(t_k)$ from t_k and t_{k+1} given by

$$\Delta\boldsymbol{\theta}_s(t_k) \equiv \boldsymbol{\theta}_s(t_{k+1}) - \boldsymbol{\theta}_s(t_k) \tag{171}$$

The angles must be unwrapped during the calculation of $\Delta\boldsymbol{\theta}_s(t_k)$ in order to get correct or even reasonable results. The four sense axis increments $\Delta\boldsymbol{\theta}_s(t_k)$ can be converted to three SIRU frame angular increments $\Delta\boldsymbol{\theta}_{SIRU}(t_k)$ by

$$\Delta\boldsymbol{\theta}_{SIRU}(t_k) = (\mathbf{W}\mathbf{W}^T)^{-1}\mathbf{W}\Delta\boldsymbol{\theta}_s(t_k) \tag{172}$$

$\boldsymbol{\theta}_s(t_k)$ and $\Delta\boldsymbol{\theta}_{SIRU}(t_k)$ are expressed about the sense axes directions or SIRU frame axes. $\Delta\boldsymbol{\theta}_{SIRU}(t_k)$ is closely related to common roll-pitch-yaw Euler angles which are also expressed about the coordinate frame axes. This suggests that $\Delta\boldsymbol{\theta}_{SIRU}(t_k)$ is useful information in its own right (and $\Delta\boldsymbol{\theta}_s(t_k)$ as well by extension) since it reflects roll-pitch-yaw magnitude. This is particularly true over time intervals short enough that the SIRU frame does not change (rotate) significantly. Over short enough time intervals the SIRU frame can be propagated using $\Delta\boldsymbol{\theta}_{SIRU}(t_k)$ alone, without involving an angular rate $\boldsymbol{\omega}_{SIRU}(t_k)$ and integration.

Angular rates about each sense axis $\boldsymbol{\omega}_s(t_k) = \mathbf{f}(\Delta\boldsymbol{\theta}_s(t_k))$ and $\boldsymbol{\omega}_{SIRU}(t_k)$ are calculated as observed angular change per unit time.

$$\boldsymbol{\omega}_s(t_k) \equiv \frac{\boldsymbol{\theta}_s(t_{k+1}) - \boldsymbol{\theta}_s(t_k)}{t_{k+1} - t_k} = \frac{\Delta\boldsymbol{\theta}_s(t_k)}{\Delta t} \tag{173}$$

$$\boldsymbol{\omega}_{SIRU}(t) = (\mathbf{W}\mathbf{W}^T)^{-1}\mathbf{W}\frac{\Delta\boldsymbol{\theta}_s(t_k)}{\Delta t} \tag{174}$$

One of the advantages of angular rates $\boldsymbol{\omega}_s(t_k)$ and $\boldsymbol{\omega}_{SIRU}(t_k)$ is that the filter estimates their biases $\hat{\mathbf{b}}$ for correcting $\hat{\boldsymbol{\omega}}$ in $\hat{\boldsymbol{\omega}} = (\mathbf{A}_b^{SIRU})^T\boldsymbol{\omega}_{SIRU} + \hat{\mathbf{b}}$.

The 50 Hz SIRU output is monitored in both the time and frequency domains for evidence of high frequency pointing variations. Due to the sampling theorem, this evidence can be more qualitative than quantitative. Correlations with entering and exiting eclipse, solar panel motion, maneuvers, changes of ATLAS state, etc are of particular interest. An important question is which forms of the output are more useful and significant in practice: $\Delta\boldsymbol{\theta}_s(t_k)$, $\Delta\boldsymbol{\theta}_{SIRU}(t_k)$, $\boldsymbol{\omega}_s(t_k)$, or $\boldsymbol{\omega}_{SIRU}(t_k)$. In principal the information content in the four forms is equivalent. In practice the ease of interpretation may vary.

4.4.3 Signal Processing

Time and frequency domain analysis of the SIRU output have a direct influence on the estimated pointing uncertainty, along with the expected performance as characterized by the pointing and jitter requirements. Jitter refers here to pointing variation at frequencies that are too high to be

observed by the SIRU, but different hypothetical cases and their effects on the SIRU output and pointing uncertainty can be characterized. In other words, the estimated pointing uncertainties should reflect both all of the information content in the SIRU output, and the expected performance based on the pointing requirements. A significant question is how as much information can be extracted from the SIRU as possible.

The discussion here focuses on time and frequency domain signal processing for a generic signal time series $x(t_k)$ at sample times t_k with approximately constant sampling intervals Δt so that $t_{k+1} - t_k \approx \Delta t$. Here $x(t_k)$ represents one component taken from of any of the time series $\Delta\boldsymbol{\theta}_s(t_k)$, $\Delta\boldsymbol{\theta}_{SIRU}(t_k)$, $\boldsymbol{\omega}_s(t_k)$, or $\boldsymbol{\omega}_{SIRU}(t_k)$. For example $x(t_k)$ can be the pitch component of $\Delta\boldsymbol{\theta}_{SIRU}(t_k)$ or $\boldsymbol{\omega}_{SIRU}(t_k)$, or the sense axis A component of $\Delta\boldsymbol{\theta}_s(t_k)$ or $\boldsymbol{\omega}_s(t_k)$. No distinction is necessary in the signal processing here; the signal here is simply a generic time series $x(t_k)$. In the interpretation of the results the units associated with the signals should be carefully distinguished: $\Delta\boldsymbol{\theta}_s(t_k)$ and $\Delta\boldsymbol{\theta}_{SIRU}(t_k)$ are arcseconds or radians, $\boldsymbol{\omega}_s(t_k)$ and $\boldsymbol{\omega}_{SIRU}(t_k)$ are arcsec/s or rad/s.

In practice we are primarily interested here in the high frequency components $x_H(t_k)$ within $x(t_k)$ and the first step is to remove the lowest frequency components $x_L(t_k)$ leaving

$$x_H(t_k) = x(t_k) - x_L(t_k) - b \tag{175}$$

where b is a constant bias and $x_H(t_k)$ is approximately zero-mean, $E\{x_H(t_k)\} \approx 0$, over longer time scales The low frequency components in $x_L(t_k)$ represents trends, variations, and deviations from the constant b over longer time scales. In short, removing the bias and low frequency components leaves the approximately zero-mean high frequency components $x_H(t_k)$.

The question here is how to estimate $x_L(t_k)$ in the time domain in order to subtract it from $x(t_k)$. One approach is to Fourier transform the time domain signal $x(t_k)$ into the frequency domain $X(\omega)$ and remove the low frequencies $X_L(\omega)$ using a frequency domain high-pass filter. Instead, the same effect will be achieved here by directly estimating $x_L(t_k)$ in the time domain for ease of physical interpretation.

One method for estimating $x_L(t_k)$ is a moving average (moving window average, boxcar average, etc). The moving average function is represented here by $ma_\alpha(\ )$ where the subscript α is a parameter for the amount of data to use for each average, or equivalently the averaging window size.

A more sophisticated method is locally weighted scatterplot smoothing (LOESS), represented here by the function $loess_{\alpha,\lambda}(\ )$. There are two parameters α and λ: α again represents the

amount of data to use for each fit, and λ is the degree of the local fit polynoial. When $\lambda = 0$ LOESS is exactly equivalent to the moving average function, $loess_{\alpha,\lambda=0}(\ ) = ma_{\alpha}(\ )$. For $\lambda = 1$ and $\lambda = 2$ linear or quadratic polynomials are fit within each data window. Examples of LOESS results for two time series are shown in Figure 8. In the figure on the right, LOESS results for different parameters α and λ are shown in red and blue. Different low frequency ranges can be estimated and removed depending on the LOESS tuning.

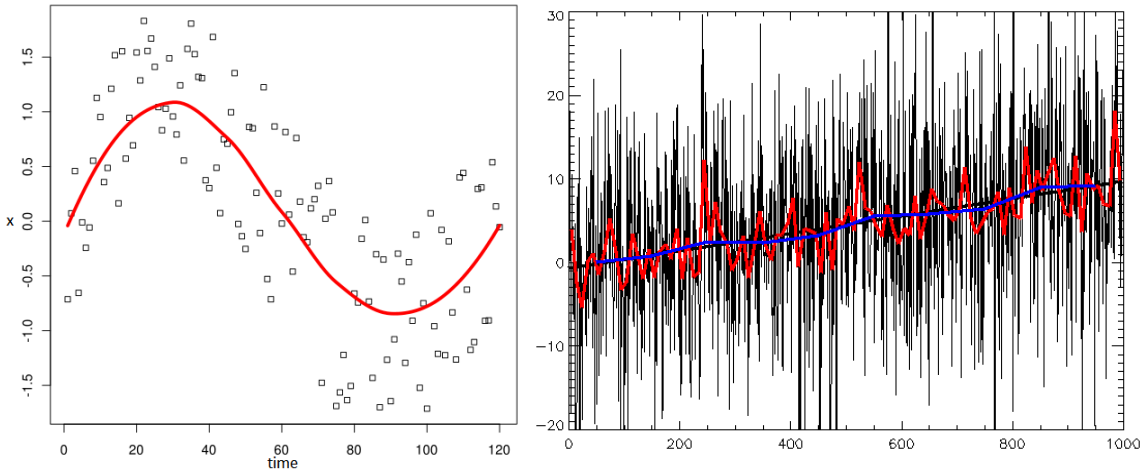

Figure 8 Examples of LOESS results for the low frequency signals (red and blue) in two time series.

With $x_L(t_k) = loess_{\alpha,\lambda}(x, t_k)$ and

$$x_H(t_k) = x(t_k) - loess_{\alpha,\lambda}(x, t_k) - b \tag{176}$$

the approximately zero mean high frequency variations can be analyzed in the time domain $x_H(t_k)$ or Fourier transformed into the frequency domain $X_H(\omega)$.

With 50 Hz sampling of the SIRU output the sampling theorem states that the usable bandwidth for detecting periodic signals is $50Hz/2 = 25Hz$. In practice signals up to approximately $0.9(50Hz/2) = 22.5Hz$ may be detectable in $X_H(\omega)$ using the rule of thumb that about 0.1 of the usable bandwidth is lost to filter roll-off and noise. This is a useful amount of bandwidth for monitoring the time series $\Delta\boldsymbol{\theta}_s(t_k)$, $\Delta\boldsymbol{\theta}_{SIRU}(t_k)$, $\boldsymbol{\omega}_s(t_k)$, and $\boldsymbol{\omega}_{SIRU}(t_k)$. For example, the types of pointing variations observed on ICESat-1 during solar array rotation (1 Hz and 3 Hz, Ref. [43]) should be easily detected and characterized in roll and pitch from $\Delta\boldsymbol{\theta}_{SIRU}(t_k)$ alone.

4.4.4 Measurement Model and Parameters

The SIRU measurement model combines the four observed sense axes rates into the three-component angular rate vector for the SIRU frame. This is a linear geometric transformation,

summing the contributions from the rates about the four sense axes to the rates about the three SIRU frame axes. It plays a role similar to the first-order pinhole camera model for the LRS, converting centroid positions to a three-dimensional vector observation.

The measurement model includes several types of corrections for each sense axes including geometric misalignment from the ideal octahedral tetrad, and scale factors of various types. Ground test values for these parameters are provided by NG, and parameter estimation is performed using flight data. Angular rate variations are required to make many of the parameters observable. Special SIRU calibration maneuvers will be performed, and the periodic ocean scan maneuvers may be useable as well.

The SIRU measurement model is the matrix $\mathbf{G}$ given by

$$\mathbf{G} = (\mathbf{I} - \mathbf{\Lambda})(\mathbf{W} - \mathbf{U}\mathbf{\Delta}_{\mathbf{v}} - \mathbf{V}\mathbf{\Delta}_{\mathbf{u}})^T \tag{177}$$

where $\mathbf{\Lambda} \equiv diag(\boldsymbol{\lambda})$ for scale factors $\boldsymbol{\lambda}_{4\times1}$, and $\mathbf{\Delta}_{\mathbf{u}} \equiv diag(\mathbf{u})$, $\mathbf{\Delta}_{\mathbf{v}} \equiv diag(\mathbf{v})$ for sense axes misalignments $\mathbf{u}_{4\times1}$ and $\mathbf{v}_{4\times1}$. The sense axes outputs are incorporated into the filter as the SIRU frame angular increment and angular rate

$$\Delta\boldsymbol{\theta}_{SIRU}(t) = (\mathbf{G}^T\mathbf{G})^{-1}\mathbf{G}^T\Delta\boldsymbol{\theta}_s(t) \tag{178}$$

$$\boldsymbol{\omega}_{SIRU}(t) = (\mathbf{G}^T\mathbf{G})^{-1}\mathbf{G}^T\boldsymbol{\omega}_s(t) \tag{179}$$

and the body frame angular rate estimate

$$\hat{\boldsymbol{\omega}} = (\mathbf{A}_b^{SIRU})^T\boldsymbol{\omega}_{SIRU} + \hat{\mathbf{b}} \tag{180}$$

The rate bias estimate $\hat{\mathbf{b}}$ is also classed as part of the measurement model. The rate bias for a sense axis is the observed rate when the true rate is zero. The time varying corrections $\hat{\mathbf{b}}(t)$ are critical and updated as frequently as possible. When the angular rates are approximately constant the effects of the model parameters in $\mathbf{G}$ are effectively absorbed in $\hat{\mathbf{b}}(t)$. The $\hat{\mathbf{b}}(t)$ term also plays an important alignment role by effectively absorbing the effects of variations in $\mathbf{A}_b^{SIRU}$ [9, 10].

The misalignment terms $\mathbf{\Delta}_{\mathbf{u}} \equiv diag(\mathbf{u})$ and $\mathbf{\Delta}_{\mathbf{v}} \equiv diag(\mathbf{v})$ correct for deviations of the sense axes away from the ideal octahedral tetrad pyramid shape defined by

$$\mathbf{W} = \frac{1}{\sqrt{3}}\begin{bmatrix} 1 & 1 & -1 & -1 \\ 1 & -1 & -1 & 1 \\ 1 & 1 & 1 & 1 \end{bmatrix} \tag{181}$$

The ideal sense axes directions expressed in the SIRU frame are the columns of the geometry matrix $\mathbf{W}$. A $\hat{\mathbf{u}}, \hat{\mathbf{v}}, \hat{\mathbf{w}}$ coordinate frame is defined for each sense axis, with the $\hat{\mathbf{w}}$ axis along the ideal direction and appearing as one of the columns in $\mathbf{W}$. The $\hat{\mathbf{u}}$ and $\hat{\mathbf{v}}$ axes can be defined by convention (agreement) or deterministic methods described in the literature [9, 11, 17]. The geometry matrices $\mathbf{U}$ and $\mathbf{V}$ are defined as

$$\mathbf{U} = \begin{bmatrix} \hat{\mathbf{u}}_1 & \hat{\mathbf{u}}_2 & \hat{\mathbf{u}}_3 & \hat{\mathbf{u}}_4 \end{bmatrix} \tag{182}$$

$$\mathbf{V} = \begin{bmatrix} \hat{\mathbf{v}}_1 & \hat{\mathbf{v}}_2 & \hat{\mathbf{v}}_3 & \hat{\mathbf{v}}_4 \end{bmatrix} \tag{183}$$

with the columns again expressing the ideal direction in the SIRU frame.

The deviation of each sense axis away from its ideal direction is expressed as a two-dimensional rotation vector u, v in the plane orthogonal to the ideal direction. Collected together, the deviations for all the axes form the misalignment vectors $\mathbf{u}_{4\times1}$ and $\mathbf{v}_{4\times1}$.

The scale factor term $\mathbf{\Lambda} \equiv diag(\boldsymbol{\lambda})$ corrects for differences between the real and observed rate variations. If the real rate is varied as a linear ramp, the observed rate should also vary as a linear ramp with the same slope. The scale factor λ_i is the correction for the *i*th sense axis. There are variations on this concept, such as symmetric scale factors that are the same for positive and negative rates, or asymmetric scale factors that are different for positive and negative rates [11, 17].

4.4.5 Error Model and Parameters

The SIRU error model describes stochastic processes contributing to the SIRU output. The error model is closely associated with the uncertainties in the pointing knowledge product. The dominant uncertainties appear in the filter as attitude and rate process noise, which are tied to the error model.

Kalman filter gyro error models are commonly based on parameter estimates for angular white noise (AWN), angular random walk (ARW), and rate random walk (RRW). The filter is assumed here to be of the model replacement type with gyros replacing dynamical modeling in the filter state equation.

In model replacement mode the SIRU measurements do not enter the filter via measurement updates, and error modeling does not enter the filter as measurement noise. Instead, SIRU error modeling enters via the process or state noise, and is characterized by parameters for AWN, ARW, and RRW. These parameters serve as approximations and simplifications for the parameters in a full gyro error model such as the IEEE standard model in reference [44].

Stochastic errors over short time scales are associated with AWN and ARW and can generically be associated with gyro noise (as opposed to gyro drift). Pointing uncertainty over short time scales is of special importance here because the SIRU provides all of the available shorter time scale (higher frequency) pointing information. SIRU noise, parameterized as σ_{awn}^2 and σ_{arw}^2, and the SIRU output recording rate of 50 Hz are the main limitations on 50 Hz pointing knowledge.

In practice the output from a rate integrating gyro held motionless in inertial space does not remain constant. AWN is a zero-mean Gaussian white noise variation of the output. Its parameter estimate is angular white noise variance σ_{awn}^2 and has units of radians^2. Its effects can be driven down by increasing the sample size.

ARW is a stochastic process described as integrated white noise and results in a angular bias in the output time series $\boldsymbol{\theta}(t_k)$. The angular bias growth is proportional to the root of the time span so slows over time. Its parameter estimate is angular random walk variance σ_{arw}^2 and has units of radians^2/second.

In the filter process noise matrix

$$\mathbf{Q}_k(t) = \begin{bmatrix} (\sigma_{awn}^2 + t\sigma_{arw}^2 + (t^3/3)\sigma_{rrw}^2)\mathbf{I} & (t^2/2)\sigma_{rrw}^2\mathbf{I} \\ (t^2/2)\sigma_{rrw}^2\mathbf{I} & t\sigma_{rrw}^2\mathbf{I} \end{bmatrix} \tag{184}$$

$\sigma_{awn}^2 + t\sigma_{arw}^2$ are the dominant terms over short time scales. Over longer time scales the σ_{rrw}^2 terms become dominant. In MEKF-based alignment and attitude filtering, RRW is used to characterize bias instability and can generically be associated with gyro drift (as opposed to gyro noise). With 10 Hz observations from the LRS star tracker and two SSTs, the filter does not experience long time intervals between measurement updates and the cumulative effects of gyro drift are kept small.

4.4.6 Filter Propagation

Propagation of the body frame attitude estimate $\mathbf{A}_i^b$ over a specified time interval is performed by integrating the body frame angular rate estimate $\hat{\boldsymbol{\omega}}$ given by

$$\hat{\boldsymbol{\omega}} = (\mathbf{A}_b^{SIRU})^T \boldsymbol{\omega}_{SIRU} + \hat{\mathbf{b}} \tag{185}$$

Over a time interval $t_{k+1} - t_k$ short enough that $\hat{\boldsymbol{\omega}}$ is approximately constant, the propagation rotation vector is given by

$$\mathbf{a} = (t_{k+1} - t_k)\hat{\boldsymbol{\omega}}(t_k) \tag{186}$$

For $\mathbf{A}_i^b$ expressed as a quaternion q_{ref} and the rotation vector $\mathbf{a}$ expressed as a quaternion $q(\mathbf{a})$, propagation of the attitude and state from t_k to t_{k+1} is given by

$$q_{ref}(t_{k+1}) = q(\mathbf{a}) \otimes q_{ref}(t_k) \tag{187}$$

$$\hat{\mathbf{x}}(t_{k+1}) = \hat{\mathbf{x}}(t_k) \tag{188}$$

Attitude propagation when the assumption of approximately constant $\hat{\boldsymbol{\omega}}$ is not valid because $t_{k+1} - t_k$ is too long or $d\hat{\boldsymbol{\omega}}/dt$ is too large is discussed in reference [15]. Note that these conditions can result if the SIRU telemetry has a high rate. In practice, with 50 Hz SIRU telemetry there may be times when the assumption that $d\hat{\boldsymbol{\omega}}/dt \approx 0$ over $t_{k+1} - t_k$ breaks down. The attitude can then be propagated using what is referred to here as the Inertial Navigation System (INS) method described in reference [15].

The INS method was designed with high frequency jitter and high gyro sampling rates in mind and is a relatively accurate way to calculate the rotation vector $\mathbf{a}$ in Eq. (187). Jitter and rapid maneuvers can cause an unwanted effect termed coning during attitude propagation. The INS method is based on the Bortz equation, the kinematic equation for the rate of change of a rotation vector $\mathbf{a}$.

The Bortz equation for $d\mathbf{a}/dt$ is given by

$$\begin{aligned} d\mathbf{a}/dt &\approx \boldsymbol{\omega} + (\boldsymbol{\alpha} \times \boldsymbol{\omega})/2 \\ &\equiv \dot{\boldsymbol{\alpha}} + \dot{\boldsymbol{\beta}} \end{aligned} \tag{189}$$

where $\boldsymbol{\alpha} \equiv \int \boldsymbol{\omega} dt$ represents integrated angular rate and $\boldsymbol{\beta} \equiv \int (\boldsymbol{\alpha} \times \boldsymbol{\omega})/2\, dt$ represents coning motion. When the coning motion is negligible $d\mathbf{a}/dt \approx \boldsymbol{\omega}$ which is equivalent to Eq. (186).

The objective of the INS method is to calculate the rotation vector $\mathbf{a}_m$ after a time interval t_m from initial conditions $t_0 = 0$ and $\mathbf{a}_0 = \mathbf{a}(t_0) = \mathbf{0}$. The time interval t_0 to t_m is termed the slow-cycle and in practice corresponds the total propagation interval, here the time between two filter measurement updates.

There are a number of sub-intervals termed the fast-cycle and defined by SIRU measurement. The index l indicates which fast-cycle is currently being processed, beginning with $l = 0$ at $t_0 = 0$. The calculations in each fast-cycle staring with $l = 1$ are shown below, where $\boldsymbol{\alpha}_0 = \mathbf{0}$ and $\boldsymbol{\beta}_0 = \mathbf{0}$. In practice $\Delta\boldsymbol{\alpha}_l$ is a SIRU angular increment $\Delta\boldsymbol{\theta}_{SIRU}(t_k)$ from Eq. (171). In other words the INS method both assumes and is designed for rate-integrating gyro output.

$$\Delta\boldsymbol{\alpha}_l = \int_{t_{l-1}}^{t_l} d\boldsymbol{\alpha} \tag{190}$$

$$\Delta\boldsymbol{\beta}_l = \frac{1}{2}\left(\boldsymbol{\alpha}_{l-1} + \frac{1}{6}\Delta\boldsymbol{\alpha}_{l-1}\right) \times \Delta\boldsymbol{\alpha}_l \tag{191}$$

$$\boldsymbol{\alpha}_l = \boldsymbol{\alpha}_{l-1} + \Delta\boldsymbol{\alpha}_l \tag{192}$$

$$\Delta\boldsymbol{\beta}_l = \boldsymbol{\beta}_{l-1} + \Delta\boldsymbol{\beta}_l \tag{193}$$

When $t_l = t_m$ the fast-cycle calculations are complete and $\mathbf{a}_m$ is given by

$$\mathbf{a}_m = \boldsymbol{\alpha}_l + \boldsymbol{\beta}_l \tag{194}$$

Essentially what the INS method provides that the basic propagation of Eq. (186) does not is the effect of the coning term $\boldsymbol{\beta}_l$.

For covariance propagation, the state transition matrix is given by

$$\boldsymbol{\Phi}_k(t) = \begin{bmatrix} \mathbf{R}(\mathbf{a}) & \mathbf{S}(\mathbf{a}) & & & & \\ \mathbf{0}_{3\times3} & \mathbf{I}_{3\times3} & & & & \\ & & \mathbf{I}_{3\times3} & & & \\ & & & \mathbf{I}_{3\times3} & & \\ & & & & \mathbf{I}_{3\times3} & \end{bmatrix} \tag{195}$$

$$\mathbf{R}(\mathbf{a}) = (\cos a)\mathbf{I} - \left(\frac{\sin a}{a}\right)[\mathbf{a}\times] + \left(\frac{1-\cos a}{a^2}\right)\mathbf{a}\mathbf{a}^{\mathbf{T}} \tag{196}$$

$$\mathbf{S}(\mathbf{a}) = t\left[\left(\frac{\sin a}{a}\right)\mathbf{I} - \left(\frac{1-\cos a}{a^2}\right)[\mathbf{a}\times] + \left(\frac{a-\sin a}{a^3}\right)\mathbf{a}\mathbf{a}^{\mathbf{T}}\right] \tag{197}$$

and the propagated covariance is $\mathbf{P}_{k+1} = \boldsymbol{\Phi}_k \mathbf{P}_k \boldsymbol{\Phi}_k^T + \mathbf{Q}_k$.

Table 7 Rotation vectors $\mathbf{a}_{k-1}^{k}$ are needed to propagate the attitude between obs.

k	t_k, msec	Δt, msec	Obs	Attitude estimate	Need
1	0	-	Gyro	$\mathbf{A}_i^b(t_1)$	-
2	4.74	4.74	Star (LRS)	$\mathbf{A}_i^b(t_2)_- = \mathbf{A}(\mathbf{a}_1^2)\mathbf{A}_i^b(t_1) \rightarrow \mathbf{A}_i^b(t_2)_+$	$\mathbf{a}_1^2$
3	9.32	4.58	Laser	$\mathbf{A}_i^b(t_3) = \mathbf{A}(\mathbf{a}_2^3)\mathbf{A}_i^b(t_2)_+$	$\mathbf{a}_2^3$
4	20.01	10.69	Gyro	$\mathbf{A}_i^b(t_4) = \mathbf{A}(\mathbf{a}_3^4)\mathbf{A}_i^b(t_3)$	$\mathbf{a}_3^4$
5	29.34	9.33	Laser	$\mathbf{A}_i^b(t_5) = \mathbf{A}(\mathbf{a}_4^5)\mathbf{A}_i^b(t_4)$	$\mathbf{a}_4^5$
6	40.01	10.67	Gyro	$\mathbf{A}_i^b(t_6) = \mathbf{A}(\mathbf{a}_5^6)\mathbf{A}_i^b(t_5)$	$\mathbf{a}_5^6$
7	49.33	9.32	Laser	$\mathbf{A}_i^b(t_7) = \mathbf{A}(\mathbf{a}_6^7)\mathbf{A}_i^b(t_6)$	$\mathbf{a}_6^7$
8	53.48	4.15	Star (SST2)	$\mathbf{A}_i^b(t_8)_- = \mathbf{A}(\mathbf{a}_7^8)\mathbf{A}_i^b(t_7) \rightarrow \mathbf{A}_i^b(t_8)_+$	$\mathbf{a}_7^8$
9	60.01	6.53	Gyro	$\mathbf{A}_i^b(t_9) = \mathbf{A}(\mathbf{a}_8^9)\mathbf{A}_i^b(t_8)_+$	$\mathbf{a}_8^9$

This table shows a representative time series of events. The events consist of the arrival of incoming observations (telemetry) from the three types of sensors: star, gyro, and laser. The star observations provide filter updates as indicated by the notation $\mathbf{A}_i^b(t_k)_- \rightarrow \mathbf{A}_i^b(t_k)_+$ for the update of the predicted attitude $\mathbf{A}_i^b(t_k)_-$ to the updated attitude $\mathbf{A}_i^b(t_k)_+$.

To form the laser pointing product, the attitude estimates $\mathbf{A}_i^b(t_3)$, $\mathbf{A}_i^b(t_5)$, and $\mathbf{A}_i^b(t_7)$ for the laser observations at t_3, t_5, and t_7 are needed. The problem reduces to estimating the eight rotation vectors $\mathbf{a}_1^2$, $\mathbf{a}_2^3$, $\mathbf{a}_3^4$, $\mathbf{a}_4^5$, $\mathbf{a}_5^6$, $\mathbf{a}_6^7$, $\mathbf{a}_7^8$, and $\mathbf{a}_8^9$.

Table 8 Estimation of the rotation vectors $\mathbf{a}_{k-1}^{k}$ using the SIRU output.

k	t_k, msec	Obs	Rate information	Estimate
1	0	Gyro $\boldsymbol{\theta}_s(t_1)$		-
2	4.74	Star (LRS)		$\hat{\mathbf{a}}_1^2 = (t_2 - t_1)\hat{\boldsymbol{\omega}}_a$
3	9.32	Laser		$\hat{\mathbf{a}}_2^3 = (t_3 - t_2)\hat{\boldsymbol{\omega}}_a$
4	20.01	Gyro $\boldsymbol{\theta}_s(t_4)$	$\hat{\boldsymbol{\omega}}_a = \mathbf{H}(\boldsymbol{\theta}_s(t_4) - \boldsymbol{\theta}_s(t_1))/(t_4 - t_1) + \hat{\mathbf{b}}$	$\hat{\mathbf{a}}_3^4 = (t_4 - t_3)\hat{\boldsymbol{\omega}}_a$
5	29.34	Laser		$\hat{\mathbf{a}}_4^5 = (t_5 - t_4)\hat{\boldsymbol{\omega}}_b$
6	40.01	Gyro $\boldsymbol{\theta}_s(t_6)$	$\hat{\boldsymbol{\omega}}_b = \mathbf{H}(\boldsymbol{\theta}_s(t_6) - \boldsymbol{\theta}_s(t_4))/(t_6 - t_4) + \hat{\mathbf{b}}$	$\hat{\mathbf{a}}_5^6 = (t_6 - t_5)\hat{\boldsymbol{\omega}}_b$
7	49.33	Laser		$\hat{\mathbf{a}}_6^7 = (t_7 - t_6)\hat{\boldsymbol{\omega}}_c$
8	53.48	Star (SST2)		$\hat{\mathbf{a}}_7^8 = (t_8 - t_7)\hat{\boldsymbol{\omega}}_c$
9	60.01	Gyro $\boldsymbol{\theta}_s(t_9)$	$\hat{\boldsymbol{\omega}}_c = \mathbf{H}(\boldsymbol{\theta}_s(t_9) - \boldsymbol{\theta}_s(t_6))/(t_9 - t_6) + \hat{\mathbf{b}}$	$\hat{\mathbf{a}}_8^9 = (t_9 - t_8)\hat{\boldsymbol{\omega}}_c$

The method for estimating the eight rotation vectors $\mathbf{a}_1^2$, $\mathbf{a}_2^3$, $\mathbf{a}_3^4$, $\mathbf{a}_4^5$, $\mathbf{a}_5^6$, $\mathbf{a}_6^7$, $\mathbf{a}_7^8$, and $\mathbf{a}_8^9$ shown here is designed to incorporate gyro measurement model information represented by $\mathbf{A}_b^{SIRU}$, $\mathbf{G}$, and $\hat{\mathbf{b}}$ with $\mathbf{H} \equiv (\mathbf{A}_b^{SIRU})^T(\mathbf{G}^T\mathbf{G})^{-1}\mathbf{G}^T$. The raw SIRU vectors $\boldsymbol{\theta}_s(t_k)$ are assumed to be unwrapped. Each $\boldsymbol{\theta}_s(t_k)$ contains four angular counts with units of 0.05 arcseconds per count. The counts range from 0 to 65,535 and wrap on underflow or overflow. Unwrapping simply means that $\boldsymbol{\theta}_s(t_k) - \boldsymbol{\theta}_s(t_{k-1})$ gives the correct, meaningful result $\Delta\boldsymbol{\theta}_s$ despite the wrapping in the raw data.

The estimated rotation vectors are essentially a linear interpolation between the four gyro observations, based on the estimated body frame angular rate.

5.0 Artificial Telemetry and Test Processing

Verification and performance analysis is discussed here in the context of the overall position, pointing, and geolocation knowledge system. Evaluation of pointing knowledge can be divided into four high-level steps:

1. Input truth, generated from true position, pointing, and geolocation.
2. Artificial telemetry (LRS, SSTs, SIRU).
3. Test processing.
4. Output knowledge, performance analysis compares output knowledge with input truth.

The inputs consist of time series of true values for position, pointing, and geolocation. The time series represent the truth underlying artificial LRS, SST, and SIRU telemetry. The basic concept of the four evaluation steps is to generate artificial telemetry based on the truth, then process the telemetry for pointing knowledge. The difference between input truth and output knowledge is the error introduced by the sensors and processing and is the basis for performance analysis.

The input and output steps can involve cooperation and information exchange with the position and geolocation portions of the ground system and are associated with interface control documents. Subsets of the four steps can easily be emphasized for limited testing, for example artificial telemetry and test processing in isolation (decoupled from the overall ground system). The focus here is on the most generalized configuration.

In practice, output pointing knowledge and performance analysis are organic by-products of processing the artificial telemetry. During processing the estimated body frame attitude $\mathbf{A}_i^b$, observed laser unit vector(s) $\mathbf{u}_{LT}$, and ocean scan correction $\mathbf{C}(t)$ are readily available and the output pointing knowledge is simply

$$\mathbf{u}_{ICRF}(t_k) = (\mathbf{A}_b^{LRS}\mathbf{A}_i^b(t_k))^T(\mathbf{C}(t_k)\mathbf{B})\mathbf{u}_{LT}(t_k) \tag{198}$$

as discussed in Section 4.3.6. This is directly equivalent to the expression for the input truth

$$\mathbf{u}_{ICRF} = (\mathbf{A}_{ATLAS}^{LRS}\mathbf{A}_i^{ATLAS})^T(\mathbf{A}_{LRS}^{LT})^T\mathbf{u}_{LT} \tag{199}$$

given above in Eq. (209). The correspondences between estimated (or observed) and true values are

$$\mathbf{u}_{ICRF,estimated} \Leftrightarrow \mathbf{u}_{ICRF,true} \tag{200}$$

$$\mathbf{u}_{LT,observed} \Leftrightarrow \mathbf{u}_{LT,true} \tag{201}$$

$$\mathbf{A}_b^{LRS}\mathbf{A}_i^b \Leftrightarrow \mathbf{A}_{ATLAS}^{LRS}\mathbf{A}_i^{ATLAS} \tag{202}$$

$$\mathbf{CB} \Leftrightarrow (\mathbf{A}_{LRS}^{LT})^T \tag{203}$$

where Eqs. (200) and (201) are equivalent since they are linked by Eqs. (202) and (203).

The significant performance questions are the errors (differences) between the estimated and true attitudes ($\mathbf{A}_b^{LRS}\mathbf{A}_i^b$ and $\mathbf{A}_{ATLAS}^{LRS}\mathbf{A}_i^{ATLAS}$) and between the observed and true laser vectors ($\mathbf{u}_{LT,observed}$ and $\mathbf{u}_{LT,true}$).

5.1 Coordinate Frames and Definitions

A number of terms and conventions are defined here for use throughout this document. Key terms and notation are: spacecraft frame $\mathbf{A}_i^{SC}$, body frame $\mathbf{A}_i^b$, ATLAS frame $\mathbf{A}_i^{ATLAS}$, and orbit frame $\mathbf{A}_i^{orbit}$.

The ATLAS frame is associated with simulation, modeling, and truth values. It is an abstract and ideal frame that is not necessarily tied to a sensor or empirical measurements. Pointing truth can be expressed as two time series representing the true attitude of the ATLAS frame $\mathbf{A}_i^{ATLAS}$ and the true laser unit vector(s) in the ATLAS frame.

A spacecraft frame $\mathbf{A}_i^{SC}$ is defined for onboard attitude control. The spacecraft frame is defined and effectively owned by OSC (they can in principal change the definition). There is motivation to make the ATLAS frame as compatible with the spacecraft frame as practical. This leads to the following general conventions to be used wherever practical (for the ATLAS frame, spacecraft frame, body frame, etc).

1. X axis along the centerline of the spacecraft and positive out through the ATLAS instrument.
2. Y axis opposite from the solar array.
3. Z axis parallel to the ATLAS telescope line of sight.

In the reference attitude mode (with ATLAS forward and the spacecraft behind) the X,Y,Z axes are aligned with the natural orbit frame roll, pitch, yaw axes and the overall angular rate is approximately -229 arcsec/sec Y (pitch).

The spacecraft frame is associated with the ideal Instrument Mounted Spacecraft Component (IMSC) frame. The IMSC is a natural semi-empirical (physical but without direct sensor measurements) definition because it is a compact and stable structure, and carries the SIRU and SSTs.

A generic body frame $\mathbf{A}_i^b$ is associated with estimation, filtering, and knowledge rather than truth values and artificial telemetry. In practice the body frame is equated with the attitude estimate for one or more attitude sensors, normally with the LRS frame (LRS star tracker).

One perspective on the ATLAS frame is that it represents attitude information that is useful in the widest context of the overall position, pointing, and geolocation ground system. Information of more limited interest is not included (for example LRS and SST alignments for generating artificial telemetry).

Information that is useful outside of the pointing determination group is incorporated into the ATLAS frame and the input truth (Section 5.2). Information that is only of interest to the pointing group is restricted to the artificial telemetry.

To make the ATLAS frame physically meaningful, it can be association with the ideal Instrument Mounted Spacecraft Component (IMSC) frame. An alternative is to involve the optical bench, but it is relatively large and is expected to have significant thermal deformations.

Unless stated otherwise, here the body frame $\mathbf{A}_i^b$ is associated with the LRS frame, and the ATLAS frame $\mathbf{A}_i^{ATLAS}$ is associated with the IMSC. This agrees with the associations of the body frame with estimation and the ATLAS frame with ideal known truth.

An orbit frame $\mathbf{A}_i^{orbit}$ can be defined from the basic orbit parameters in Table 9

Table 9 Orbit characteristics

	Orbit, km	Period, sec	Period, min	Speed, km/s	Rate, arcsec/s
ICESat-1	590	5779	96.33	7.56	224.3
ICESat-2	496	5663	94.38	7.61	228.8

Approximating the orbit as circular, the simulated-truth position $\mathbf{r}$ and velocity $\mathbf{v}$ expressed in the ECI frame can be used to define an as a local vertical and local horizontal coordinate frame with its $\hat{\mathbf{i}}$ axis parallel to $\mathbf{v}$, and its $\hat{\mathbf{k}}$ axis parallel to the nadir vector $-\mathbf{r}$.

$$\hat{\mathbf{i}} = \mathbf{v}/\|\mathbf{v}\| \tag{204}$$

$$\hat{\mathbf{j}} = \hat{\mathbf{k}} \times \hat{\mathbf{i}} \tag{205}$$

$$\hat{\mathbf{k}} = -\mathbf{r}/\|\mathbf{r}\| \tag{206}$$

$\mathbf{A}_i^{orbit}$ can be represented as a rotation matrix

$$\mathbf{A}_i^{orbit} = \left[\hat{\mathbf{i}} \quad \hat{\mathbf{j}} \quad \hat{\mathbf{k}} \right] \tag{207}$$

The ATLAS frame incorporates the orbit frame $\mathbf{A}_i^{ATLAS}(t) = \mathbf{A}_{orbit}^{ATLAS}(t)\mathbf{A}_i^{orbit}(t)$ where $\mathbf{A}_{orbit}^{ATLAS}(t) = \mathbf{A}_n(t)\ldots\mathbf{A}_2(t)\mathbf{A}_1(t)$ are rotations that can represent ocean scans, off-nadir pointing, higher-frequency rotations of ATLAS as a whole, etc. After the additional rotations the $\hat{\mathbf{i}}$ and $\hat{\mathbf{k}}$ vectors in $\mathbf{A}_i^{ATLAS} = \left[\hat{\mathbf{i}} \quad \hat{\mathbf{j}} \quad \hat{\mathbf{k}} \right]$ will generally no longer be aligned with the velocity and nadir directions.

5.2 Position, Pointing, and Geolocation Truth

In practice the laser unit vectors are empirically observed in the LRS laser tracker frame. They are therefore thought of here as being fundamentally associated with the laser tracker frame and represented by $\mathbf{u}_{LT}$. To represent pointing truth we want the true laser vectors $\mathbf{u}_{ICRF}$ in the ICRF (and the intermediary $\mathbf{u}_{ATLAS}$ in the ATLAS frame).

The true ATLAS frame attitude is $\mathbf{A}_i^{ATLAS}$ and the true laser unit pointing vector(s) $\mathbf{u}_{ATLAS}$ and $\mathbf{u}_{ICRF}$ are given by

$$\mathbf{u}_{ATLAS} = (\mathbf{A}_{LRS}^{LT}\mathbf{A}_{ATLAS}^{LRS})^T\mathbf{u}_{LT} \tag{208}$$

$$\mathbf{u}_{ICRF} = (\mathbf{A}_i^{ATLAS})^T\mathbf{u}_{ATLAS} = (\mathbf{A}_{LRS}^{LT}\mathbf{A}_{ATLAS}^{LRS}\mathbf{A}_i^{ATLAS})^T\mathbf{u}_{LT} \tag{209}$$

The essential values for the overall position, pointing, and geolocation ground system are $\mathbf{u}_{ICRF}$ and $\mathbf{A}_i^{ATLAS}$. Information that is primarily of interest to the pointing group and is therefore restricted to the artificial telemetry (Section **Error! Reference source not found.**) is represented y the sensor alignments $\mathbf{A}_{LRS}^{LT}\mathbf{A}_{ATLAS}^{LRS}$. Note that given the true values for $\mathbf{u}_{ICRF}$ and $\mathbf{A}_i^{ATLAS}$, the laser unit vectors in the laser tracker frame $\mathbf{u}_{LT}$ follow directly by

$$\mathbf{u}_{LT} = (\mathbf{A}_{LRS}^{LT}\mathbf{A}_{ATLAS}^{LRS}\mathbf{A}_i^{ATLAS})\mathbf{u}_{ICRF} \tag{210}$$

Equation (210) demonstrates that the $\mathbf{u}_{LT}$ can be viewed as a function of $\mathbf{u}_{ICRF}$ and $\mathbf{A}_i^{ATLAS}$

$$\mathbf{u}_{LT} = \mathbf{f}(\mathbf{u}_{ICRF}, \mathbf{A}_i^{ATLAS}) \tag{211}$$

Clearly $\mathbf{u}_{ICRF}$ and $\mathbf{A}_i^{ATLAS}$ are where position and geolocation information enter the true pointing. Representing the true ATLAS position vector as $\mathbf{r}$ and the true geolocation vector(s) as $\mathbf{s}$, the $\mathbf{u}_{ICRF}$, $\mathbf{A}_i^{ATLAS}$, and $\mathbf{u}_{LT}$ can be viewed as a function of $\mathbf{r}$ and $\mathbf{s}$

$$\begin{aligned} \mathbf{u}_{LT} &= \mathbf{f}(\mathbf{u}_{ICRF}(\mathbf{r},\mathbf{s}), \mathbf{A}_i^{ATLAS}(\mathbf{r},\mathbf{s})) \\ &= \mathbf{f}(\mathbf{r},\mathbf{s}) \end{aligned} \tag{212}$$

Equation (212) represents the perspective adopted here, though the more common perspective is probably to describe geolocation as a function of $\mathbf{r}$, $\mathbf{u}_{LT}$, and $\mathbf{A}_i^{ATLAS}$ in

$$\mathbf{s} = \mathbf{s}(\mathbf{r}, \mathbf{u}_{ICRF}) = \mathbf{s}(\mathbf{r}, \mathbf{u}_{LT}, \mathbf{A}_i^{ATLAS}) \tag{213}$$

For time series of true attitudes and positions $\mathbf{A}_i^{ATLAS}(t)$ and $\mathbf{r}(t)$, there are associated time series of true angular rates $\boldsymbol{\omega}(t)$ and velocities $\mathbf{v}(t)$. They are classed as components of the overall state (though $\boldsymbol{\omega}(t) \equiv d\mathbf{A}/dt$ and $\mathbf{v}(t) \equiv d\mathbf{r}/dt$) to provide compatibility with the traditional state-space perspective, where a state equation of the form $d\mathbf{x}/dt = \mathbf{f}(\mathbf{x}, t, ...)$ equates the derivate of the state vector to a force model. The state-space perspective and state equation are somewhat deemphasized in pointing determination because no attempt is made to model the angular accelerations and torques.

5.3 Artificial Telemetry and SIMV9 Truth Data

SIMV9 is a fundamental truth dataset from the geolocation group at GSFC. It provides the spacecraft frame attitude, rate, position, and velocity for a 24 hour interval that includes realistic pointing maneuvers of all types. The SIMV9 attitude truth frame $\mathbf{A}_i^{ATLAS}$ is defined here to be similar to the OSC spacecraft frame $\mathbf{A}_i^{SC}$ which is associated with the IMSC as described in section 5.1.

The dataset provides a useful example for describing artificial telemetry and test processing, and it is treated a baseline or reference case here. It provides true attitudes and rates for $\mathbf{A}_i^{ATLAS}$ at 1 second intervals. After interpolation to 0.1 second intervals these attitudes and rates are already closely related to the spacecraft star trackers and SIRU by the IMSC. The SSTs and SIRU are mounted on the IMSC, and the SIMV9 frame $\mathbf{A}_i^{ATLAS}$ is associated with the OSC spacecraft frame $\mathbf{A}_i^{SC}$ and therefore with the IMSC.

Generating artificial telemetry is a straightforward application of the measurement and error models from Chapter 4.0. The true attitude and alignments are known. The measurement models are used to introduce the sensor characteristics and deterministic errors. Stochastic errors (noise) are added and characterized in terms of the error models. The SIRU is more complex due to the nature of its observations and its role in the processor, as discussed below.

5.3.1 Artificial Star Telemetry

Artificial telemetry is generated for the SSTs based on their reference alignments $\mathbf{A}_{ATLAS}^{SST1}$ and $\mathbf{A}_{ATLAS}^{SST2}$. The telemetry simply consists of the attitudes given by

$$\mathbf{A}_i^{SST1} = \mathbf{A}_{ATLAS}^{SST1}\mathbf{A}_i^{ATLAS} \tag{214}$$

$$\mathbf{A}_i^{SST2} = \mathbf{A}_{ATLAS}^{SST2}\mathbf{A}_i^{ATLAS} \tag{215}$$

Alignment variations $\mathbf{a}_{SST1}(t), \mathbf{a}_{SST2}(t)$ and noise $\boldsymbol{\eta}_{SST1}, \boldsymbol{\eta}_{SST2}$ are added to give

$$\mathbf{A}_i^{SST1} = \mathbf{A}(\mathbf{a}_{SST1}(t))\mathbf{A}_{ATLAS}^{SST1}\mathbf{A}_i^{ATLAS} + \boldsymbol{\eta}_{SST1} \tag{216}$$

$$\mathbf{A}_i^{SST2} = \mathbf{A}(\mathbf{a}_{SST2}(t))\mathbf{A}_{ATLAS}^{SST2}\mathbf{A}_i^{ATLAS} + \boldsymbol{\eta}_{SST2} \tag{217}$$

The reference alignments $\mathbf{A}_{ATLAS}^{SST1}$ and $\mathbf{A}_{ATLAS}^{SST2}$ are based on values provided by OSC.

$$\mathbf{A}_{ATLAS}^{SST1} = \begin{bmatrix} -.5 & -.7071 & .5 \\ -.5 & .7071 & .5 \\ -.7071 & 0 & -.7071 \end{bmatrix}^{\mathbf{T}} \tag{218}$$

$$\mathbf{A}_{ATLAS}^{SST2} = \begin{bmatrix} .5 & -.7071 & -.5 \\ -.5 & -.7071 & .5 \\ -.7071 & 0 & -.7071 \end{bmatrix}^{\mathbf{T}} \tag{219}$$

In the spacecraft frame, the SST LOS vectors are $SST1 = [0.5 \quad 0.5 \quad -0.7071]^T$ and $SST2 = [-0.5 \quad 0.5 \quad -0.7071]^T$. The LRS LOS vector is $LRS = [0 \quad 0 \quad -1]^T$. This creates a pyramid geometry with each SST LOS 45° from the LRS LOS and 60° from the other SST LOS. Another perspective on SST geometry is that the LRS star tracker LOS is along the spacecraft frame -Z axis and the SST LOSs are in their own SST plane. Take the plane defined by the spacecraft X,-Z axes and rotate it about the X axis by 35.26 degrees towards the Y axis (so away from the solar array). This is the SST plane. Within the SST plane the SST LOSs are 60 degrees apart. One is 30 degrees forwards towards the X axis, one is 30 degrees back towards the -X axis.

The alignment rotation from the ATLAS frame to the LRS frame (LRS star tracker) is $\mathbf{A}_{ATLAS}^{LRS}$ and artificial LRS star observations are generated as unit vectors expressed in h, v coordinates in the LRS attitude frame $\mathbf{A}_{ATLAS}^{LRS}\mathbf{A}_i^{ATLAS}$. For additional realism they can first be represented as centroid x, y pixel positions and then converted to unit vectors as described in Section 4.2.2, but in most testing cases artificial centroids are simply redundant information.

The LRS line of sight is the $\mathbf{k}$ axis of the LRS attitude frame $\mathbf{A}_{ATLAS}^{LRS}\mathbf{A}_i^{ATLAS}$. A search is made of the mission catalog for all observable stars near the LOS using the method described in Section 4.1.8. Candidate stars from the search are expressed as unit vectors in the LRS attitude frame by

$$\mathbf{u}_{LRS} = \mathbf{A}_{ATLAS}^{LRS}\mathbf{A}_i^{ATLAS}\mathbf{u}_{ICRF} \tag{220}$$

For the 12° LRS field of view the h, v limits are

$$\tan(6\pi / 180) = 0.105 \tag{221}$$

Candidate stars with horizontal or vertical coordinates greater than 0.105 are outside of the field of view and discarded.

The remaining candidates are transformed by the measurement model

$$\mathbf{u}'_{LRS} = \mathbf{f}(\mathbf{u}_{LRS}, \mathbf{p}) + \boldsymbol{\eta} \tag{222}$$

where the parameter vector $\mathbf{p}$ characterizes the deterministic errors and $\boldsymbol{\eta}$ is zero-mean Gaussian white noise $E\{\boldsymbol{\eta}^T \boldsymbol{\eta}\} = \sigma^2$. The measurement model is described in Section 4.2.4 and the error model for $\boldsymbol{\eta}$ incorporates the magnitude dependence discussed in Section 4.2.6.

5.3.2 Artificial Laser Telemetry

The six laser beams are designed to have a constant geometry relative to one another. This is assumed true here and one vector is sufficient to specify all six beams using constant offset rotations. Extension to time-varying beam geometry is a straightforward increase in bookkeeping from one vector to six vectors.

True laser pointing in the ICRF is given by

$$\mathbf{u}_{ICRF}(t_k) = (\mathbf{A}_{ATLAS}^{LRS} \mathbf{A}_i^{ATLAS}(t_k))^T \mathbf{A}_{LT}^{LRS}(t_k) \mathbf{u}_{LT}(t_k) \tag{223}$$

As described in Section 4.3.6 the laser tracker alignment is modeled as $\mathbf{A}_{LT}^{LRS} = \mathbf{C}(t)\mathbf{B}$ where $\mathbf{B}$ is the reference alignment between the laser tracker frame and LRS frame (LRS star tracker), and $\mathbf{C}(t)$ is a time-varying alignment correction, so that

$$\mathbf{u}_{ICRF}(t_k) = (\mathbf{A}_{ATLAS}^{LRS} \mathbf{A}_i^{ATLAS}(t_k))^T (\mathbf{C}(t_k)\mathbf{B}) \mathbf{u}_{LT}(t_k) \tag{224}$$

Given the true laser pointing $\mathbf{u}_{ICRF}(t_k)$, artificial laser observations $\mathbf{u}'_{LT}(t_k)$ are generated from the $\mathbf{u}_{LT}(t_k)$ by

$$\mathbf{u}'_{LT} = \mathbf{f}(\mathbf{u}_{LT}, \mathbf{p}) + \boldsymbol{\eta} \tag{225}$$

where $\mathbf{p}$ are the measurement model parameters described in Section 4.3.3 and $\boldsymbol{\eta}$ is zero-mean Gaussian white noise $E\{\boldsymbol{\eta}^T \boldsymbol{\eta}\} = \sigma^2$ error model described in Section 4.3.4.

Generally the unit vectors are represented using h, v coordinates in the laser tracker frame. For additional realism they can be represented as equivalent centroid x, y pixel positions at any time as described in Section 4.3.3. Conversion from centroids to unit vectors and unit vectors to centroids is deterministic and the two representations are redundant.

5.3.3 Artificial Gyro Telemetry

ICESat-2 pointing knowledge requires attitude estimates every 20 milliseconds. Over this timescale most of the available attitude information comes from gyro observations recorded every 20 milliseconds asynchronously from the attitude estimates. The true situation is more complex with additional attitude estimates needed intermittently between the 20 millisecond boundaries, but the basic 20 millisecond problem demonstrates the principals and methods involved.

The gyro observations represent changes of direction over time. Past observations are required to interpret new observations and functionally the gyros act as a memory unit. By contrast, the star trackers observe directions in space and are memoryless in the sense that information from the past is not required to interpret new observations.

In practice the problem reduces to extracting rotation vectors for each 20 millisecond interval from the asynchronous gyro observations. The rotation vectors represent the desired attitude estimates. Starting from an initial attitude they specify the following attitudes.

The questions become what information is expected in the gyro observations, how much smoothing should be performed given the noise characteristics, and how should the 20 millisecond rotation vectors be interpolated.

The interpolation method should reflect both the predicted motion of the spacecraft and the predicted resolution[3] of the gyro observations over appropriate timescales. The predictions are based primarily on available information from Orbital Sciences and Northrop Grumman respectively.

The problem can be posed in two spaces: raw angular increments (sense-axes integrated rates) and inertial navigation methods[4], or reduced angular rates (differentiation) and re-integration. In principal the information content is the same in both spaces, but the interpretations as rotation vectors are different.

Smoothing (moving average, LOESS, frequency domain signal processing filters such as Butterworth, Chebyshev, Elliptic, etc) can be useful depending on the characteristics of the motion and the noise. Noise refers here to any stochastic (non-deterministic) components in the

[3] The term resolution refers here to the overall ability to reconstruct the true motion from the gyro observations.

[4] Savage, P. G., "Strapdown Inertial Navigation Integration Algorithms Design Part 1: Attitude Algorithms," *Journal of Guidance, Control, and Dynamics*, Vol. 21, No. 1, 1998, pp. 19-28.

gyro observations. Decisions regarding smoothing are based on noise predictions and flight experiences from Northrop Grumman.

These considerations should ultimately be incorporated in the artificial gyro telemetry. Initially simple biases and noise can be added to the true body rate $\boldsymbol{\omega}$, followed by the full measurement model discussed in Section 4.4.4 (sense axes misalignments, scale factors).

5.4 Preprocessor

Flight telemetry is delivered from SIPS as ATL02 files in HDF5 format that are functionally similar to the ICESat-1 GLA04 granules. The artificial telemetry format evolves over time to converge with and become identical to the flight ATL02 HDF5 format. The objective is that by the ground readiness test in 2016 the artificial telemetry format will be the same as the flight HDF5 format. In other words the ground readiness test will use artificial telemetry formatting that is as flight-like as possible.

Telemetry (artificial and flight) is handled in a preprocessor that functions as an abstraction layer. When there is a change of telemetry format, or multiple formats for the same telemetry, corresponding adaptations are made in the preprocessor but no changes are needed within the primary processing.

After launch, minor changes should be expected to the flight format over time. There were cases of this with the ICESat-1 GLA04 flight format. For example there was a change of the GLA04 definition for IST star position coordinates. The preprocessor outputs are stable representations of sensor observations for processing and the question becomes which representations are preferable, for example in terms of performance or clarity.

One of the most important jobs of the preprocessor is to sort and group the sensor observations in time. The output is a timetag sorted event list of all observations (LRS, SST1, SST2, and SIRU) during a specified time interval t_{start} and t_{end}. The information can come from multiple telemetry files. ICESat-1 GLA04 format for example used a separate physical file for each sensor. The time interval t_{start} and t_{end} may span multiple telemetry files as well. An example event list is shown in Table 10 for a time interval with $t_{start} = 0 msec$ and $t_{end} = 60.01 msec$.

Table 10 Event list example

k	Timetag t_k, msec	Δt, msec	Observation type
1	0	-	Gyro
2	4.74	4.74	Star (LRS)
3	9.32	4.58	Laser
4	20.01	10.69	Gyro
5	29.34	9.33	Laser
6	40.01	10.67	Gyro
7	49.33	9.32	Laser
8	53.48	4.15	Star (SST)
9	60.01	6.53	Gyro

The data structure representing the event list has three key components per record:

1. Timetag
2. Observation type, signifying how to handle the record and its associated observation.
3. Observation parameters, or a pointer to the observation parameters if they are located in a different data structure.

This intermediate or interface event list data structure provides practical abstraction between the telemetry and the processor. The definitions of the observation parameters are processor dependent and decoupled from telemetry formatting.

The event list also provides a useful map and overview of the incoming telemetry. Data gaps of various types (LRS star tracker blinding, SIRU telemetry malfunctions, etc) are easily detectable. Sanity checking, outlier detection, and quality monitoring are important preprocessor functions and it is convenient and practical to focus on analyzing the centralized event list wherever possible, particularly because of the independence from telemetry formatting. Some sanity checking is necessarily telemetry format dependent, but it is kept to a minimum to promote code

maintainability and reuse. If there is a change of telemetry format, it should not break sanity checking and quality monitoring functionality.

5.5 Processor

For processing the event list, adequate attitude estimates $\mathbf{A}_i^b$ for many purposes (particularly LRS star identification) are provided by the SST1 and SST2 observations, which directly represent the estimated attitude rotations $\mathbf{A}_i^{SST1}$ and $\mathbf{A}_i^{SST2}$. Body frame attitude estimates from the SST observations are given by

$$\mathbf{A}_i^b(t_k) = (\mathbf{A}(\mathbf{a}_{SST1}(t_k))\mathbf{A}_b^{SST1})^T \mathbf{A}_i^{SST1}(t_k) \tag{226}$$

$$\mathbf{A}_i^b(t_k) = (\mathbf{A}(\mathbf{a}_{SST2}(t_k))\mathbf{A}_b^{SST2})^T \mathbf{A}_i^{SST2}(t_k) \tag{227}$$

One aspect of the overall problem is to find the SST1 and SST2 alignment corrections $\mathbf{a}_{SST1}(t_k)$ and $\mathbf{a}_{SST2}(t_k)$ that result in the best LRS star predictions $\mathbf{u}_{LRS} = \mathbf{A}_b^{LRS}\mathbf{A}_i^b(t_k)\mathbf{u}_{ICRF}$ (the LRS star predictions that produce the smallest observed minus predicted residuals).

When an even list record contains an SST attitude observation $\mathbf{A}_i^{SST1}$ or $\mathbf{A}_i^{SST2}$, an update is applied to the corresponding SST alignment correction

$$\mathbf{a}_{SST1}(t_k)_- \rightarrow \mathbf{a}_{SST1}(t_k)_+ \tag{228}$$

$$\mathbf{a}_{SST2}(t_k)_- \rightarrow \mathbf{a}_{SST2}(t_k)_+ \tag{229}$$

Using an SST observation to also update the attitude estimate $\mathbf{A}_i^b(t_k)$ is optional, the update can be configured either way and can be an adaptive decision. For example, when the LRS is blinded the SSTs can be used to update $\mathbf{A}_i^b(t_k)$ but not otherwise. This is a significant tuning choice for the overall processor and a topic for performance analysis.

In practice the alignment corrections $\mathbf{a}_{SST1}(t_k)$ and $\mathbf{a}_{SST2}(t_k)$ are small enough that the LRS star predictions are always adequate for performing filter updates using the LRS star observations. For normal stars with adequate flight catalog parameters there is no difficulty in performing star identification and filter updates. In other words, the reference alignments between the LRS, SST1, and SST2 are stable and well known enough to easily interpret the LRS star observations based on the SST attitude observations.

Normally the LRS frame alignment estimate $\mathbf{A}_b^{LRS}$ is held approximately constant so that the LRS attitude estimate $\mathbf{A}_i^{LRS}(t_k)$ is identified with body frame attitude estimate $\mathbf{A}_i^b(t_k)$ by

$$\mathbf{A}_i^{LRS}(t_k) = \mathbf{A}_b^{LRS}\mathbf{A}_i^b(t_k) \tag{230}$$

When an event list record contains LRS star unit vector observations an update is applied to the body frame estimate

$$\mathbf{A}_i^b(t_k)_- \rightarrow \mathbf{A}_i^b(t_k)_+ \tag{231}$$

These LRS star observation updates are critical for performance analysis. The post-update LRS attitude estimate $\mathbf{A}_i^{LRS}(t_k)_+ = \mathbf{A}_b^{LRS}\mathbf{A}_i^b(t_k)_+$ should be as close as possible to the true LRS attitude $\mathbf{A}_{ATLAS}^{LRS}\mathbf{A}_i^{ATLAS}(t_k)$.

In-between star updates from the LRS and SSTs are gyro attitude estimates. As discussed in Section 5.3.3, the characteristic timescale of both the gyro observations and attitude estimates is 20 milliseconds. On this timescale the motion of the spacecraft is relatively uncertain and performance analysis is necessarily more complex.

An interesting question for investigation using artificial telemetry is the empirical effects of various types of high frequency motion on the gyro observations and attitude estimates. Ultimately the results can be represented as lower bounds on the attitude uncertainty. The concept here is that high frequency motion may be at best partially observable. There may be qualitative evidence of significant high frequency motion that is not characterized quantitatively. Testing using artificial gyro telemetry can be used to estimate reasonable lower bounds for the uncertainties on timescales near 20 milliseconds.

One of the difficulties at these timescales is that there are not filter residuals to monitor. The gyro observations enter the filter via the propagation phase rather than the update phase. The key principal here is that there are no external references and no predictions for the gyro observations. In a sense the gyro observations are used open-loop with no feedback to generate an error signal and evaluate performance.

5.6 Case A: Spacecraft Star Trackers and SIRU

The simplest case includes the spacecraft star trackers and SIRU alone, setting aside the LRS. In a sense this shrinks the spacecraft down to the IMSC and its three sensors. The true attitude $\mathbf{A}_i^{ATLAS}$ is conceptually tied to the IMSC, and the true values for $\mathbf{A}_i^{ATLAS}$ are interpolated from the SIMV9 data. The SST alignments are assumed to be constant. Errors introduced in the artificial telemetry are attitude noise (SST quaternion output noise) and rate noise (SIRU rate bias instability).

One way in which this is effectively the simplest useful test case is the absence of direct star observations. What is referred to here as the broad class of star telemetry is involved through the

SSTs, but the star observations are already reduced to attitude estimates. The SSTs and SIRU provide noisy observations of the attitude and rate that are filtered together for overall attitude and rate estimates. The fundamental question is how well the processor tracks the true $\mathbf{A}_i^{ATLAS}$ given noisy SST and SIRU attitude and rate observations.

5.6.1 Artificial Telemetry

SIMV9 describes nadir pointing, calibration scans, and target scans as realistically as possible, particularly the transitions to and from scans where the angular accelerations are high. It consists of true attitudes at 1 second intervals over 86400 seconds (approximately 1 day). During this period two ocean scans, an around the world scan, and a sequence of target scans are performed. This is not a realistic day for on-orbit operations, but is convenient for studying scans and transitions.

Rates are derived from the attitudes and both are interpolated to 0.1 second intervals to match the fundamental frequency of the attitude determination problem (determined by the frequency of star tracker observations). The interpolated attitudes and rates represent the true state. This means that they are also the ideal observations from the spacecraft star trackers and SIRU. If the sensor observations contain negligible errors then they are equal to the true attitude and rate. It is a given that the attitude time series represents the ideal SST observations, but the rates have to be derived carefully to insure that they represent the ideal SIRU observations.

A test is immediately performed on the angular rates to see if they are valid for use as the ideal SIRU output, in other words if they are in fact the true rates. The initial attitude is propagated forward in time using the rates alone to predict the attitude time series. If significant errors accumulate in the predicted attitudes the rates are not a valid representation of the truth or of the ideal SIRU output.

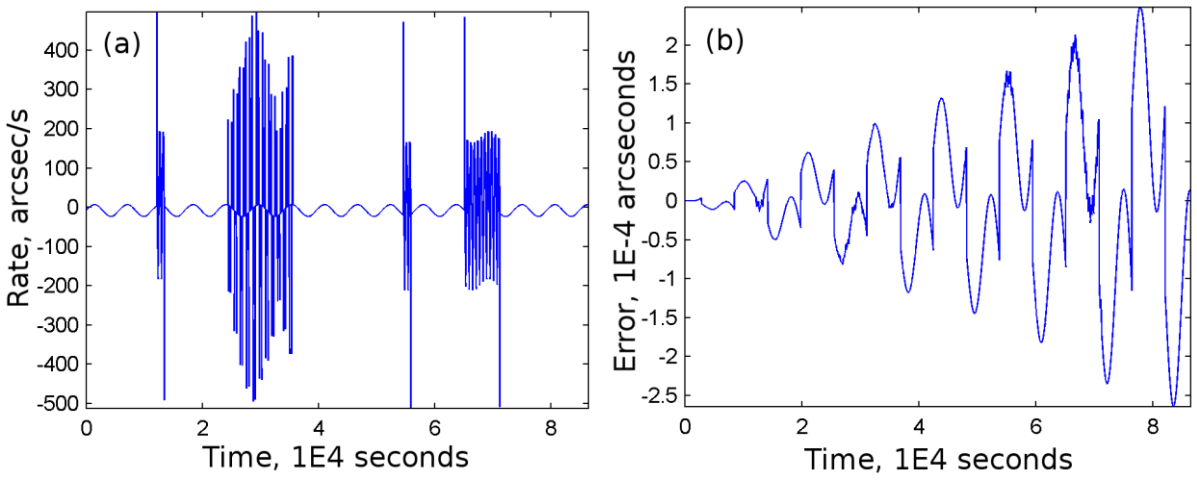

Fig. 9 Roll a) true angular rate b) error in predicted attitude.

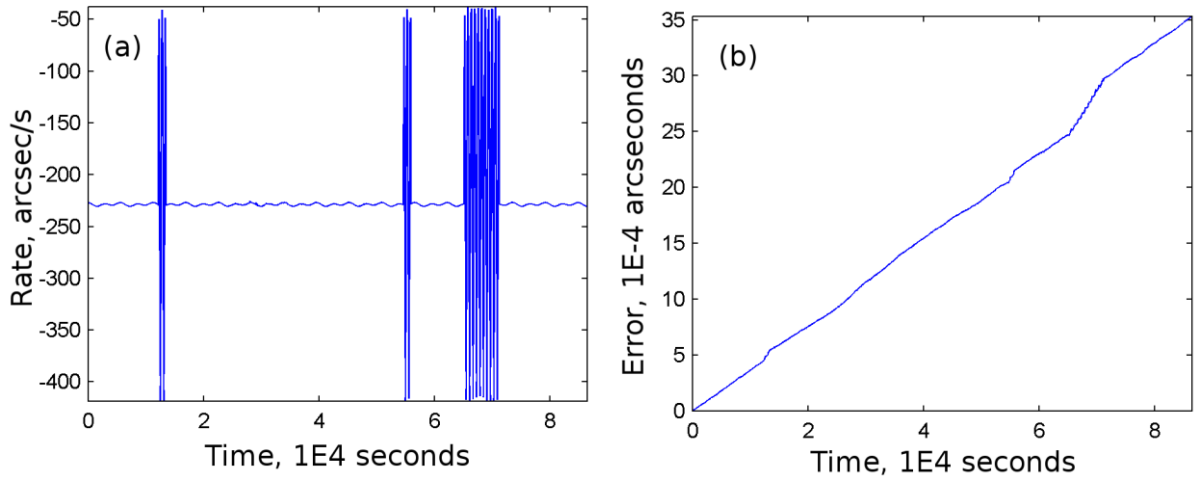

Fig. 10 Pitch a) true angular rate b) error in predicted attitude.

For the SIRU, a rate bias is added to the true rate to form the observed rate. The initial rate bias is random, and each of its components performs a random walk over time based on the SIRU parameters reported in specification documents.

$$\sigma_{awn} = .003 arcsec / Hz^{1/2} \rightarrow 1.454e-8 rad / Hz^{1/2} \tag{232}$$

$$\sigma_{arw} = 1.5e-4 arcsec / s^{1/2} \rightarrow 7.272e-10 rad / s^{1/2} \tag{233}$$

$$\sigma_{rrw} = .0003 arcsec / s / \sqrt{3600 s} = 5e-6 arcsec / s^{3/2} \rightarrow 2.424e-11 rad / s^{3/2} \tag{234}$$

Alternate values reported in other sources include $\sigma_{awn} = 0.645e-7 rad/Hz^{1/2}$ and $\sigma_{arw} = 4.363e-8 rad/s^{1/2}$. In general the larger values are used as a worst case precaution.

The rate random walk parameter σ_{rrw} is used to characterize the rate bias variations. As shown by Eq. (184), the growth in rate bias uncertainty over time is given by $\sqrt{t}\sigma_{rrw}$ and over a 0.1 second interval

$$\sqrt{0.1}(2.424e-11) = 7.6e-12 rad/s \tag{235}$$

This value is used as a rough order-of-magnitude estimate for the random walk during each 0.1 second step.

On short time scales the random walk steps are effectively noise and over longer time scales they accumulate as rate bias. For the ICESat-1 SIRU, rate biases magnitudes were on the order of 0.1 to 1 arcsec/s. In the artificial telemetry using the random walk values discussed above, the magnitude of the rate bias variation is on the order of 0.1 arcsec/s over a 12 hour interval.

SST1 is used here as a representative for both SSTs. The true SST1 attitude is given immediately by

$$\mathbf{A}_i^{SST1} = \mathbf{A}_{ATLAS}^{SST1}\mathbf{A}_i^{ATLAS} \tag{236}$$

and a random noise rotation is included to create the observed attitude

$$\mathbf{A}_i^{SST1} = \mathbf{A}(\boldsymbol{\eta}_{SST1})\mathbf{A}_{ATLAS}^{SST1}\mathbf{A}_i^{ATLAS} \tag{237}$$

Noise estimates for use in $\boldsymbol{\eta}_{SST1}, \boldsymbol{\eta}_{SST2}$ based on initial flight experience are available in Reference [45]. The reference gives three-sigma values resulting in the factor of 3 seen here.

$$\sigma_x = \frac{(2.7/3)}{\sqrt{16Hz}} = \frac{.22asec}{\sqrt{Hz}} \rightarrow .22asec\sqrt{10Hz} = .7asec \text{ at 10 Hz} \tag{238}$$

$$\sigma_y = \frac{(2.6/3)}{\sqrt{16Hz}} = \frac{.22asec}{\sqrt{Hz}} \rightarrow .22asec\sqrt{10Hz} = .7asec \text{ at 10 Hz} \tag{239}$$

$$\sigma_z = \frac{(23.8/3)}{\sqrt{16Hz}} = \frac{1.98asec}{\sqrt{Hz}} \rightarrow 1.98asec\sqrt{10Hz} = 6.3asec \text{ at 10 Hz} \tag{240}$$

Calculating the rotational differences between the true and observed attitudes, in other words the observation errors, over a time series provides confirmation that the noise effects have the proper statistical characteristics about each of the three SST frame axes.

5.6.2 Preprocessor

From a preprocessor perspective this case is particularly simple because individual star observations are not included. There are only attitudes (four component vectors) and rates (three component vectors). Both the truth values and the artificial telemetry are easily represented by two-dimensional arrays with each record including a timetag and a vector of attitude and rate components.

The event list reduces to a list of attitude observations (SST1, SST2) and rate observations (SIRU). In reality the observations from the three instruments are asynchronous but little fidelity is lost by modeling them as synchronous at 10 Hz, effectively reducing or compressing both the 50 Hz SIRU output and the overall complexity of the event list. Every 0.1 seconds the event list receives a rate vector from the SIRU and an attitude vector from each SST.

5.6.3 Processor

Case A provides an ideal study of attitude filtering. The fundamental principles are not obscured by superficial complexity. The true attitudes $\mathbf{A}_i^{ATLAS}$ and rates are known. They are used to create artificial telemetry consisting of observed attitudes and rates with known error characteristics. The observations are filtered to estimate the attitude and rate. The differences between the truth and the estimates are the overall error.

There is a difference or asymmetry in the use of the attitude and rate information reflecting a basic principle of attitude filtering: attitude observations enter through filter updates, and rate observations enter through filter predictions (propagations). The filter does not treat the rate observations as measurements but instead uses them to replace dynamical modeling in the state equation (model replacement). A summary of the asymmetries is shown in Table 11.

Table 11 Attitude filter asymmetries between attitude and rate observations

	Attitude obs	Rate obs
Filter phase	Update	Prediction
Noise type	Quaternion noise	Rate bias instability
Noise represented in filter by	**R** Measurement noise	**Q** State process noise

Case A reduces the attitude filter to its most basic principles. There are two knobs to turn for tuning: $\mathbf{R}$ and $\mathbf{Q}$. The emphasis put on filter updates is changed by varying $\mathbf{R}$. Smaller values in $\mathbf{R}$ mean there is less uncertainty in the attitude observations and results in larger update gains $\mathbf{K}$ and stronger update corrections of the filter state. The emphasis put on filter predictions is changed by varying $\mathbf{Q}$. Larger values in $\mathbf{Q}$ mean there is more uncertainty in the filter states and predictions and again results in larger update gains $\mathbf{K}$ and stronger update corrections of the filter state.

$\mathbf{Q}$ characterizes how attitude prediction uncertainty grows over time and is tied to the SIRU and complex measurement and error models. It is parameterized in the filter by $\sigma_{awn}, \sigma_{arw}$ and particularly by σ_{rrw}. Values are taken from the SIRU specifications and testing. With 10 Hz updates coming from the spacecraft star trackers the prediction time spans are relatively short. Over 0.1 second intervals the predictions from the SIRU are relatively good and the question may reduce to how good are the attitude observations and how much should they be trusted. Filter tuning then becomes focused on $\mathbf{R}$ and the emphasis is placed on filter updates and attitude observations. Can the filtered spacecraft star tracker attitude observations keep the errors in the attitude estimates within the requirement of 2 microradians, even during maneuvers?

Glossary

Ancillary inputs refers to inputs that come from outside the ICESat-2 mission. Some examples are ephemeris data for the sun and moon (from JPL), fundamental star catalogs (SKY2000, Hipparcos), etc.

ATLAS frame the concept of an ATLAS frame comes up particularly in modeling and simulation of the overall geolocation process (level L2A product). It is an abstract and ideal frame. For ICESat-1 there was often discussion of a GLAS frame and it was usually equivalent to a GLAS optical bench frame. For ICESat-2 the IMSC platform (carrying the SIRU and SSTs) is the obvious choice for an ATLAS frame.

Bad stars have LRS position measurements that are biased (from their reference positions given in the mission catalog) due to near-neighbor stars.

Body frame the term body frame may be local to the processor and filter, particularly the theory. A convention in attitude and alignment estimation theory to express the attitude as rotation from the ICRF to the body frame $\mathbf{A}_i^b$. Here we express the star tracker alignments as rotations from this body frame $\mathbf{A}_b^{LRS}$, $\mathbf{A}_b^{SST1}$, $\mathbf{A}_b^{SST2}$. In general in this document the body frame is the same as the LRS frame, and often the ATLAS frame, and even the spacecraft frame (which is associated with the OSC onboard ACS).

Calibration parameter inputs refers to input parameters that are not included in the telemetry but are local to the ICESat-2 mission. They consist of ground testing and calibration information for the LRS, SST, and SIRU measurement and error models. Mission star catalogs can be loosely identified with the calibration inputs.

Centroiding errors or **high spatial frequency errors (HSFE)** are deviations away from the pinhole camera model that are a function of small changes of position on the focal plane, on the scale of individual pixels.

Coordinate frames these are abstract, ideal frames not directly associated with a sensor or empirical observations. In general the **Body Frame** is associated with estimation, filtering, and knowledge. The **ATLAS Frame** is associated with simulation, modeling, and "truth". The **orbit frame** is associated with the simplest orbit model. The **spacecraft frame** is associated with the OSC onboard ACS system.

Distortion errors or **low spatial frequency errors (LSFE)** refers here to deviations away from the simple pinhole camera model that are a function of the overall position on the focal plane [35, 37, 39].

Error models are stochastic equations involving random processes and represent uncertainties in sensor measurements and their interpretation.

Filter cold start means that default values for the states and uncertainties are used. An example is starting the filter without information from a previous run using telemetry that is nearby temporally.

Filter warm start means that state and uncertainty information from a previous run is available. The simplest case is starting a filter run using information from a previous run that is adjacent and even overlapping in time.

Focal plane coordinates represent unit vectors in an $\mathbf{i, j, k}$ sensor frame.

Gyro telemetry is received from the SIRU and used for propagation between measurement updates.

High spatial frequency errors (HSFE) or **centroiding errors** are deviations away from the pinhole camera model that are a function of small changes of position on the focal plane, on the scale of individual pixels

Laser Telemetry is received from the LRS laser tracker, which measures laser and reference spot centroids at 50 Hz.

Laser Reference Sensor consists of two trackers, referred as the **LRS star tracker** (LRSST) and the **LRS laser tracker (LRSLT)**, joined back-to-back. The laser side functions like a star tracker, but observes artificial stars generated by the altimetry lasers and reference signals.

Local Tangent Plane (LTP) coordinates represent unit vectors in an $\mathbf{i, j, k}$ frame based on the body frame. Closely related to **sensor frame coordinates** or **focal plane coordinates** that represent unit vectors in an $\mathbf{i, j, k}$ sensor frame.

Low spatial frequency errors (LSFE) or **distortion errors** refers here to deviations away from the simple pinhole camera model that are a function of the overall position on the focal plane.

Measurement Models are deterministic equations for transforming and interpreting the sensor measurements.

Mission Star Catalogs are tied to the LRS star tracker. They can also be referred to as mission catalogs or LRS catalogs; the terms are completely equivalent here.

Orbit frame this is a basic LVLH frame for a circular orbit. It represents the simplest possible model $\mathbf{A}_i^{orbit}$ for the ATLAS frame attitude $\mathbf{A}_i^{ATLAS} = \mathbf{A}_{orbit}^{ATLAS}\mathbf{A}_i^{orbit}$ when $\mathbf{A}_{orbit}^{ATLAS} = \mathbf{I}$.

Telemetry Inputs refers to inputs from ATLAS and the spacecraft. These are the time series data sent from SIPS as HDF5 data files. They consist of 10 Hz LRS star measurements, 50 Hz LRS laser side measurements, 10 Hz quaternions and uncertainties from the two SSTs; 50 Hz SIRU measurements, ACS state estimates, temperature data, etc.

Spacecraft frame this frame is associated with the OSC onboard ACS. They express their alignments in the spacecraft frame so it is useful to keep in mind.

Star Telemetry is based on star measurements and is used to perform the filter measurement updates. It therefore determines propagation time intervals and filter cycle boundaries. It is a general term here for star measurements from the LRS and attitude estimates from the SSTs.

Acronyms

ACS	Attitude Control System
AF	ATLAS Frame
ARW	Angular Random Walk in gyro output
ASAS	ATLAS Science Algorithm Software
ASU	Adaptive Star Updates
ATLAS	Advanced Topographic Laser Altimeter System
AWN	Angular White Noise in gyro output
CSR	Center for Space Research, University of Texas at Austin
GLAS	Geoscience Laser Altimeter System
GSFC	Goddard Space Flight Center
HDF5 data	Telemetry input data files for PPD, produced and sent by SIPS in HDF5 format
HSFE	High Spatial Frequency Error
ICESat	Ice, Cloud, and Land Elevation Satellite
ICESat-2	Ice, Cloud, and Land Elevation Satellite 2
IMSC	Instrument Mounted Spacecraft Component
INS	Inertial Navigation System
IQR	Interquartile Range Q3-Q1
LF	LRS Frame, identified with the LRS star side frame
LOS	Line of Sight, the optical axis of a sensor
LRS	Laser Reference Sensor
LRSICD	LRS Interface Control Document
LRSLT	Laser Reference Sensor Laser Tracker
LRSST	Laser Reference Sensor Star Tracker
LRSTC	LRS Team Catalog or LRS Tom Catalog (Tom Correll)
LSFE	Low Spatial Frequency Error
LT	Laser tracker or laser side of the LRS
LTP	Local Tangent Plane coordinates for representing unit vectors
MOC	Mission Operations Center
NG	Northrop Grumman
OF	Orbit Frame, LVLH Orbital Coordinate Frame
OSC	Orbital Sciences Corporation

POD	Precision Orbit Determination
PPD	Precision Pointing Determination
PPDBMC	PPD Baseline Mission Catalog
PSO	Project Science Office
RRW	Rate Random Walk in gyro output
SDMS	Scheduling and Data Management System
SF	Spacecraft Frame, Spacecraft Coordinate Frame
SIPS	Science Investigator Led Processing System
SIRU	Space Inertial Reference Unit
SKY2KV5	SKY2000 Version 5 NASA star tracker catalog
SST	Spacecraft Star Tracker
SIMV9	SIMV9 is a fundamental truth dataset from GSFC (Scott Lutchcke)

References

[1] Sande, C., Brasoveanu, D., Miller, A. C., Home, A. T., and Tracewell, D., "Improved Instrumental Magnitude Prediction Expected from Version 2 of the NASA SKY2000 Master Star Catalog," AAS 98-362, AAS Space Flight Dynamics, Advances in the Astronautical Sciencs, Vol. 100, Univelt, 1998, pp. 765-778.

[2] Sande, C., Natanson, G., and Tracewell, D., "Effects of Uncataloged Near-Neighbor Stars on CCDST Operation," Proceedings NASA-CP-2005-212789, Proceedings of the NASA Goddard Flight Mechanics Symposium, 2005.

[3] Sande, C., Natanson, G., and Tracewell, D., "Effects of Uncataloged Near-Neighbor Stars on CCDST Operation," Goddard Space Flight Center, Maryland, 2005.

[4] Sande, C., Ottenstein, N., Tracewell, D., and Oza, D., "SKYMAP Requirements, Functional, and Mathematical Specifications," Report No. CSC-96-932-24, Computer Sciences Corporation, Falls Church, Virginia, Report CSC-96-932-24, Aug. 1999 1999.

[5] Sande, C. B., Warren, W. H., and Tracewell, D. A., "Recent Enhancements to and Future Plans for the SKY2000 Star Catalog," *Journal of the American Association of Variable Star Observers*, Vol. 29, No. 2, 2000, pp. 123-128.

[6] Lucke, R. L., Sirlin, S. W., and San Martin, A. M., "New Definitions of Pointing Stability: AC and DC Effects," *AAS Journal of the Astronautical Sciences*, Vol. 40, No. 4, 1992, pp. 557-576.

[7] Bayard, D. S., "A State-Space Approach to Computing Spacecraft Pointing Jitter," *Journal of Guidance, Control, and Dynamics*, Vol. 27, No. 3, 2004, pp. 426-433.

[8] Pittelkau, M. E., "Pointing Error Definitions, Metrics, and Algorithms," AAS 03-559, AAS/AIAA Astrodynamics Specialists Conference, Big Sky, MT, 2003.

[9] Pittelkau, M. E., "RIMU Misalignment Vector Decomposition," AIAA 2004-4856, AIAA Astrodynamics Specialist Conference, Providence, RI, 2004.

[10] Pittelkau, M. E., "Observability and Calibration of a Redundant Inertial Measurement Unit (RIMU)," AAS 05-105, AAS Space Flight Mechanics Meeting, Advances in the Astronautical Sciences, Vol. 120, Univelt, 2005, pp. 71-84.

[11] Pittelkau, M. E., "Calibration and attitude determination with Redundant Inertial Measurement Units," *Journal of Guidance, Control, and Dynamics*, Vol. 28, No. 4, 2005, pp. 743-752.

[12] Pittelkau, M. E., "Attitude Determination and Calibration with Redundant Inerital Measurement Units," AAS 04-116, AAS Space Flight Mechanics Meeting, Advances in the Astronautical Sciences, Vol. 119, Univelt, 2005, pp. 229-248.

[13] Markley, F. L., "Attitude Error Representation for Kalman Filtering," *Journal of Guidance, Control, and Dynamics*, Vol. 26, No. 2, 2003, pp. 311-317.

[14] Pittelkau, M. E., "Rotation Vector in Attitude Estimation," *Journal of Guidance, Control, and Dynamics*, Vol. 26, No. 6, 2003, pp. 855-860.

[15] Savage, P. G., "Strapdown Inertial Navigation Integration Algorithms Design Part 1: Attitude Algorithms," *Journal of Guidance, Control, and Dynamics*, Vol. 21, No. 1, 1998, pp. 19-28.

[16] Bayard, D. S., "High Precision Three-Axis Pointing and Control," in *Encyclopedia of Aerospace Engineering: Attitude Dynamics and Orbit Control of Spacecraft*. vol. 5 Part 26, R. Blockley and W. Shyy, Eds., ed Hoboken, NJ: Wiley-Blackwell Publishers, 2010, pp. 172-181.

[17] Pittelkau, M. E., "Survey of Calibration Algorithms for Spacecraft Attitude Sensors and Gyros," AAS 07-295, AAS Astrodynamics Specialist Conference, Advances in the Astronautical Sciences, Vol. 129, Univelt, 2007.

[18] Gray, C. W., Herman, L. K., Kolve, D. I., and Westerlund, G. L., "On-Orbit Attitude Reference Alignment and Calibration," AAS 90-042, AAS Guidance and Control Conference, Advances in the Astronautical Sciences, Vol. 72, Univelt, 1990, pp. 275-292.

[19] Bayard, D. S., "An Overview of the Pointing Control System for NASA's Space Infra-Red Telescope Facility (SIRTF)," AIAA 2003-5832, AIAA Guidance, Navigation, and Control Conference, Austin, TX, 2003.

[20] Bayard, D. S. and Kang, B. H., "A High-Order Kalman Filter for Focal Plane Calibration of NASA's Space Infrared Telescope Facility (SIRTF)," AIAA 2003-5824, AIAA Guidance, Navigation, and Control Conference, Austin, TX, 2003.

[21] Li, R., Needelman, D., Fowell, R., Tsao, T.-C., and Wu, Y.-W., "Reusable Stellar Inertial Attitude Determination (SIAD) Design For Spacecraft Guidance, Navigation & Control," AIAA 2005-5928, AIAA Guidance, Navigation, and Control Conference, San Francisco, CA, 2005.

[22] Li, R. and Wu, Y.-W., "Absolute and Relative Attitude Determination for Multiple Payloads On Spacecraft," AIAA 2006-6048, AIAA Guidance, Navigation, and Control Conference, Keystone, CO, 2006.

[23] Pittelkau, M. E., "A Kalman Filter Approach to System Alignment Calibration," AAS 00-127, AAS/AIAA Space Flight Mechanics Meeting, 2000.

[24] Pittelkau, M. E., "Kalman Filtering for Spacecraft System Alignment Calibration," *Journal of Guidance, Control, and Dynamics*, Vol. 24, No. 6, 2001, pp. 1187-1195.

[25] Pittelkau, M. E., "Everything Is Relative In Spacecraft System Alignment Calibration," *Journal of Spacecraft and Rockets*, Vol. 39, No. 3, 2002, pp. 460-466.

[26] Pittelkau, M. E. and Dellinger, W. F., "Attitude Sensor Alignment And Calibration For The TIMED Spacecraft," AAS 03-153, AAS/AIAA Space Flight Mechanics Meeting, Ponce, Puerto Rico, 2003.

[27] O'Shaughnessy, D. and Pittelkau, M. E., "Attitude Sensor and Gyro Calibration for Messenger," NASA International Symposium on Space Flight Dynamics, NASA Conference Proceedings, Vol. NASA CP-2007-214158, NASA, 2007.

[28] Hanlon, P. D. and Maybeck, P. S., "Multiple-Model Adaptive Estimation Using a Residual Correlation Kalman Filter Bank," *IEEE Transactions on Aerospace and Electronic Systems*, Vol. 36, No. 2, 2000, pp. 393-406.

[29] Markley, F. L., "Attitude Determination and Parameter Estimation Using Vector Observations: Application," *The Journal of the Astronautical Sciences*, Vol. 39, No. 3, 1991, pp. 367-381.

[30] Fowell, R. A., Smith, N., Bae, S., and Schutz, B. E., "Bad Stars," AAS 09-012, AAS Guidance and Control Conference, Advances in the Astronautical Sciences, Vol. 133, Univelt, 2009, pp. 20-36.

[31] Smith, N., Fowell, R., Bae, S., and Schutz, B. E., "Improved Star Tracker Instrument Magnitude Prediction From ICESat Flight Telemetry," Paper AAS 11-086, AAS Guidance and Control Conference, Advances in the Astronautical Sciences, Vol. 141, Univelt, 2011, pp. 639-654.

[32] Smith, N., Bae, S., and Schutz, B. E., "Biased Star Tracker Measurements of Forty-Nine Stars from Flight Data," *Journal of Spacecraft and Rockets*, Vol. 47, No. 6, 2010, pp. 1023-1028.

[33] Mortari, D. and Neta, B., "K-vector Range Searching Techniques," Advances in the Astronautical Sciences, Vol. 105, Univelt Inc., 2000, pp. 449-463.

[34] Liebe, C. C., "Accuracy performance of star trackers - A Tutorial," *IEEE Transactions on Aerospace and Electronic Systems*, Vol. 38, No. 2, 2002, pp. 587-599.

[35] Lam, Q. M., Woodruff, C., Ashton, S., and Martin, D., "Noise Estimation for Star Tracker Calibration and Enhanced Precision Attitude Determination," IEEE Information Fusion Conference, IEEE Conference Proceedings, IEEE, 2002, pp. 235-242.

[36] Wu, Y.-W. and Li, R., "Star Tracker Error Characteristics and Their Compensation Techniques," Proceedings NASA CP-2003-212246, Proceedings of the NASA Goddard Flight Mechanics Symposium, NASA-CP-2003-212246, 2003.

[37] Griffith, T. D., Singla, P., and Junkins, J. L., "Autonomous On-orbit Calibration Approaches for Star Tracker Cameras," AAS 02-102, AAS Space Flight Mechanics Meeting, Advances in the Astronautical Sciences, Vol. 112, Univelt, 2002, pp. 39-57.

[38] Singla, P., Griffith, T. D., Crassidis, J. L., and Junkins, J. L., "Attitude determination and autonomous on-orbit calibration of star tracker for the gifts mission," AAS 02-101, Spaceflight Mechanics 2002, Advances in the Astronautical Sciences, Vol. 112, 2002, pp. 19-38.

[39] Smith, N., "Localized Distortion Estimation and Correction for the ICESat Star Trackers," M.S. Thesis, Aerospace Engineering, University of Texas at Austin, Austin, 2006.

[40] Shuster, M. D., "Stellar Aberration and Parallax: A Tutorial," *Journal of the Astronautical Sciences*, Vol. 51, No. 4, 2003, pp. 477-494.

[41] Lauer, M., Jauregui, L., and Kielbassa, S., "Operational Experience with Autonomous Star Trackers on ESA Interplanetary Spacecraft," Proceedings NASA-CP-2007-214158, Proceedings of the 20th International Symposium on Space Flight Dynamics, NASA-CP-2007-214158, 2007.

[42] Luthcke, S. B., Rowlands, D. D., McCarthy, J. J., Pavlis, D. E., and Stoneking, E., "Spaceborne Laser-Altimeter-Pointing Bias Calibration from Range Residual Analysis," *Journal of Spacecraft and Rockets*, Vol. 37, No. 3, 2000, pp. 374-384.

[43] Yoon, S., Bae, S., and Schutz, B. E., "High Frequency Attitude Motion Of ICESat," AAS 05-108, AAS Space Flight Mechanics Meeting, Advances in the Astronautical Sciences, Vol. 120, Univelt, 2005, pp. 117-131.

[44] IEEE, "IEEE Std 647-2006 Standard Specification Format Guide and Test Procedure for Single-Axis Laser Gyros," ed: IEEE, 2006.

[45] Piot, D., Oddos-Marcel, L., Gelin, B., Thieuw, A., Genty, P., Martinez, P.-E., and Airey, S., "Hydra Star Tracker On-Board SPOT-6," AAS 13-046, 2013.